People's Democratic Republic of Algeria
Ministry of Higher Education and Scientific Research

Saad Dahlab University - Blida 1

Institute of Aeronautics and Space Studies

Master's degree in Aeronautics

Option: **Space Propulsion**

Impact of Combustion Conditions on the Performance and Emissions of Internal Combustion Engines: A Coupled Experimental and Numerical Approach

---

Presented by

- Imene CHAOUCHE
- Soundous BOUAZIZ

Supervised by

- Dr.Rachid RENANE
- Dr.Ahmed NECHE

Jury Members:

Dr.Rachid ALLOUCHE	President
Dr.Nadir BEKKA	Examiner
Dr.Hamid OUELDBESSI	Examiner

2024/2025

Acknowledgements

First and foremost, we express our deepest gratitude to God, whose guidance and blessings have accompanied us throughout this journey and made this achievement possible.

We extend our warmest thanks to our families—our beloved parents, brothers, and sisters—for their endless support, love, and encouragement. Your presence and faith in us have been a pillar of strength.

We would also like to take a moment to sincerely thank ourselves—for the dedication, perseverance, and effort we invested in carrying out this work. It has not been easy, but we are proud of what we have accomplished.

Our heartfelt appreciation goes to our promoters, Dr. R. RENANE and Dr. A. NECHE, who generously offered us this opportunity and provided continuous support and valuable guidance throughout the project. Their trust, mentorship, and insightful feedback have played a key role in the realization of our work.

A very special thank you goes to Ahmed BAOUCHI, Chaima DJEBABLA, Nihad BENFREDJ, Wiam ELAIHAR, and Lina REGIGE for their generosity, assistance, and kindness. You have truly made a difference in our experience.

We also express our gratitude to the Mechanical Engineering Department of Blida 1 University and the Mechanical Engineering Department of Boumerdès University for their support and the resources provided during this study.Finally, we thank all those who believed in us, supported us, or simply offered a kind word of encouragement—it truly meant a lot.

Thank you all.

Dedication 01

Eighteen years—a journey of learning, perseverance, and countless sleepless nights—has led me here. As I stand at this summit, looking back at every struggle and triumph, my heart swells with gratitude. Above all, I thank Allah, who guided me to this moment.

With a soul brimming with love and a spirit lifted by joy, I dedicate this milestone to:

My mother—the first home I ever knew. You carried me, nurtured me, and taught me with endless patience. Your sacrifices were my foundation, your love my compass. No words can hold the depth of my gratitude.

My father—my unshakable hero. You crossed oceans so my path would be smooth, fought battles so mine would be lighter. You are my strength, my shelter. May life always honor you as you've honored me.

My siblings (Muhammad, Abdulrahman, Ibrahim, and Yusuf)—my first friends, my forever confidants. You shared my laughter, my dreams, and even my stubbornness. May your journeys shine brighter than mine.

My husband—the one who stepped into my story and made it ours. Your love is my anchor, your presence my peace. With you, every step forward feels like a new beginning.

My grandparents, aunts, uncles, and cousins—your prayers and love wrapped around me like a shield. May Allah bless you with long, joyful lives.

My dearest friends—the ones who turned dorm rooms into sanctuaries and stress into laughter. You made the hard days lighter and the best days unforgettable.

Soundous—my partner in late-night study sessions and endless coffee cups. You turned challenges into triumphs, and I'll always cherish our shared struggles.

And to **everyone** who lifted me, whether with wisdom, a kind word, or even a silent moment of solidarity—this achievement is yours as much as mine. Your faith in me became my fuel.

This is not an ending, but a promise—to keep climbing, to keep striving, and to carry your light with me always.

Imene CHAOUCHE

Dedication 02

In the name of Allah, the Most Merciful, the Most Compassionate. All praise belongs to Him alone — the One by whose grace every good deed is completed, and by whose mercy I found the strength and guidance to finish this work. His hands are the keys to all goodness.

To my beloved father, Taher — you who crossed endless roads and scorching days to clear a path for my dreams. You faced the sun and the restless winds to offer me warmth and safety. This work is but a drop in the ocean of your sacrifices. No words can repay you, but may these lines remind you of a heart that will never forget.

To my gentle mother, Assia — you turned hardship into comfort, and a weary world into a safe home. You taught me that love is a prayer whispered without end. These pages carry the scent of your sleepless nights and the blessing of your whispered prayers, which were my strongest shelter on this journey.

To my dear siblings (Abdelraouf, Nour El Hoda, Mohsen, Hasnaa, and Houssam) — you made our house a garden of laughter and a fortress of love. This achievement is the fruit of your smiles, your tears, and countless moments we shared — memories too precious ever to fade.

To my faithful companions, Ayadi Takoua and Bensaadi Hanane — you were my light in dark times, my steady hands when I stumbled, my joy in every triumph. Without the warmth of your hearts, this road would have lost its meaning and its beauty.

To my cherished friends, Chaima, Wiam, and Nihad — thank you for walking beside me through every chapter of this story, for hearts that were always a safe haven and a

source of laughter, even on the hardest days.

And finally, to my soul's twin in this journey, Imene Chaouche — you shared sleepless nights and secret questions with me, and smiled with me when answers finally dawned. This work carries your mark as much as it carries mine. You were the sister I chose for myself, and the sun that never sets from my sky.

Because some love is written in tears, and some gratitude is carved from sleepless nights, I offer you these words as an open heart — too small to repay all you gave me, yet too grateful to stay silent.

May Allah make this effort the beginning of goodness, forgive my shortcomings, let it be a token of thanks to every hand that lifted me up, and a guiding light to all who may need it.

Soundous BOUAZIZ

Abstract

This final-year project focuses on a combined experimental and numerical study of the impact of combustion conditions on the performance and emissions of internal combustion engines, particularly gasoline and diesel engines. The main objective is to better understand the mechanisms influencing thermal efficiency and pollutant formation, in a context where energy efficiency and emission reduction have become major challenges.

The experimental part is based on tests carried out on an engine test bench, enabling the measurement of key parameters such as torque, effective power, specific fuel consumption, air/fuel ratio, and exhaust gas temperature. These measurements allow for a detailed comparison between diesel and gasoline engines, highlighting the effect of operating conditions on overall performance.

In parallel, an in-depth numerical study was conducted using two complementary approaches. A first thermodynamic approach, based on chemical equilibrium (Gibbs law), enables the calculation of adiabatic flame temperatures and the molar fractions of species resulting from the complete and dissociated combustion of hydrocarbons (kerosene, methane, diesel). The model incorporates thermodynamic functions (enthalpy, entropy, specific heat) calculated using Bonni McBride coefficients, and the equilibrium equations were solved using the Newton-Raphson method in Fortran.

Résumé

Ce projet de fin d'études porte sur l'étude couplée, expérimentale et numérique, de l'impact des conditions de combustion sur les performances et les émissions des moteurs à combustion interne, en particulier les moteurs essence et diesel. L'objectif principal est de mieux comprendre les mécanismes influençant le rendement thermique et la formation des polluants, dans un contexte où l'efficacité énergétique et la réduction des émissions sont devenues des enjeux majeurs.

La partie expérimentale repose sur des essais réalisés sur banc moteur, permettant de mesurer des paramètres clés tels que le couple, la puissance effective, la consommation spécifique de carburant, le rapport air/carburant et la température des gaz d'échappement. Ces mesures ont permis une comparaison détaillée entre les moteurs diesel et essence, soulignant l'effet des conditions de fonctionnement sur les performances globales.

En parallèle, une étude numérique approfondie a été menée selon deux approches complémentaires. Une première approche thermodynamique, basée sur l'équilibre chimique (loi de Gibbs), permet de calculer les températures de flamme adiabatique ainsi que les fractions molaires des espèces issues de la combustion complète et dissociée d'hydrocarbures (kérosène, méthane, gasoil). Le modèle intègre les fonctions thermodynamiques (enthalpie, entropie, chaleur spécifique) calculées à l'aide des coefficients de Bonni McBride, et les équations d'équilibre ont été résolues via la méthode de Newton-Raphson en Fortran.

ملخص

يركّز هذا المشروع النهائي على دراسة مزدوجة، تجريبية وعددية، لتأثير ظروف الاحتراق على أداء وانبعاثات محركات الاحتراق الداخلي، وخاصة محركات البنزين والديزل. الهدف الرئيسي هو فهم أفضل للآليات التي تؤثر على الكفاءة الحرارية وتكوّن الملوّثات، في ظل تزايد أهمية كفاءة الطاقة وتقليل الانبعاثات.

الجزء التجريبي يعتمد على اختبارات أجريت على منصة اختبار محرك، حيث تم قياس معلمات رئيسية مثل العزم(torque) ، القدرة الفعلية، الاستهلاك النوعي للوقود، نسبة الهواء إلى الوقود، ودرجة حرارة غازات العادم. سمحت هذه البيانات بإجراء مقارنة مفصلة بين محركات الديزل والبنزين، مظهرة تأثير ظروف التشغيل على الأداء العام.

في المقابل، أجريت دراسة عددية باستخدام نهج ديناميكي حراري مبني على التوازن الكيميائي (قانون Gibbs) لحساب درجات حرارة اللهب الأديباتيكي والنسب المولية للنواتج الناتجة عن الاحتراق الكامل وغير الكامل لهيدروكربونات مثل الكيروسين، الميثان، والديزل. يتضمن النموذج دوالّ حرارية مثل enthalpy، entropy، وspecific heat، وتم حل معادلات التوازن باستخدام طريقة Newton-Raphson بلغة Fortran.

Keywords

Internal combustion engines (ICE), Combustion conditions, Engine performance, Emissions, Experimental approach, Numerical simulation, Thermal efficiency, Pollutant formation, Gasoline engine, Diesel engine, Engine test bench, Torque, Effective power, Specific fuel consumption, Air/fuel ratio, Exhaust gas temperature, Thermodynamic modeling, Chemical equilibrium, Gibbs law, Adiabatic flame temperature, Dissociation reactions, Equivalence ratio, Hydrocarbons (kerosene, methane, diesel), Thermodynamic functions (enthalpy, entropy, specific heat), Bonni McBride coefficients, Newton-Raphson method, Fortran programming, ANSYS Fluent, Computational fluid dynamics (CFD), Species transport model, Turbulence modeling, Numerical methods, Emission control, Preheating temperature, Stoichiometry, Experimental validation.

Contents

List of Figures

List of Tables

Abbreviations List

A	Piston Area (cm^2)
BDC	Bottom Dead Centre
C	Torque ($N \cdot m$)
Cd	Coefficient of discharge
c	Molar concentration (mol/m^3)
CI	Compression Ignition
CO	Carbon Monoxide
c_p	Specific heat at constant pressure ($J/kg \cdot K$)
c_v	Specific heat at constant volume ($J/kg \cdot K$)
CV	Calorific Value (kJ/kg)
d	Cylinder Bore (mm)
D	Air/Fuel ratio (mass-based)
ΔP	Pressure difference (Pa)
ΔU	Change in internal energy (J)
F/A or A/F	Fuel–Air Ratio / Air–Fuel Ratio
h	Enthalpy (J)
HO	Water vapor
ICE	Internal Combustion Engine
IDC/ODC	Inner / Outer Dead Centre (horizontal engines)
K_p	Equilibrium Constant
L	Stroke (mm)
M	Mean molar mass (g/mol)
M_i	Molar mass of species i (g/mol)

N	Engine Speed (rpm)
NO_x	Nitrogen Oxides
n	Number of moles
O	Ground-level ozone
P	Pressure (Pa)
P_e	Effective Power (kW)
p_m	Mean Effective Pressure (Pa)
P_s	Specific Power Output (kW/kg)
Q	Heat added to the system (J)
R	Universal gas constant ($8.314\,\mathrm{J/mol \cdot K}$)
r	Compression Ratio
r_{air}	Air-specific gas constant ($\mathrm{J/kg \cdot K}$)
ρ	Mass density ($\mathrm{kg/m^3}$)
ρ_c	Fuel density (kg/L)
S	Entropy (J/K)
sfc	Specific Fuel Consumption (g/kWh)
SI	Spark Ignition
S_p	Mean Piston Speed (m/s)
T_a	Ambient temperature (K)
T_{ad}	Adiabatic Flame Temperature (K)
TDC	Top Dead Centre
U	Internal Energy (J)
UHC	Unburned Hydrocarbons
$\dot{m}_a$	Air consumption (kg/s)
$\dot{m}_c$	Hourly fuel consumption (g/h)
V	Volume ($\mathrm{m^3}$)
V_{cc}	Cylinder volume ($\mathrm{m^3}$)
V_c	Clearance Volume ($\mathrm{m^3}$)
V_s	Swept Volume or Displacement Volume ($\mathrm{m^3}$)
w_i	Mass fraction of species i
W	Work done by the system (J)
x_i	Mole fraction of species i

η_{ith}	Indicated Thermal Efficiency
η_m	Mechanical Efficiency
η_v	Volumetric Efficiency
η_{rel}	Relative Efficiency or Efficiency Ratio
ϵ_p	Pressure energy
ϕ	Equivalence Ratio
CFD	Computational Fluid Dynamics
DI	Direct Injection
IDI	Indirect Injection
$HCCI$	Homogeneous Charge Compression Ignition
$RCCI$	Reactivity Controlled Compression Ignition
PM	Particulate Matter
SO_2	Sulfur dioxide
PbO_2	Lead dioxide
RPM	Revolutions per minute
μ	Dynamic viscosity ($\mathrm{Pa} \cdot \mathrm{s}$)
μ_t	Turbulent dynamic viscosity ($\mathrm{Pa} \cdot \mathrm{s}$)
κ	Turbulent kinetic energy ($\mathrm{m}^2/\mathrm{s}^2$)
ε	Turbulent dissipation rate ($\mathrm{m}^2/\mathrm{s}^3$)
λ	Thermal conductivity ($\mathrm{W}/(\mathrm{m} \cdot \mathrm{K})$)
δ_{ij}	Kronecker delta
γ	Ratio of specific heats
ϵ	Error tolerance
Pr_t	Turbulent Prandtl number
$C_{\varepsilon 1}, C_{\varepsilon 2}, C_\mu$	Turbulence model constants
g_i	Gravity component in i-direction (m/s^2)
P_b	Turbulent kinetic energy production due to buoyancy
T	Temperature (K)
t	Time (s)
u_i, u_j, u_k	Velocity components (m/s)
τ_{ij}	Viscous stress tensor (Pa)
q_j	Heat flux vector (W/m^2)

h	Specific enthalpy (J/kg)
e	Specific internal energy (J/kg)
∇	Gradient operator
Δ	Increment or change operator
Σ	Summation operator

foreword

As part of the work carried out for this memoir, we conducted two important technical visits to specialized laboratories working on internal combustion engines. These experimental campaigns were crucial for gathering real-world data and enhancing the practical relevance of our study.

Our first visit took place at the LaboMoteur laboratory within the Mechanical Engineering Department of Saad Dahlab University – Blida 1. This laboratory is equipped with a test bench dedicated to diesel internal combustion engines. During our experimental sessions, we actively worked on the test bench to observe and measure the engine's performance. A key aspect of the procedure was the systematic variation of the engine's rotational speed across a defined range. For each speed setting, we recorded critical operating parameters such as torque, fuel consumption, engine power, exhaust gas temperature, and other performance indicators using the bench's digital monitoring system.

The second visit was made to the Mechanical Engineering Department at the University of M'hamed Bougara – Boumerdès, where we conducted a similar set of experiments on a gasoline (essence) internal combustion engine. The engine was also mounted on a test bench, and again, we varied the rotational speed during the tests to study the engine's behavior under different operating conditions. For each speed increment, we collected important measurements including power output, airflow rate, fuel usage, and exhaust temperature, allowing us to evaluate the performance of the gasoline engine with precision.

These experimental efforts enabled us to acquire a reliable and comparative dataset for both diesel and gasoline engines. The practice of varying rotational speed during test-

ing allowed for a more comprehensive performance evaluation and helped highlight how different engine types respond to changes in operating conditions.

Overall, these field visits provided hands-on experience with engine diagnostics and test bench operation, and they played a central role in the development of this memoir by offering solid experimental data on which the performance analysis is based.

General Introduction

Internal combustion engines (ICEs) remain indispensable across a wide array of industries, including transportation, agriculture, and energy production. Their widespread use is driven by their robustness, high power-to-weight ratio, and ability to operate under diverse conditions. Although global energy trends are increasingly favoring electrification and renewable alternatives, ICEs continue to dominate in applications where electric technologies are not yet feasible or sufficiently developed.

Nevertheless, rising environmental concerns and stricter emissions regulations have made it imperative to improve the efficiency and sustainability of ICEs. The combustion process within these engines involves complex interactions between thermodynamic, fluid dynamic, and chemical processes. Key parameters such as air–fuel ratio, ignition timing, and in-cylinder pressure significantly influence performance metrics and pollutant emissions, including nitrogen oxides (NO), carbon monoxide (CO), and unburned hydrocarbons (UHCs).

To address these challenges, advanced combustion strategies such as Homogeneous Charge Compression Ignition (HCCI) and Reactivity Controlled Compression Ignition (RCCI) have gained attention due to their potential for high efficiency and low emissions. At the same time, numerical tools like Computational Fluid Dynamics (CFD), especially ANSYS Fluent, are increasingly used for simulating combustion phenomena within engine cylinders, offering detailed insight into flame development, heat release, and pollutant formation.

This final-year project (PFE) explores the impact of combustion parameters on engine performance and emissions using both experimental and numerical approaches. The goal

is to evaluate and compare diesel and gasoline engine performance, investigate the effects of combustion characteristics, and understand the influence of air–fuel equivalence ratio on in-cylinder combustion temperature through simulation.

The methodology integrates two complementary approaches. On the experimental side, performance data were collected from two different test benches—one for a gasoline engine and another for a diesel engine—allowing for a direct comparison between spark-ignition and compression-ignition systems. On the numerical side, a CFD simulation using ANSYS Fluent was conducted to model combustion within an ICE chamber, focusing on the variation of combustion temperature as a function of the equivalence ratio.

This report is organized as follows:

Chapter 1 presents the theoretical background of internal combustion engine operation and combustion fundamentals.

Chapter 2 defines the scope of the numerical study and outlines the simulation strategy used to analyze combustion behavior.

Chapter 3 details the two separate experimental setups used to evaluate the performance of gasoline and diesel engines, including the test conditions and measurement procedures.

Chapter 4 presents the CFD simulation of combustion within an internal combustion engine chamber using ANSYS Fluent, with particular emphasis on how the equivalence ratio affects combustion temperature.

Finally, Chapter 5 provides a discussion of the combined results, highlights key findings, and offers conclusions on the performance differences and combustion characteristics observed in both experimental and simulated contexts.

By integrating theoretical principles, practical experimentation, and advanced simulation techniques, this study aims to contribute valuable insights into the optimization of ICEs and support efforts toward cleaner and more efficient engine technologies.

Chapter 1

Fundamentals of Internal Combustion and Review of Theoretical Principles

1.1 Introduction

Internal combustion engines (ICEs) have long been the cornerstone of modern transportation and industrial applications due to their efficiency, reliability, and adaptability to various fuels. These engines operate based on the conversion of chemical energy from fuel into mechanical work through controlled combustion processes. Despite the global transition towards alternative energy systems, ICEs remain critical in engineering research, particularly in the quest for optimizing performance, reducing emissions, and enhancing fuel efficiency.

This chapter provides a comprehensive overview of internal combustion engines, including their classifications, operating principles, thermodynamic cycles, and key performance parameters. Special emphasis is placed on the combustion process, as it is central to both engine efficiency and pollutant formation. Additionally, this chapter introduces the fundamental scientific principles—thermodynamics, fluid mechanics, and chemical kinetics—that govern combustion in engines, forming the theoretical basis for the numerical and simulation work in subsequent chapters.

1.2 Thermodynamics Review

1.2.1 General Definitions

Thermodynamic State

A system is in a "thermodynamic state" if macroscopic observable properties have fixed, definite values, independent of 'how you got there'. These properties are variables of state or functions of state. Examples are volume, pressure, temperature etc. In thermal equilibrium these variables of state have no time dependence.

Functions of state can be:

- Extensive (proportional to system size) e.g., energy, volume, magnetization, mass
- Intensive (independent of system size) e.g., temperature, pressure, magnetic field, density

Total work done on a system and total heat put into a system are not functions of state - you cannot say a system has a certain amount of heat, or a certain amount of work [20].

Closed Thermodynamic System

A closed system is a type of thermodynamic system that can exchange heat with its surroundings but mass cannot be exchanged. A pressure cooker is an example of a closed system. The energy/heat can be transferred to the surroundings, but the mass within the cooker cannot be transferred.[21]

Thermodynamic Equilibrium

A system is said to be in thermodynamic equilibrium if it does not spontaneously change its state after it has been isolated.[22]

Isothermal

Transformation at constant temperature. [20]

Isentropic

Transformation at constant entropy. [20]

Isovolumetric

Transformation at constant volume. [20]

Isobaric

Transformation at constant pressure. [20]

Adiabatic

Transformation adiathermal and reversible. Put a system in thermal contact with some new surroundings. Heat flows and/or work is done. Eventually no further change takes place: the system is said to be in a state of thermal equilibrium .[20]

Adiathermal

Transformation without flow of heat. A system bounded by adiathermal walls is thermally isolated. Any work done on such a system produces an adiathermal change. Diathermal walls allow flow of heat. Two systems separated by diathermal walls are said to be in thermal contact.[20]

Entropy (S)

Entropy is a measure of the disorder of a system. Entropy also describes how much energy is not available to do work. The more disordered a system and higher the entropy, the less of a system's energy is available to do work.[23]

Enthalpy (h)

The enthalpy of a thermodynamic system is defined as the sum of its internal energy and the product of its pressure and volume: where U is the internal energy, p is pressure, and V is the volume of the system; pV is sometimes referred to as the pressure energy ϵ_p .[24]

Mole Fraction

The mole fraction x_i of the species i denotes the ratio of the mole number n_i of species i to the total mole number $n = \sum n_i$ of the mixture ($x_i = n_i/n$) .[17]

Mass Fraction

The mass m is a fundamental property of matter (units of kg in the SI system). The mass fraction w_i is the ratio of the mass m_i of the species i and the total mass $m = \sum m_i$ of the mixture ($w_i = m_i/m$).[17]

Molar Mass

The molecular weight (now outdated) The mass of one mol of species i is denoted by M_i (units of, say, g/mol). It is common practice to represent mass fractions w_i and mole fractions x_i as percentages. Simple computations may be used to confirm the following relations (1.1) and (1.2), where S stands for the number of distinct compounds [17]:

$$w_i = \frac{M_i n_i}{\sum_{j=1}^{S} M_j n_j} = \frac{M_i x_i}{\sum_{j=1}^{S} M_j x_j} \tag{1.1}$$

$$x_i = \frac{w_i}{M_i}\overline{M} = \frac{w_i/M_i}{\sum_{j=1}^{S} w_i/M_j} \tag{1.2}$$

Densities are independent of a system's size or scope. These variables are referred to as intense properties, and their definition is the system volume V divided by the equivalent extensive characteristics, which are dependent on the system's extent. Intense qualities include, for example [17]:

- **Mass density (density):** $\rho = m/V$ (in e.g., mol/m^3)
- **Molar density (concentration):** $c = n/V$ (in e.g., mol/m^3)

It follows that the mean molar mass is given by the expression (1.3) [17]:

$$\frac{\rho}{c} = \frac{m}{n} = \overline{M} \tag{1.3}$$

In chemistry, concentration c of chemical species defined in this way are usually denoted by species symbols in square brackets (e.g., $c_{H_2O} = [H_2O]$).

For gases and gas mixtures in combustion processes, an equation of state relates to the temperature, pressure, and density of the gas. For many conditions, it is satisfactory to use the Ideal gas equation $PV = nRT$.[17]

Where p denotes the pressure (in units of Pa), V the volume (in m^3), n the mole number (in mol), T the absolute temperature (in K), and R the universal gas constant ($R = 8.314\,\mathrm{J}\cdot\mathrm{mol}^{-1}\cdot\mathrm{K}^{-1}$). It follows that relation (1.4) [17]:

$$c = \frac{p}{RT} \quad \text{and} \quad \rho = \frac{p\overline{M}}{RT} = \frac{p}{RT\sum_{i=1}^{S}\frac{w_i}{M_i}} \tag{1.4}$$

The ideal gas equation of state provides an insufficient prediction of concentration or density when temperature is close to or below the critical temperature or when pressure is close to or above the critical pressure. It is more accurate to think of the system as a genuine gas.[17]

Equation of State

The equation of state relates the thermodynamic properties of the fluid, namely pressure, density (or specific volume), and temperature. For ideal gases, it is written as [17]:

$$p = \rho RT \tag{1.5}$$

Where:

- p: is the pressure,
- ρ: is the density,
- R: is the specific gas constant,
- T: is the temperature.

1.3 History of Internal Combustion Engines

The internal combustion engine (ICE) originated in theory in the 17th century but became practical in the 19th century. Lenoir built the first gas-fueled engine in 1860, and Otto's four-stroke engine in 1876 laid the groundwork for modern ICEs [25]. Diesel's 1897

compression-ignition engine marked a major efficiency improvement and became especially significant after the 1973 oil crisis, with advances like direct injection and electronic control [26].

Although turbine engines took over aviation in the 1950s, ICEs continued to advance in automobiles, becoming cleaner and more fuel-efficient. Today, they still dominate transportation, particularly in diesel variants using modern systems like common-rail injection [27].

While electric vehicles are rising, ICEs are expected to persist—especially in heavy-duty uses—due to energy density and mature infrastructure. Future developments will likely focus on hybridization and cleaner fuels.

Figure 1.1: Diesel engine of 1897.[1]

1.4 Definition of an Internal Combustion Engine

An internal combustion engine (ICE) generates mechanical work by burning fuel directly within its cylinders, distinguishing it from external combustion systems. This direct combustion allows for compactness and quick response. Most ICEs operate on a four-stroke cycle—intake, compression, combustion, and exhaust—common in automotive use for their efficiency and lower emissions. Combustion is triggered by a spark (gasoline) or compression (diesel). Piston motion is converted to rotational torque via the crankshaft.

Efficiency typically ranges from 20% to 40%, influenced by factors like compression ratio and heat loss [28].

1.5 Basic Engine Components and Nomenclature

1.5.1 Engine Components

Internal combustion engines operate through the integration of several coordinated systems that ensure efficient performance. Figure 1.2 illustrates the principal components, including the air intake system—comprising the air cleaner and carburettor—the valve train, which consists of the camshaft, rocker arms, and valves, and the power assembly, made up of the piston, connecting rod, and crankshaft. In addition, auxiliary systems such as the oil pump and timing belt play essential roles in maintaining proper lubrication and ensuring precise synchronization of engine operations.

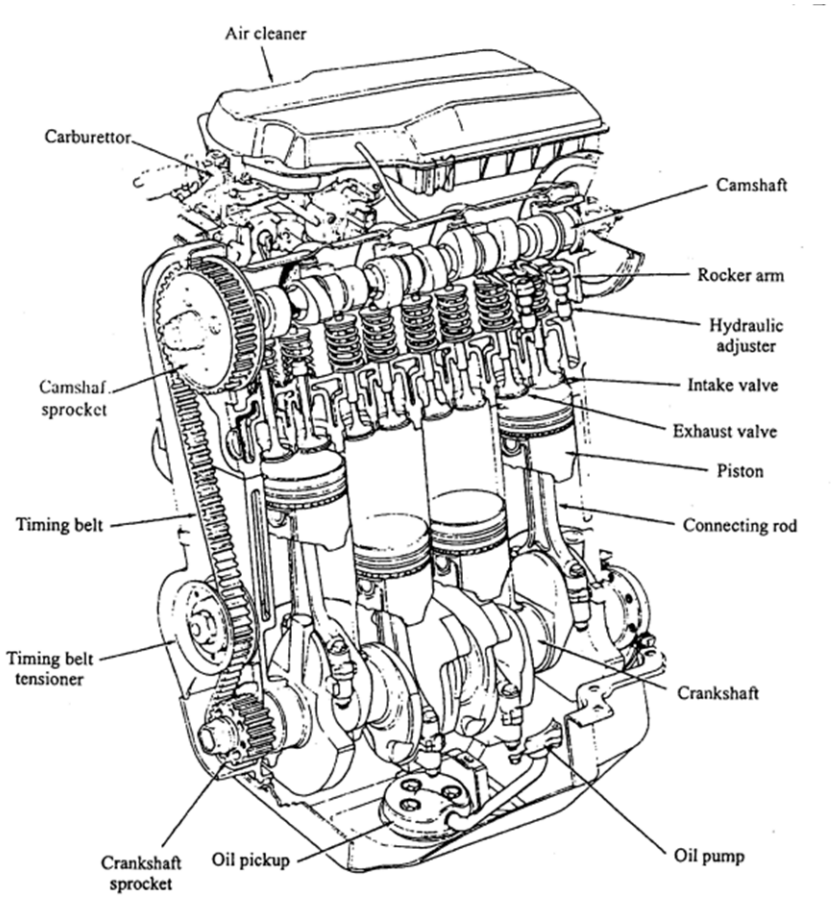

Figure 1.2: General component of ic engine. [2]

1.6 Nomenclature

In internal combustion engines, the **cylinder bore** (d) refers to the nominal inner diameter of the working cylinder, typically expressed in millimeters. The **piston area** (A) corresponds to the cross-sectional area of the cylinder bore and is given in cm^2. The **stroke** (L) is the nominal distance the piston travels between its two dead centres, also expressed in millimeters. The **stroke-to-bore ratio** (L/d) is used to classify engine types as under-square, square, or over-square, where an over-square engine ($d > L$) allows higher operating speeds. The **dead centres** mark the piston's extreme positions: **Top Dead Centre** (TDC) when it is farthest from the crankshaft and **Bottom Dead Centre** (BDC) when it is nearest. The **displacement volume** (V_s) is the volume swept by the piston during one stroke, while the **engine capacity** is the displacement volume multiplied by the number of cylinders. The **clearance volume** (V_c) is the volume above the piston at TDC, and the **compression ratio** (r) is the ratio of total cylinder volume at BDC to clearance volume. [3]

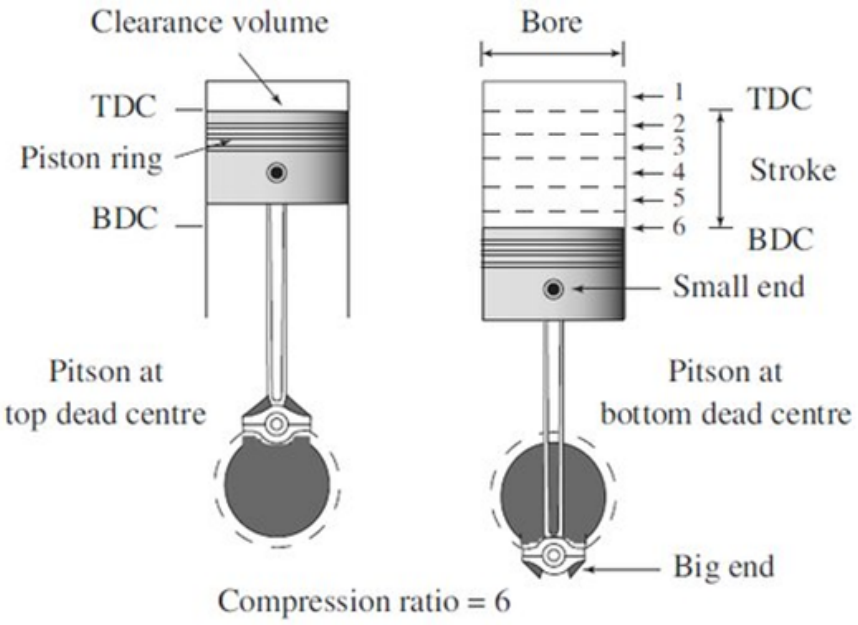

Figure 1.3: Top and bottom dead centres [3]

1.7 Classifications of Internal Combustion Engines

IC engines can be classified based on the number of strokes, type of fuel consumed and arrangement of engine cylinders. An insight into this classification of the IC engine is enumerated below [29]:

1.7.1 Based on Number of Strokes

Two-stroke Engine

A two-stroke engine is an internal combustion engine that completes a power cycle with two strokes of the piston, making it simpler but less fuel-efficient compared to its counterpart, the four-stroke engine. Two-stroke engines are commonly found in small power tools, scooters, and some motorcycles. They have a simpler design compared to four-stroke engines and complete a power cycle in two strokes of the piston. [29]

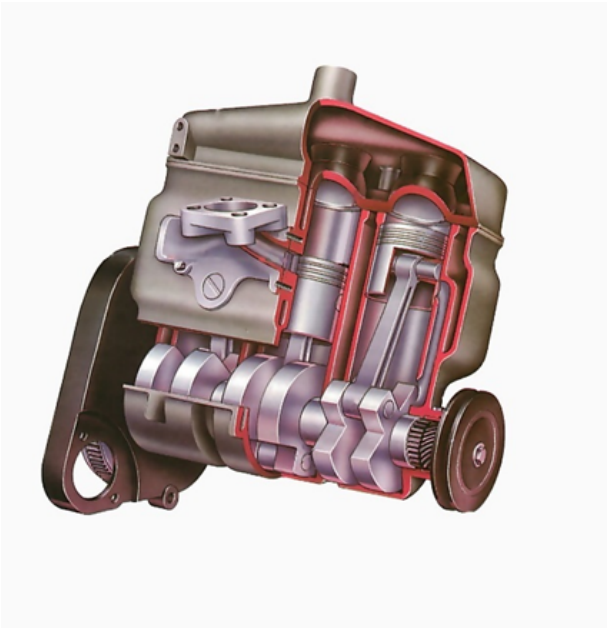

Figure 1.4: Two-stroke engine. [4]

Four-stroke Engine

A four-stroke engine is a type of internal combustion engine that completes four distinct phases in one complete cycle: intake, compression, power, and exhaust. It is commonly used in cars, motorcycles, and other vehicles. These engines have a more complicated

design compared to the Two-stroke engines. [29]

Figure 1.5: Four-stroke engine. [5]

Comparison of Four and Two-Stroke Cycle Engines

Table 1.1: Comparison Between Two-Stroke and Four-Stroke Engines. [3]

Two-Stroke Engine	**Four-Stroke Engine**
Power stroke every revolution of the crankshaft.	Power stroke every two revolutions of the crankshaft.
More uniform turning moment; lighter flywheel.	Less uniform turning moment; heavier flywheel.
Higher power for the same engine size; compact and light.	Lower power for the same engine size; heavier and bulkier.
Greater cooling and lubrication needs; more wear and tear.	Less cooling and lubrication needed; lower wear.
No valves, only ports (some use reed or exhaust valves).	Uses valves with actuating mechanism for intake/exhaust.
Lightweight and simpler; lower initial cost.	Heavier and complex; higher initial cost.
Lower volumetric and thermal efficiency.	Higher volumetric and thermal efficiency.
Used in low-cost, light applications (scooters, mopeds).	Used in high-efficiency applications (cars, buses, planes).

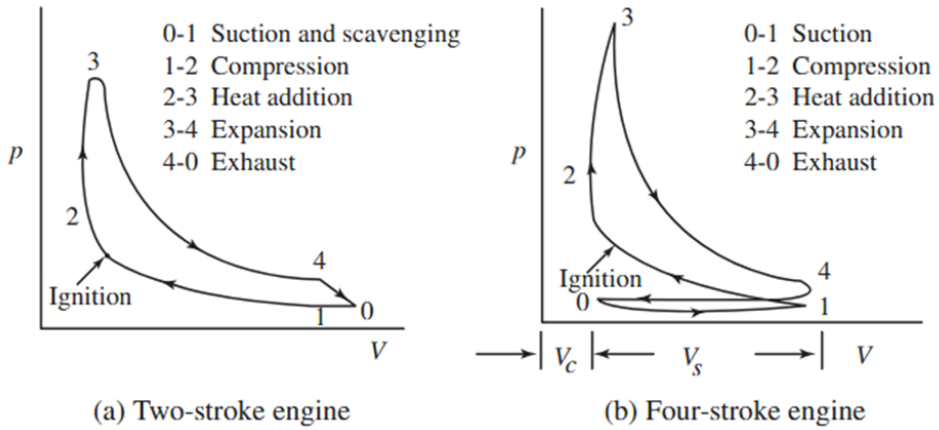

(a) Two-stroke engine (b) Four-stroke engine

Figure 1.6: Actual p-V diagrams. [3]

1.7.2 Based on Injection System

Direct Injection

Direct injection (DI) is a fuel system that delivers fuel straight into the engine's combustion chamber, eliminating pre-chamber air-fuel mixing. Compared to indirect injection (IDI) engines, DI engines typically use lower compression ratios (15:1 to 18:1), feature flat-faced cylinder heads, and are usually turbocharged. Although IDI engines reach peak torque at lower RPMs, DI engines generally produce significantly more torque overall.[6]

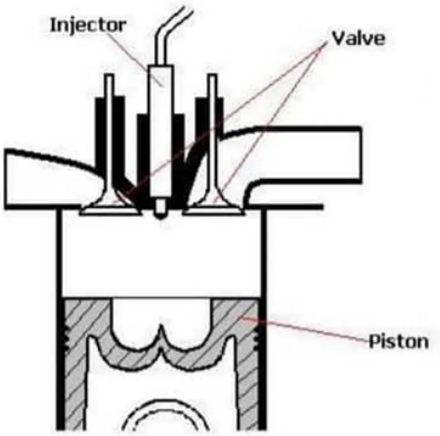

Figure 1.7: Direct injection. [6]

Indirect Injection

Indirect injection (IDI) systems inject fuel into a pre-chamber connected to the main combustion chamber, promoting mixing before ignition. IDI diesel engines usually have high compression ratios (over 20:1), distinct cylinder heads with integrated pre-chambers, and are often naturally aspirated rather than turbocharged. While they generate peak torque at low RPMs, their maximum horsepower tends to occur at higher engine speeds compared to direct injection (DI) engines.[6]

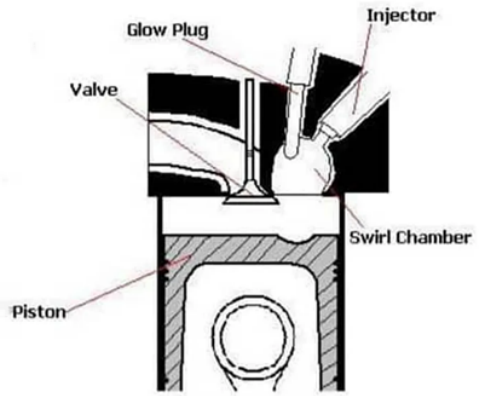

Figure 1.8: Indirect Injection. [6]

1.7.3 Based on Fuel Type

Diesel Engine (Spark-Ignition Engine (SI))

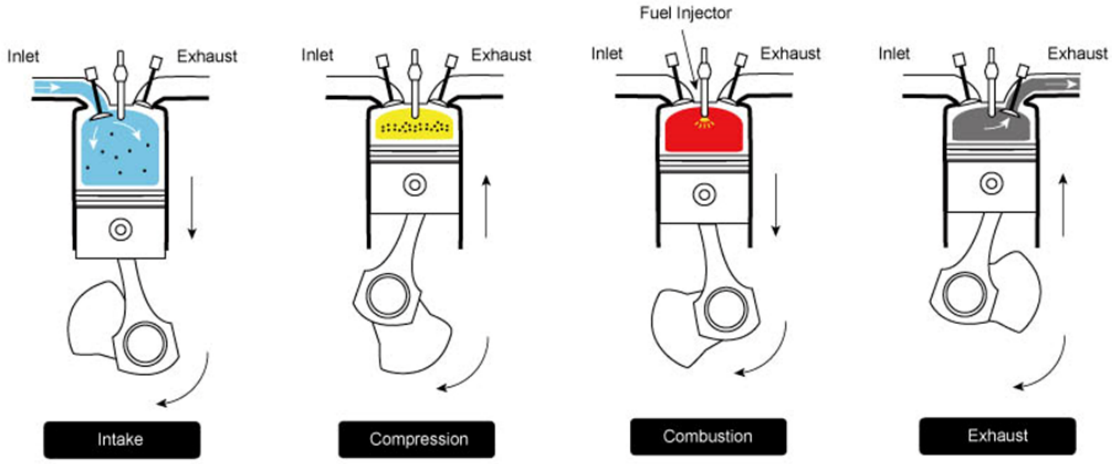

Figure 1.9: Operating principle of Diesel Engine. [7]

Diesel engines operate on the principle of compression ignition, distinguishing them from gasoline engines, which rely on spark ignition. In a diesel engine, air is compressed at high pressure, reaching temperatures high enough for the fuel to ignite spontaneously when injected. This process largely depends on compressed air, which facilitates efficient and uniform combustion.

The cycle of four stroke engines consists of four main phases [30]:

- **Intake:** The intake valve opens, and the piston moves down, allowing the entry of

compressed air without fuel mixture.

- **Compression:** The intake valve closes, and the piston moves up, compressing the air until its temperature is high enough to ignite the diesel. The use of compressed air at this stage is crucial for improving the engine's thermal efficiency.
- **Power Stroke (Combustion):** At the peak of compression, the injection system sprays diesel fuel into the chamber. The mixture ignites instantly due to the heat generated by compression, causing a controlled explosion that pushes the piston downward and generates mechanical power.
- **Exhaust:** The piston moves back up, opening the exhaust valve to expel combustion gases from the cylinder. In some modern systems, compressed air is used in this phase to improve gas evacuation and reduce resistance in the engine cycle.

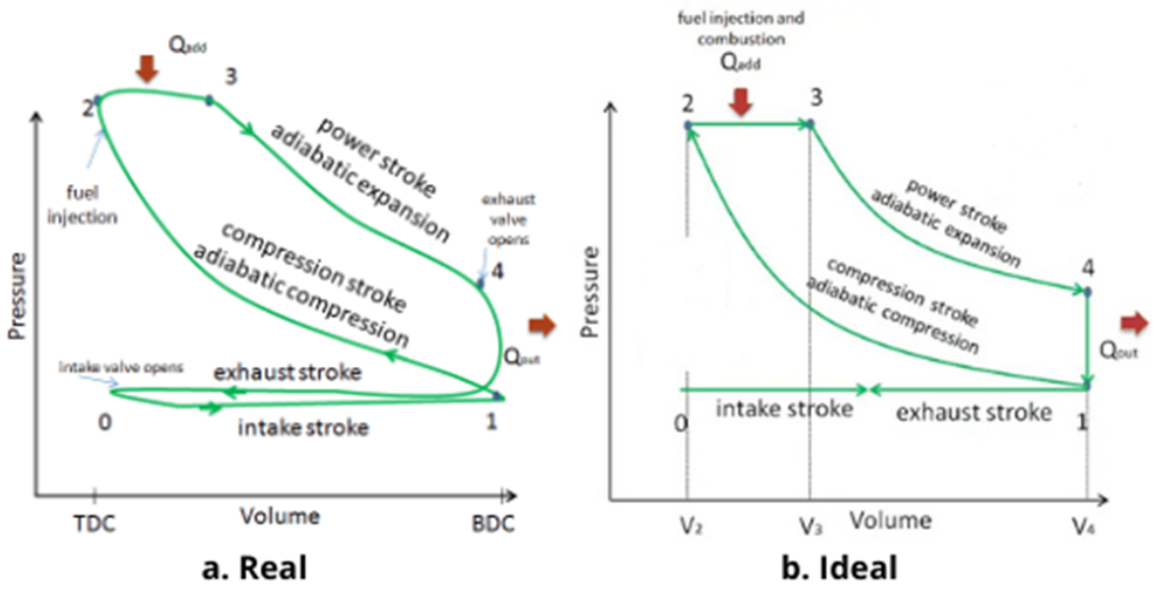

Figure 1.10: Ideal and real diesel cycle. [8]

Gasoline Engine (Compression-Ignition Engine (CI))

The kinetic energy is generated by burning the gasoline in the cylinder, which drives the crank connecting rod mechanism connected to the piston to make a reciprocating circular motion around the crankshaft to output power. [31]

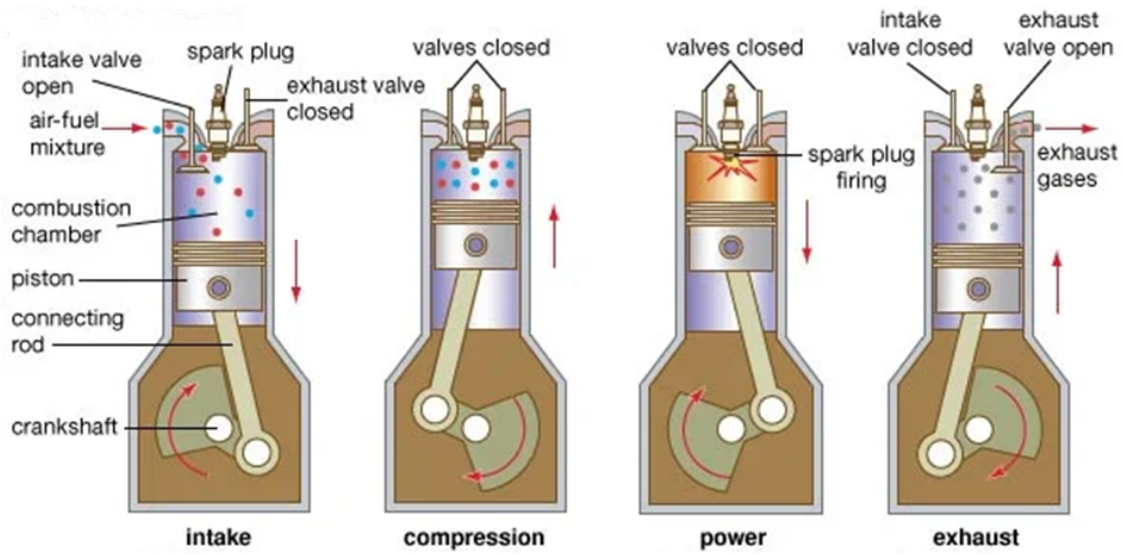

Figure 1.11: Operating principle of gasoline engine. [9]

A four-stroke engine is composed of four strokes (strokes) of intake, compression, work, and exhaust.

- The intake stroke piston is driven by the crankshaft to move from top dead center to bottom top dead center. At the same time, the intake valve opens and the exhaust valve closes. When the piston moves from the top dead center to the bottom dead center, the volume above the piston increases, the gas pressure in the cylinder decreases, and a certain degree of vacuum is formed. As the intake valve opens, the cylinder communicates with the intake pipe, and the mixture is sucked into the cylinder. When the piston moves to the bottom dead center, the cylinder is filled with fresh mixed gas.

- The compression stroke piston moves from the bottom dead center to the top dead center, and the intake and exhaust valves are closed. The crankshaft is driven to rotate under the action of inertial force such as the flywheel, and the piston is pushed upward through the connecting rod. The gas volume in the cylinder gradually decreases, the gas is compressed, and the pressure and temperature of the mixed gas in the cylinder increase.

- At this time of the work stroke, the intake and exhaust valves are closed at the same time, the spark plug is ignited, and the mixed gas is violently burned. The temperature and pressure in the cylinder rise sharply. The high temperature and

high-pressure gas push the piston down and drives the crankshaft to rotate through the connecting rod. In the four strokes of the engine, only this stroke can realize the conversion of heat energy into mechanical energy.

- Exhaust strokes the exhaust valve opens, the piston moves from the bottom dead center to top dead center, and exhaust gas is discharged from the cylinder along with the upward movement of the piston. Because the exhaust system has resistance and the combustion chamber also occupies a certain volume, it is impossible to exhaust the exhaust gas at the end of the exhaust gas. This part of the remaining exhaust gas is called the residual exhaust gas. Residual exhaust gas not only affects the intake of air but also has an adverse effect on combustion. At the end of the exhaust stroke, the piston returns to the top dead center.

This completes a work cycle. Subsequently, the crankshaft continues to rotate depending on the inertia of the flywheel, and the next cycle begins. After repeating this cycle, the engine keeps running. [31]

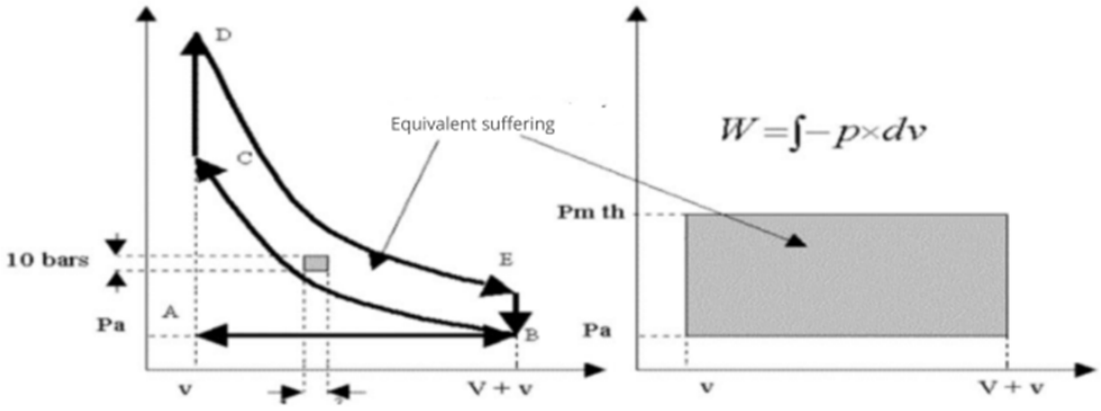

Figure 1.12: Example of (P,V) Diagrams for an ICE. [1]

Comparison Between Diesel and Gasoline Engines

Table 1.2: Difference Between gasoline and Diesel Engine. [18]

Diesel Engine	**Gasoline Engine**
These engines work on the diesel cycle	Works on the Otto cycle
The fuel is mixed with air inside the cylinder	Air and fuel are mixed in a carburetor
Ignition is achieved with the help of the hot, compressed air.	Fuel is ignited with an electric spark
High compression ratio	Relatively low compression ratio
High power production	Relatively low amounts of power are produced in a gasoline engine
These engines work with fuels that have low volatilities	Highly volatile fuels are used in these internal combustion engines
Generally used in heavy vehicles such as trucks and buses	Used in light vehicles such as motorcycles and cars.
Relatively low fuel consumption	High fuel consumption.
High initial and maintenance costs	Comparatively low initial cost and maintenance cost

1.8 Combustion

Combustion is a chemical reaction in which certain elements of the fuel like hydrogen and carbon combine with oxygen liberating heat energy and causing an increase in temperature of the gases. The conditions necessary for combustion are the presence of combustible mixture and some means of initiating the process. The theory of combustion is a very complex subject and has been a topic of intensive research for many years. In spite of this, not much knowledge is available concerning the phenomenon of combustion. [3]

1.8.1 Chemical Kinetics Concept

Combustion is a rapid chemical reaction accompanied by light emission and massive release of heat, following the general scheme [19]:

Fuel + Oxidizer → Combustion Products + Heat

The chemical process is [19]:

- Molecular bond breaking/formation as elementary reactions
- Reaction mechanisms involving hundreds of species and thousands of elementary reactions
- Final state controlled by chemical equilibrium laws

For hydrocarbon combustion in air (stoichiometric) [19]:

$$C_nH_m + (n + m/4)(O_2 + 3.76N_2) \rightarrow nCO_2 + m/2H_2O + 3.76(n + m/4)N_2 \quad (1.6)$$

1.8.2 Combustion Chemistry

Combustion features[19]:

- Rapid exothermic reaction with flame formation
- Heat release calculation:

$$Q_{comb} = m_f \times LHV \quad (1.7)$$

  Where:

  - m_f: Fuel mass per cycle (kg)
  - LHV: Lower Heating Value (kJ/kg).

Classification of Different Combustion Varieties

Inflammation processes (i.e., the initiation of combustion) must be separated from the flame propagation process[27]:

- The inflammation process requires an external energy input:
  - Heating the walls of the reactor containing the mixture

  - Adiabatic compression of the mixture by a shock wave or a reduction in volume
  - Creation of a plasma between two electrodes
- The flame propagation process occurs without external intervention in the system
  - Successive layers of the combustible mixture ignite using the energy released by the combustion of the previous layers.

Different Forms of Combustion

Homogeneous: The oxidizer and fuel are pre-mixed in a given ratio. Heterogeneous: Combustion occurs at the boundary between the oxidizer and fuel. The oxidizer and fuel can both be, or one can be, solid, liquid, or gaseous. Stratified: The oxidizer and fuel are pre-mixed in a variable ratio ranging from a value allowing ignition to a ratio representing pure oxidizer presence.[19]

Table 1.3: Different forms of combustion. [19]

Type	**Characteristics**	**Examples**
Homogeneous	Premixed fuel/oxidizer	Spark-ignition engines
Heterogeneous	Reaction at fuel-oxidizer interface	Diesel combustion
Stratified	Variable mixture ratio	Lean-burn engines

The Distribution Between Physical and Chemical Time

- **Physical time:** the ratio of the square of the characteristic length of the system and of the diffusion coefficient
- **Chemical time:** time required to consume half of the reagents. [32]

Combustion in Homogeneous Medium

- **Slow Combustion:** A managed oxidation procedure that begins at the point of ignition where the rate of energy release is equal to the rate of heat transfer out of the reaction zone and thermal equilibrium is maintained.

- **Deflagration:** An ignition event, that develops into a self-sustaining "combustion wave" where the rate of heat generation is greater than the rate of heat transfer, can propagate pseudo-sub-sonically via thermal diffusion (i.e., laminar regime) or via turbulent mixing, and has a stable combustion front that can continually propagate irrespective of the ignition source.
- **Detonation:** An ignition sequence that develops into a supersonic combustion wave accompanied by a shock front, where the heat and pressure produced by the incident shock wave ignites the combustible mixture resulting in a combustion reaction zone which propagates at Chapman-Jouguet velocity. Following ignition, the flame front is kinetically coupled to the leading shock front. [27]

1.9 Fire Triangle

The fire triangle is a model for understanding the necessary components for most fires: heat, fuel, and oxygen. Each element plays a crucial role in the ignition and propagation of a fire.[33]

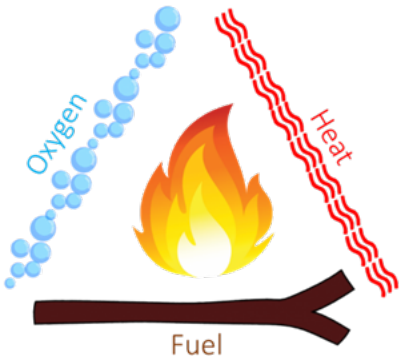

Figure 1.13: Fire triangle. [10]

- **Heat:** is the ignition source that raises a material's temperature to its combustion point. It can originate from sparks, flames, or friction. Once ignition occurs, the fire produces its own heat, sustaining the burning process. Cooling, typically with water or fire suppressants, is a primary method of extinguishing fires.[33]
- **Fuel:** refers to any combustible substance—solid, liquid, or gas—such as wood,

paper, gasoline, or natural gas. The fire's intensity and spread depend on the type and quantity of fuel. Removing or isolating the fuel source is a common firefighting technique.[33]

- **Oxygen:** is vital for sustaining combustion. Atmospheric oxygen is usually sufficient, but reducing or eliminating its availability—via smothering (e.g., fire blankets) or using suppression systems—can effectively extinguish a fire. [33]

1.10 Flame

1.10.1 Flame Definition

A flame is the visible part of a fire. It gives light and heat. It is the result of an exothermic reaction. The color and temperature of a flame depend on the type of fuel that is used to make the fire. A blue or white flame is often very hot, while a red, orange, or yellow flame is less hot. [34]

1.10.2 Classification of Flame Types

- **Diffusion flame:** A flame in which the initially separated fuel and oxidant are diffused into each other during combustion.[11]
- **Premix flame:** (premixed flame, deflagrating flame) A flame where fuel and oxidizer are mixed before combustion. [11]

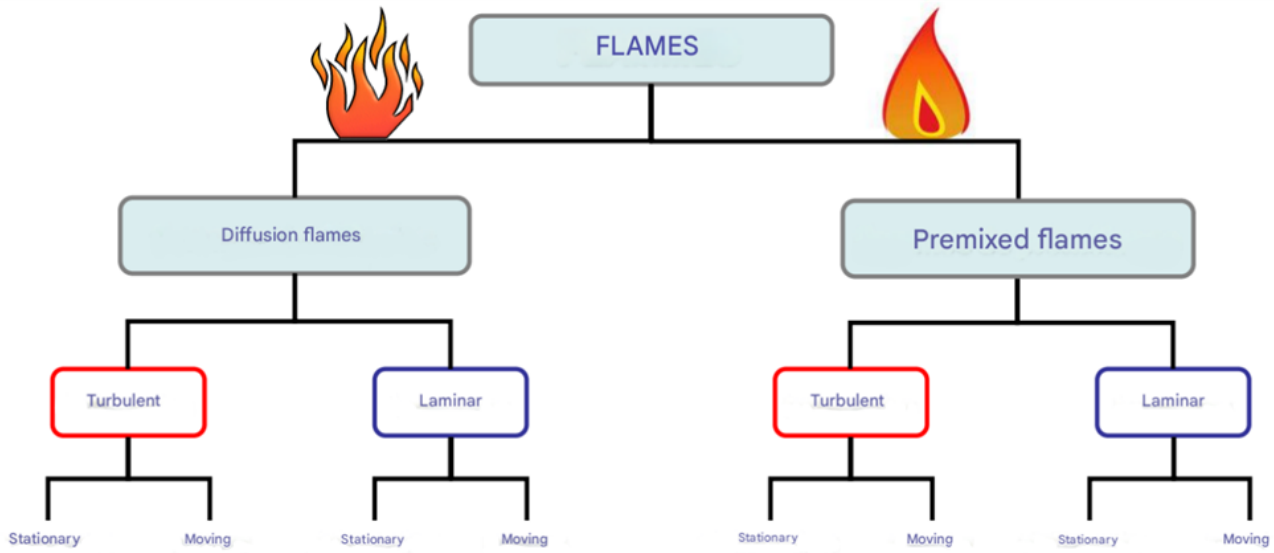

Figure 1.14: Proposed Classification of Flame Types. [11]

Flow

Movement of fluid under the action of external forces. The flow has two types [11]:

- **Laminar flow:** An orderly and predictable flow characterized by regular and linear velocities of fluid layers.
- **Turbulent flow:** A disorderly flow characterized by velocity fluctuations and mixing of fluid layers.

1.11 Emission Formation in IC Engines

The emissions of internal combustion engines (ICE), used for transportation and industry, are a major environmental problem. The rising curve in the number of vehicles since the mid-20th century, resulting from rising energy demands and better standards of living, has led to heightened use of fossil fuels and air pollution. The principal pollutants from IC engines are hydrocarbons (HC), carbon monoxide (CO), nitrogen oxides (NOx), particulate matter (PM), carbon dioxide (CO), and water vapor (HO). HC and CO result from incomplete combustion, while NOx is formed under high temperature. PM consists of fine carbon particles, and CO, though less hazardous, is involved in global warming. Secondary pollutants like ground-level ozone (O) are formed when primary emissions react with atmospheric compounds and pose threats in the way of respiratory disease and

environmental damage. They are due to reasons like inefficient burning, fuel evaporation, and lack of oxygen, making them a problem of critical concern for scientists and policymakers aiming to look for sustainable measures. [12]

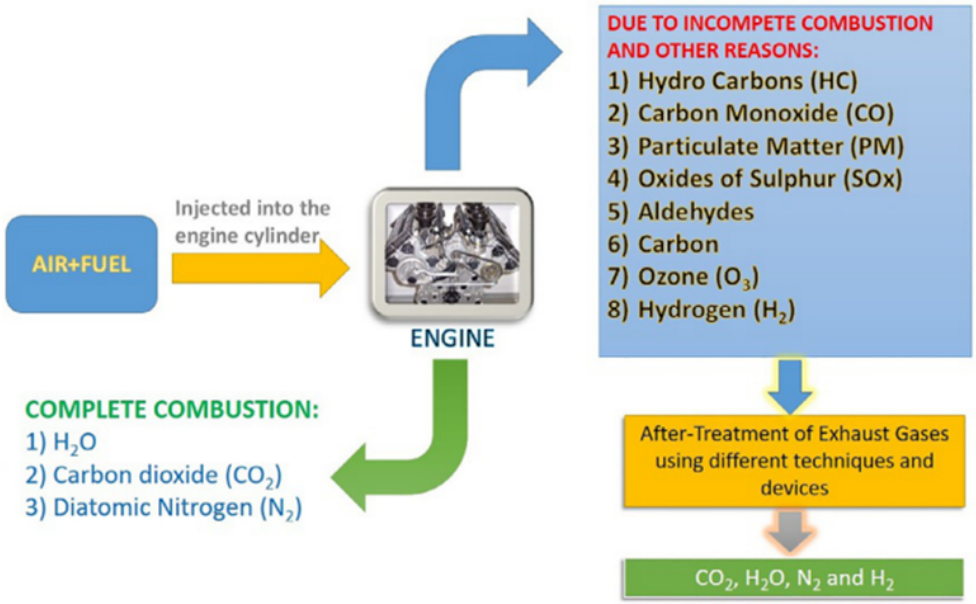

Figure 1.15: Emissions resulting from complete and incomplete burning. [12]

Table 1.4: Pollutants formed in IC engines and their characteristics. [12]

Type of pollutant	**Characteristics of pollutant**
Particulate matter	Tiny particles with diameters less than 2.5 µm that primarily contain carbon.
Hydrocarbons	Compounds containing carbon and hydrogen atoms.
Carbon dioxide	Odorless at low concentrations but exhibits acidic color at high concentrations. Contains a carbon atom bonded to two oxygen atoms.
Carbon monoxide	Contains each atom of carbon and oxygen with bond length of 112.8 pm. It is a colorless, tasteless, and odorless gas.

Table 1.4 Pollutants formed in IC engines and their characteristics. [12]

Type of pollutant	**Characteristics of pollutant**
Oxides of nitrogen emissions (NO and NO_2)	NO is a colorless, flammable gas having little odor. NO has one unpaired electron (free radical). NO_2 is a nonflammable gas but poisonous and has a deep orange-red color.
Sulfur oxides (SO_2) and Lead oxides (PbO_2)	SO_2 is colorless, toxic, and has a suffocating odor. Furthermore, SO_2 leads to the formation of sulfuric acid and results in acid rain. PbO_2 is dark brown in color, nonflammable, and insoluble in water.
Ozone (O_3)	Ozone (O_3) is bluish in color and a strong oxidizer with good solubility. Ozone can be explosive if its concentration exceeds 20% in a mixture.
Aldehydes and ketones	They are organic compounds that are soluble in water, but their solubility decreases with an increase in carbon length. With an increase in molecular weight, their boiling point increases.

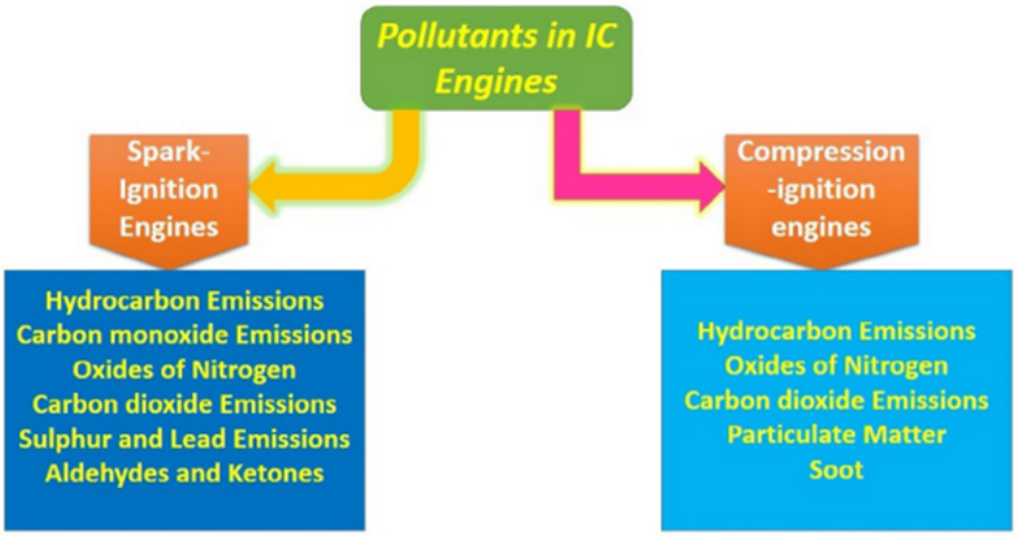

Figure 1.16: Pollutants Formed in Spark-Ignition and Compression-Ignition Engines. [12]

1.12 State of the Art

Table 1.5: People Studies: A Comprehensive Overview of Research and Methodologies.

Reference	**Objective**
[35]	Evlampiev's Numerical Combustion Modeling for Complex Reaction Systems (2007) introduces advanced computational tools, including the TROT program (C++) and the C-MECH format, for simulating combustion in Diesel engines. The study examines high-pressure effects on auto-ignition and NO formation, comparing real gas models (e.g., Redlich-Kwong) with ideal gas assumptions. It also presents a validated laminar flame let model for counter flow diffusion flames and analyzes soot formation under different mixing conditions. Applied to turbulent combustion cases like the Sandia Flame D, this work provides key insights for optimizing engine performance and reducing emissions.
[36]	This study investigates the numerical simulation of methane (CH) combustion in combustion chambers of varying sizes (lengths of 0.5 m, 1 m, and 1.5 m). The primary objective is to analyze the influence of chamber geometry and flow conditions on combustion efficiency and pollutant emissions, particularly carbon dioxide (CO) and nitrogen oxides (NOx) .

Table 1.5 – People Studies: A Comprehensive Overview of Research and Methodologies.

Reference	**Objective**
[37]	This study analyzes the performance and emissions of an unmodified internal combustion engine running on gasoline and gasoline/n-butanol blends at speeds of 2600-3400 r/min. While n-butanol blends slightly reduce torque, power, volumetric efficiency, exhaust temperature, and in-cylinder pressure due to their leaning effect, they significantly lower CO, CO, and unburned hydrocarbon (UHC) emissions thanks to n-butanol's oxygen content improving combustion. The results show that engine speed has a greater influence on emissions than fuel blend ratio, emphasizing the role of operating conditions. The findings suggest n-butanol can effectively reduce emissions without requiring engine modifications.
[38]	This study examines a DI diesel engine running on bio diesel/diesel blends from soybean oil without engine modifications. Results show bio diesel blends have slightly higher fuel consumption (BSFC) and lower thermal efficiency (BTE) than pure diesel, but significantly reduce CO and smoke emissions—especially at high loads—while HC levels stay similar. NOx emissions increase marginally due to better combustion. Combustion analysis confirms bio diesel behaves similarly to diesel, making it a viable drop-in alternative. The findings suggest soybean bio diesel can partially replace diesel in existing engines, reducing emissions with only minor performance impacts .

Thesis Objectives

This final-year project aims to conduct an in-depth study on the influence of combustion conditions on the performance and emissions of internal combustion engines, with a particular focus on diesel and gasoline engines. A combined **experimental and numerical approach** was employed. The main objectives of the work are as follows:

- To analyze combustion behavior under varying operating conditions (e.g., air–fuel ratio, temperature, equivalence ratio).
- To study the effects of these parameters on thermal efficiency, specific fuel consumption, and pollutant formation (NOx, CO, unburned hydrocarbons).
- To perform a **numerical simulation** of the combustion process using **ANSYS Fluent**, focusing on methane–air combustion modeling.
- To implement a **thermodynamic model** based on chemical equilibrium (Gibbs law) in order to calculate:
  - Adiabatic flame temperatures,
  - Molar fractions of combustion products.
- To apply advanced **numerical methods** such as the Newton-Raphson method, Gaussian elimination, and the bisection method to solve nonlinear systems related to combustion equilibrium.
- To conduct **experimental tests** on real engine test benches:
  - A diesel engine at Blida 1 University,
  - A gasoline engine at Boumerdès University.
- To collect and analyze key performance parameters, including:
  - Torque, effective power,
  - Hourly and specific fuel consumption,
  - Exhaust gas temperature, air/fuel ratio, and thermal efficiency.
- To **validate** the numerical simulation results using data obtained from experimental measurements.
- To **compare** the performance, efficiency, and emission profiles of diesel and gasoline engines under different operating conditions.
- To contribute to the advancement of **cleaner and more energy-efficient combustion technologies** through the integration of theoretical, numerical, and experimental tools.

1.13 Conclusion

This chapter has laid a comprehensive theoretical foundation for understanding internal combustion engines (ICEs), emphasizing key thermodynamic principles, combustion mechanisms, and the classification and operation of both diesel and gasoline engines. Through detailed coverage of concepts such as thermodynamic cycles, chemical kinetics, flame characteristics, and pollutant formation, it becomes evident how combustion plays a pivotal role in engine performance and emissions. Furthermore, the discussion of emission sources and control highlights the growing environmental concerns that shape current research directions.

By reviewing the state of the art, we have identified the scientific and technological gaps that modern studies aim to fill—particularly through advanced combustion modes and numerical simulation techniques designed to enhance efficiency and reduce emissions. This foundational knowledge provides the essential background for the next chapter, which will develop a detailed theoretical and mathematical framework for analyzing combustion. Specifically, Chapter 2 will introduce the parameters, stoichiometry, and computational tools needed to characterize reactive flows, forming the basis for the numerical and experimental studies that follow.

Chapter 2

Effects of preheating temperature and fuel-air equivalence ratio on pollution control in hydrocarbon combustion

2.1 Introduction

Combustion is a complex chemical process involving the reaction of fuel and oxidizer to produce heat and combustion products. Understanding this process requires a detailed analysis of key parameters such as mass fractions, mole fractions, mixture equivalence ratio, and adiabatic flame temperature. These factors influence combustion efficiency, pollutant formation, and energy release, making them essential for optimizing combustion systems in real-world applications. This chapter presents a rigorous theoretical framework for combustion analysis, covering stoichiometry, dissociation effects, and numerical methods for calculating combustion properties. The discussion includes fundamental definitions, thermodynamic principles, and equilibrium conditions, supported by mathematical formulations and computational techniques. A significant focus is placed on numerical methods, particularly the Newton-Raphson and Gaussian elimination methods, which are employed to solve nonlinear and linear systems of equations, respectively. Additionally, the chapter highlights the use of Futron, a specialized program for combustion analysis, which facilitates the computation of species concentrations, flame temperatures, and other critical combustion parameters. By integrating theoretical concepts with computational

tools, this chapter provides a comprehensive foundation for analyzing reactive flows, optimizing combustion efficiency, and minimizing emissions. The systematic approach ensures clarity and precision, making it a valuable resource for researchers and engineers in the field of combustion science.

2.2 Basic definition

In a chemically reactive flow, it is necessary to define in addition to classical state variables (pressure, temperature, velocity) variables characterizing the medium's composition. [39]

2.2.1 Fundamental Quantities

To characterize the composition of a reactive mixture, each chemical substance is assigned an index "j". The mass of species "j" is then defined as [39]:

$$m_j = n_j M_j \tag{2.1}$$

M_j represents the molar mass and n_j denotes the number of moles. The total mass m_t of the mixture is consequently given by [39]:

$$m_t = \sum_{j=1}^{N} m_j \tag{2.2}$$

N represents the total number of species constituting the mass m_t. Similarly, the total number of moles N_t is given by [39]:

$$N_t = \sum_{j=1}^{N} n_j \tag{2.3}$$

This definition yields the expression for the mixture of molar mass [39]:

$$M = \frac{1}{N_t} \sum_{j=1}^{N} n_j M_j \tag{2.4}$$

The relative quantity of species j in the mixture is given either by the mole fraction (2.5) or by the mass fraction (2.6) [39]:

$$X_j = \frac{n_j}{N_t} \tag{2.5}$$

$$Y_j = \frac{m_j}{m_t} \tag{2.6}$$

The two relations (2.5) and (2.6) automatically satisfy expression (2.7):

$$\sum_{j=1}^{N} X_j = \sum_{j=1}^{N} Y_j = 1 \tag{2.7}$$

The conversion between these parameters is achieved through the following relation [39]:

$$Y_j = \frac{M_j}{M} X_j \tag{2.8}$$

Chemists preferentially employ molar concentration, which expresses composition relative to volume [39]:

$$C_j = \frac{n_j}{V_t} \tag{2.9}$$

Alternatively, the mass density can be expressed as [39]:

$$\rho_j = \frac{m_j}{V_t} \tag{2.10}$$

V_t represents the total mixture volume. The global molar concentration C and total mass density r are derived from the preceding relations as follows [39]:

$$C = \sum_{j=1}^{N} C_j \tag{2.11}$$

$$\rho = \sum_{j=1}^{N} \rho_j \tag{2.12}$$

2.2.2 Equivalence Ratio

To describe combustion energy, take the following example: the oxidation of methane with oxygen. Methane, a hydrocarbon with the formula CH_4, in full combustion with oxygen (O_2) produces carbon dioxide (CO_2) and water vapor (H_2O) as significant gaseous products. The stoichiometric burning reaction can be expressed as [39]:

$$\mathrm{CH_4 + 2O_2 \rightarrow CO_2 + 2H_2O} \tag{2.13}$$

By adopting the following molar masses: M_o=16, M_c=12.01, M_H=1.008, M_N=14.001, Reaction (2.13) indicates that the complete combustion of one gram of methane requires a mass of oxygen equal to 3.989 g.[39]

When combustion occurs in air, it must be noted that air contains 21% oxygen (O_2) by volume or 23% by mass, with the remainder being essentially nitrogen (N_2), which does not participate in the reaction.[39]

In this context, an "air molecule" can be represented by the fictitious pair($O_{0.42}$, $N_{1.58}$), allowing the chemical reaction of methane with air to be written as [39]:

$$\mathrm{CH_4 + 2(O_2 + \beta N_2) \rightarrow CO_2 + 2H_2O + 2\beta N_2} \tag{2.14}$$

Where:

$\beta = 3,76$

The knowledge of the mass flow rate of fuel $\dot{m}_f$ and oxidizer $\dot{m}_a$ allows us to define the mixture equivalence ratio (ϕ) [39]:

$$\Phi = \frac{\alpha}{\alpha_s} = \frac{\left(\frac{\dot{m}_f}{\dot{m}_a}\right)}{\left(\frac{\dot{m}_f}{\dot{m}_a}\right)_s} \tag{2.15}$$

In this expression, the subscript "s" corresponds to stoichiometric conditions. That is, we assume complete combustion of methane occurs according to reaction (2.14). In this case, the stoichiometric mixture equivalence ratio (ϕ_s) is given by [39]:

$$\alpha_s = \left(\frac{\dot{m}_f}{\dot{m}_a}\right)_s = \frac{M_f}{2M_a(1+\beta)} = 0.0526 \tag{2.16}$$

where:

M_f and M_a correspond to the molar masses of methane and air, respectively.

If the mixture equivalence ratio equals 1, the mixture is said to be stoichiometric. Conversely, if the equivalence ratio is less than 1, the mixture is fuel-lean, while if it exceeds 1, the mixture is fuel-rich. For air-based combustion systems, fuel-lean mixtures are typically employed, as this represents the only practical approach to achieving complete combustion since perfect homogeneity of the (fuel, oxidizer) mixture can never be attained. It is evident that the final combustion temperature reaches it's maximum when combustion is complete and the gases are least diluted - that is, for a homogeneous mixture with a equivalence ratio of exactly 1. [39]

2.2.3 The Dissociation

At high temperatures, the primary combustion products decompose or dissociate into other species. For example, complete combustion of hydrocarbons with air yields CO_2, H_2O, N_2 (and O_2 in lean combustion) as products. However, dissociation of these products and reactions between the resulting species can produce many other compounds, such as O, H, OH, N, NO, and others. The major dissociation reactions are: (2.32), (2.33), (2.34), (2.35), (2.36), (2.37), (2.38).

Molecular dissociation occurs at elevated temperatures when and only when a significant number of molecules possess sufficient kinetic energy during collisions to break one or more internal bonds. At typical combustion temperatures, dissociation primarily affects CO_2 and H_2O, though other species are also impacted at higher temperatures. The presence of CO and H_2 in the products indicates incomplete oxidation, and consequently, the final temperature is lower than the adiabatic flame temperature calculated for complete combustion products. [39]

2.3 Hypotheses

We describe the procedures used to determine the final combustion temperature and molar fractions of combustion products for a hydrocarbon-air mixture, based on the following assumptions:

- All gaseous species behave as ideal gases.
- Air composition: 79% N_2 and 21% O_2 (by volume).
- Adiabatic, isobaric combustion process.
- The thermodynamic equilibrium is achieved post-combustion.
- Flow Mach number is sufficiently small that kinetic energy and viscous dissipation are negligible.
- Both premixed and non-premixed (diffusion) flames are considered. This assumption depends on reactant introduction into the combustion zone, which is a key parameter controlling the combustion regime. Fuel and oxidizer may be premixed before reaction occurs (premixed flame) or they may enter the reaction zone separately (non-premixed/diffusion flame).

2.4 Calculation of the Final Combustion State

The global combustion equation is[40]:

$$rc\,C_nH_m + \left(n + \frac{m}{4}\right)(O_2 + 3.76\,N_2) \rightarrow n_1CO_2 + n_2H_2O + n_3O_2 + n_4N_2 + n_5NO + n_6OH + n_7CO + n_8H_2 + n_9O + n_{10}H + n_{11}N \tag{2.17}$$

According to the First Principle of Thermodynamics, we have:

For an open system [40]:

$$W + Q = \Delta H \tag{2.18}$$

Since the combustion is isobaric, no work will be produced: W=0

And since the process is adiabatic: so Q=0

Give as this:

$$\Delta H = 0 \tag{2.19}$$

or:

$$H_r(T_e) = H_P(T_{ad}) \tag{2.20}$$

or:

$$f(T) = H_P(T_{ad}) - H_r(T_i) = 0 \tag{2.21}$$

This constitutes the fundamental relation. By solving this equation, we can determine T_{ad}, the final adiabatic combustion temperature. [40]

2.4.1 Calculation of Reactants Enthalpy

$$Hr = r_c(H_{RC}) + (n + \frac{m}{4})H_a \tag{2.22}$$

Fuel Enthalpy H_{Rc}

There are two methods [40]:

a) Using hydrocarbons enthalpy of formation:

$$H_{RC} = \Delta H_F^0 + H_C^S(T) \tag{2.23}$$

$$H_C^S(T) = \frac{0.403\,T + 0.000405\,T^2}{\sqrt{0.9952\,d_4^{20} + 0.00806}}\,(12n + m) \quad \text{[cal/mole]} \tag{2.24}$$

Where:

ΔH_F^0 is the enthalpy of hydrocarbon formation, given by standard Enthalpy tables.

$H_C^S(T)$ is the sensible enthalpy variation.

b) Using the comprehensive formula derived from integrating Cp with respect to T:

$$\frac{Cp(T)}{R} = a_1T^{-2} + a_2T^{-1} + a_3 + a_4T + a_5T^2 + a_6T^3 + a_7T^4 \tag{2.25}$$

Will give us:

$$H(T) = \big(- a_1T^{-2} + \frac{a_2 \ln T}{T} + a_3 + \frac{a_4T}{2} + \frac{a_5T^2}{3} + \frac{a_6T^3}{4} + \frac{a_7T^4}{5} + \frac{b_1}{T}\big) RT \tag{2.26}$$

Where:

a_i, b_i are the Gordon-McBride constants.

The enthalpy of air Ha

We have (1 mole of O_2 + 3.76 moles of N_2), corresponding to 4.76 moles of air. Therefore, we use formula (2.7) with the coefficients of air.

2.4.2 Calculation of Products' Enthalpy

We have as products 11 species with unknown mole numbers:

- 4 primary products: CO_2, H_2O, O_2, N_2
- 7 dissociation products: NO, OH, CO, H_2, O, H, N

Governed by the enthalpy relation:

$$H_P = \sum_{i=1}^{11} n_i H_i \tag{2.27}$$

Thus, calculating the enthalpy of the products reduces determining the mole numbers of each product species.

Calculation of the number of moles of combustion products

To achieve this, we use the following equations:

a) Species conservation:

From the global combustion balance equation, we derive:

Carbon conservation:

$$n \times r_c = n_1 + n_7 \tag{2.28}$$

Hydrogen conservation:

$$m \times r_c = 2n_2 + n_6 + 2n_8 + n_{10} \tag{2.29}$$

Oxygen conservation:

$$2 \times \left(n + \frac{m}{4}\right) = 2n_1 + n_2 + 2n_3 + n_5 + n_6 + n_7 + n_9 \tag{2.30}$$

Azote conservation:

$$7.52 \times \left(n + \frac{m}{4}\right) = 2n_4 + n_5 + n_{11} \tag{2.31}$$

b) Equilibrium equations for dissociation reactions:

There are 7 balance equations:

$$2\,CO_2 \rightleftharpoons 2\,CO + O_2 \tag{2.32}$$

$$2\,H_2O \rightleftharpoons 2\,OH + H_2 \tag{2.33}$$

$$2\,H_2O \rightleftharpoons 2\,H_2 + O_2 \tag{2.34}$$

$$H_2 \rightleftharpoons 2\,H \tag{2.35}$$

$$O_2 \rightleftharpoons 2\,O \tag{2.36}$$

$$N_2 \rightleftharpoons 2\,N \tag{2.37}$$

$$N_2 + O_2 \rightleftharpoons 2\,NO \tag{2.38}$$

For these balance equations, the equilibrium constant will be:

$$K_p(13) = \frac{P_{CO}^2 P_{O_2}}{P_{CO_2}^2}$$

And we have the partial pressures for each species i:

$$P_i = \frac{n_i}{\sum_p n_i} P \tag{2.39}$$

where P is the total pressure.

With:

$$\sum n_i = N_t \tag{2.40}$$

By combining with the global equation, we obtain:

$$K_p(13) = \frac{n_7^2\, n_3}{n_1^2} \cdot \frac{P}{N_t} \tag{2.41}$$

P is known (isobaric transformation), equal to the initial pressure $P_{initial}$ and k_p is calculated by the formula:

$$K_{p_k} = \exp\left(-\frac{\Delta H_K^0}{RT} + \frac{\Delta S_K^0}{R}\right) \tag{2.42}$$

So, for the past 6 equations we got

$$K_p(14) = \frac{n_6^2\, n_8}{n_2^2} \cdot \frac{P}{N_t} \tag{2.43}$$

$$K_p(15) = \frac{n_8^2\, n_3}{n_2^2} \cdot \frac{P}{N_t} \tag{2.44}$$

$$K_p(16) = \frac{n_{10}^2}{n_8} \cdot \frac{P}{N_t} \tag{2.45}$$

$$K_p(17) = \frac{n_9^2}{n_3} \cdot \frac{P}{N_t} \tag{2.46}$$

$$K_p(18) = \frac{n_{11}^2}{n_4} \cdot \frac{P}{N_t} \tag{2.47}$$

$$K_p(19) = \frac{n_5^2}{n_3\, n_4} \tag{2.48}$$

We set a fixed value for T. We have 12 equations with 12 unknowns:

$$f_1 = n_1 + n_7 - (n \times r_c) \tag{2.49}$$

$$f_2 = 2n_2 + n_6 + 2n_8 + n_{10} - (m \times r_c) \tag{2.50}$$

$$f_3 = 2n_1 + n_2 + 2n_3 + n_5 + n_6 + n_7 + n_9 - \left(2 \times \left(n + \frac{m}{4}\right)\right) \tag{2.51}$$

$$f_4 = 2n_4 + n_5 + n_{11} - \left(7.52 \times \left(n + \frac{m}{4}\right)\right) \tag{2.52}$$

$$f_5 = n_7^2\, n_3 - \left(\frac{K_p(13)}{P}\, n_1^2 N_t\right) \tag{2.53}$$

$$f_6 = n_6^2\, n_8 - \left(\frac{K_p(14)}{P} n_2^2 N_t\right) \tag{2.54}$$

$$f_7 = n_8^2\, n_3 - \left(\frac{K_p(15)}{P} n_2^2 N_t\right) \tag{2.55}$$

$$f_8 = n_{10}^2 - \left(\frac{K_p(16)}{P} n_8 N_t\right) \tag{2.56}$$

$$f_9 = n_9^2 - \left(\frac{K_p(17)}{P} n_3 N_t\right) \tag{2.57}$$

$$f_{10} = n_9^2 - \left(\frac{K_p(17)}{P} n_3 N_t\right) \tag{2.58}$$

$$f_{11} = n_{11}^2 - \left(\frac{K_p(18)}{P} n_4 N_t\right) \tag{2.59}$$

$$f_{12} = n_5^2 - \left(\frac{K_p(19)}{P} n_3 n_4\right) \tag{2.60}$$

To solve such a system, we employ appropriate numerical methods. For example, the Newton-Raphson method for nonlinear systems, which relies on a linear system solver.

2.4.3 Calculation of Products' Enthalpy

Once the mole numbers n_i are determined, the enthalpy can be calculated using the following formula:

$$\begin{aligned} H_p = {} & n_1 H_{\mathrm{CO_2}} + n_2 H_{\mathrm{H_2O}} + n_3 H_{\mathrm{O_2}} + n_4 H_{\mathrm{N_2}} + n_5 H_{\mathrm{NO}} + n_6 H_{\mathrm{OH}} \\ & + n_7 H_{\mathrm{CO}} + n_8 H_{\mathrm{H_2}} + n_9 H_{\mathrm{O}} + n_{10} H_{\mathrm{H}} + n_{11} H_{\mathrm{N}} \end{aligned} \tag{2.61}$$

Where:

the Hi are calculated by formula (2.26), using the coefficients ai corresponding to species ii and temperature T.

2.4.4 Calculation of Final Combustion Temperature

This calculation requires the application of a numerical method, such as the "BISECTION METHOD".

Application of the Bisection Method:

a. Reactant enthalpy is calculated using relation (2.26).

b. For Tad, select a temperature interval [T_1,T_2] and evaluate each value in (2.21) to obtain:

$$\begin{cases} f(T_1) = H_p(T_1) - H_r(T_i) \\ f(T_2) = H_p(T_2) - H_r(T_i) \end{cases} \tag{2.62}$$

If $f(T_1) \times f(T_2) > 0$, the condition is satisfied and the interval $[T_1, T_2]$ must be adjusted.

If $f(T_1) \times f(T_2) < 0$, the target temperature is within this interval.

To proceed, calculate:

$$T_{\mathrm{ad}}^0 = \frac{T_1 + T_2}{2} \tag{2.63}$$

With:

$f(T_{\text{ad}}^0) = H_p(T_{\text{ad}}^0) - H_r(T_i)$.

If $f(T_{\text{ad}}^0) \times f(T_1) < 0$, then T_{ad1} is in the interval $[T_1, T_{\text{ad}}^0]$.

Either:

$$T_{\text{ad}}^1 = \frac{T_{\text{ad}}^0 + T_1}{2} \tag{2.64}$$

Otherwise, T_{ad}^1 belongs to the interval $[T_{\text{ad}}^0, T_2]$.

Either:

$$T_{\text{ad}}^1 = \frac{T_{\text{ad}}^0 + T_2}{2} \tag{2.65}$$

The calculations are repeated until:

$$\left|T_{\text{ad}}^i - T_{\text{ad}}^{i-1}\right| \leq \varepsilon \tag{2.66}$$

where ε epsilone represents the error tolerance value.

Finally, we obtain:

The Final Combustion Temperature:

$$T_{\text{ad}} \approx T_{\text{ad}}^i \tag{2.67}$$

The previous steps are summarized in the following organization chart.

2.5 organization chart (org chart)

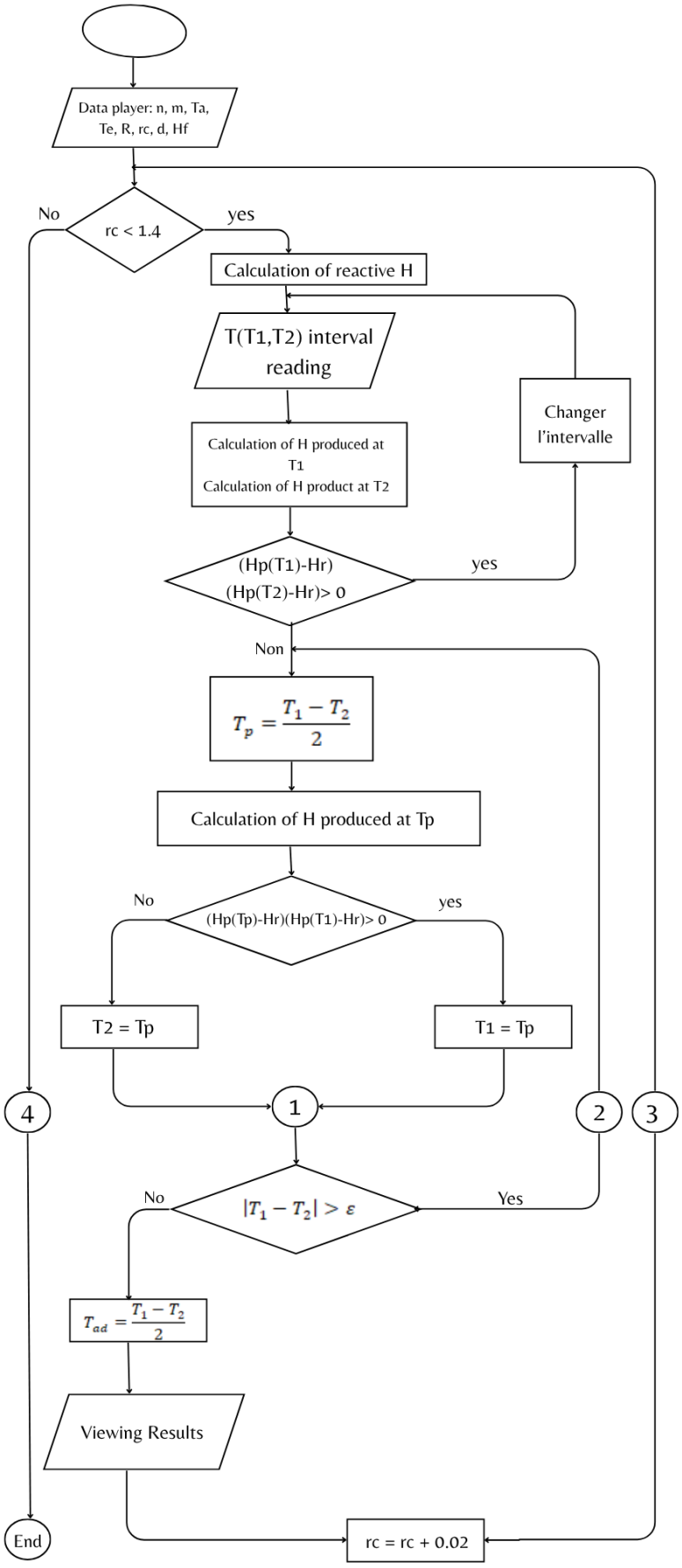

Figure 2.1: Organizations chart for Determining Combustion Temperature and Product Mole Fractions.

For enthalpy calculations, we use the following subroutines:

2.5.1 Reactant enthalpy

Subroutine calcul H_r(T, H) for air enthalpy.

Subroutine calcul H_c(T, H) for fuel enthalpy.

Subroutine calcul H_f(T, H) for fuel enthalpy.

2.5.2 Product Enthalpy

For this purpose, we use subroutine fractions (T, n, m, re, p, x_i) to determine the molar fractions of the various products. This subroutine calls other subroutines: Calculation of K_p(T, K_p) for equilibrium constants Eligaus (n, a, b, x): a numerical method for solving systems of linear equations.

The subroutine calcul K_p in turn calls two other subroutines: calc H_p(T,H_p) for determination of product species enthalpy. calc S_P (T, S_p) for determination of product species entropy.

We will describe the Newton-Raphson method for solving systems of nonlinear equations. This method calls upon another method for solving linear systems - we have selected Gaussian elimination with partial pivoting.

2.6 Newton-Raphson Method

2.6.1 History

Newton's method was discovered by Isaac Newton and published in 'Method of Fluxions' in 1736. Although the method was described by Joseph Raphson in 'Analysis Aequationum' in 1690, the relevant sections of 'Method of Fluxions' had already been written in 1671.[40]

In numerical analysis, Newton's method (or the Newton-Raphson method) is an efficient algorithm for finding approximations to the zeros (or roots) of a real-valued function, or systems of nonlinear equations. [40]

2.6.2 Method Description

We focus on solving the following system of equations:

$$\begin{cases} f_1(x_1, x_2, \ldots, x_n) = 0 \\ f_2(x_1, x_2, \ldots, x_n) = 0 \\ \vdots \\ f_n(x_1, x_2, \ldots, x_n) = 0 \end{cases} \tag{2.68}$$

Where the f_i are nonlinear functions of the real variables x_i

In our case, the f_i are as follows:

$$f_1 = n_1 + n_7 - (n \times r_c) \tag{2.69}$$

$$f_2 = 2n_2 + n_6 + 2n_8 + n_{10} - (m \times r_c) \tag{2.70}$$

$$f_3 = 2n_1 + n_2 + 2n_3 + n_5 + n_6 + n_7 + n_9 - \left(2(n + \tfrac{m}{4})\right) \tag{2.71}$$

$$f_4 = 2n_4 + n_5 + n_{11} - \left(7.52(n + \tfrac{m}{4})\right) \tag{2.72}$$

$$f_5 = n_7^2 n_3 - \frac{K_p(13)}{P} n_1^2 N_t \tag{2.73}$$

$$f_6 = n_6^2 n_8 - \frac{K_p(14)}{P} n_2^2 N_t \tag{2.74}$$

$$f_7 = n_8^2 n_3 - \frac{K_p(15)}{P} n_2^2 N_t \tag{2.75}$$

$$f_8 = n_{10}^2 - \frac{K_p(16)}{P} n_8 N_t \tag{2.76}$$

$$f_9 = n_9^2 - \frac{K_p(17)}{P} n_3 N_t \tag{2.77}$$

$$f_{10} = n_9^2 - \frac{K_p(17)}{P} n_3 N_t \tag{2.78}$$

$$f_{11} = n_{11}^2 - \frac{K_p(18)}{P} n_4 N_t \tag{2.79}$$

$$f_{12} = n_5^2 - \frac{K_p(19)}{P} n_3 n_4 \tag{2.80}$$

Where $n_1, \ldots, n_{11}, N_t$ represent the variables x_i.

The relation used for each iteration i is:

$$x_{i+1} = x_i - \frac{f(x_i)}{f'(x_i)} \tag{2.81}$$

If each function f_i is continuous and continuously differentiable, then by Taylor series expansion we obtain:

$$f_i(\hat{x} + \delta) = f_i(\hat{x}) + \frac{\partial f_i}{\partial x_1}\,\delta_1 + \cdots + \frac{\partial f_i}{\partial x_n}\,\delta_n. \tag{2.82}$$

Thus, to ensure that $f(\hat{x} + \delta) \to 0$, we must solve a linear system of n equations with n unknowns.

$$\begin{bmatrix} \frac{\partial f_1}{\partial x_1} & \frac{\partial f_1}{\partial x_2} & \cdots & \frac{\partial f_1}{\partial x_n} \\ \vdots & \vdots & \ddots & \vdots \\ \frac{\partial f_n}{\partial x_1} & \frac{\partial f_n}{\partial x_2} & \cdots & \frac{\partial f_n}{\partial x_n} \end{bmatrix} \begin{bmatrix} \delta_1 \\ \vdots \\ \delta_n \end{bmatrix} = \begin{bmatrix} -f_1 \\ \vdots \\ -f_n \end{bmatrix}. \tag{2.83}$$

This system can be solved using numerical methods for linear equations, such as Gaussian elimination.

This resolution determines the x_i and subsequently, the xi can be obtained using the relation:

$$x_{i+1} = x_i + \delta_i. \tag{2.84}$$

Note: The initial vector is provided as the first approximation.

An initial guess $\begin{bmatrix} x_1^0 \\ x_2^0 \\ \vdots \\ x_n^0 \end{bmatrix}$ is necessary to provide a starting point for the subsequent iterations.

The following loop should be iterated upon until the stopping conditions are reached: Construct the Jacobian (left-hand side of Eq. (2.71)),Solve the linear system, Calculate new values of x_i.

2.6.3 The stopping conditions

$$\begin{cases} \left|\frac{\delta_j}{x_j}\right| \leq 10^{-7} & \text{if } |x_j| \geq 10^{-7} \\ \text{or} & \\ |\delta_j| \leq 10^{-7} & \text{if } |x_j| \leq 10^{-7}. \end{cases} \tag{2.85}$$

2.6.4 Convergence method

To ensure proper convergence, the following steps must be followed:

a. Compare the norm of the newly computed function $f_i(x_1, x_2, \ldots, x_n)$ with that of the previous function $f_{i-1}(x_1, x_2, \ldots, x_n)$, where:

$$\text{norm} = \sum_{i=1}^{n} |f_i(\hat{x})| . \tag{2.86}$$

b. If the new norm is larger than the old vector's norm, divide δ by an arbitrary constant; otherwise, do nothing. [40]

2.7 Gauss method

Principle: The Gaussian elimination method transforms the system Ax=b into an equivalent system where A' is an upper triangular matrix.[40]

2.7.1 Description method

Consider the following system [40]:

$$\begin{bmatrix} a_{11} & a_{12} & \cdots & a_{1n} \\ a_{21} & a_{22} & \cdots & a_{2n} \\ \vdots & \vdots & \ddots & \vdots \\ a_{n1} & a_{n2} & \cdots & a_{nn} \end{bmatrix} \begin{bmatrix} x_1 \\ x_2 \\ \vdots \\ x_n \end{bmatrix} = \begin{bmatrix} b_1 \\ b_2 \\ \vdots \\ b_n \end{bmatrix}. \tag{2.87}$$

Given that the same transformations will be applied to both A and b to preserve the system, the algorithm is simplified by forming the augmented matrix $[A \,|\, b]$, where the vector b becomes the $(n+1)$-th column. The system is now represented as:

$$\begin{bmatrix} a_{11} & a_{12} & \cdots & a_{1n} \\ a_{21} & a_{22} & \cdots & a_{2n} \\ \vdots & \vdots & \ddots & \vdots \\ a_{n1} & a_{n2} & \cdots & a_{nn} \end{bmatrix} \begin{bmatrix} x_1 \\ x_2 \\ \vdots \\ x_n \end{bmatrix} = \begin{bmatrix} a_{1,n+1} \\ a_{2,n+1} \\ \vdots \\ a_{n,n+1} \end{bmatrix}. \tag{2.88}$$

First step

We transform [A,b] into a matrix where the sub-diagonal terms of the first column are zero:

$a_{21}^{(1)} = a_{31}^{(1)} = \ldots = a_{n1}^{(1)} = 0.$

Premultiply $[A, b]$ by $E_{21}\big(-\frac{a_{21}}{a_{11}}\big)$. Only the second row is modified, and its terms become:

$$\begin{bmatrix} a_{21}^{(1)} \\ a_{22}^{(1)} \\ \vdots \\ a_{2,n+1}^{(1)} \end{bmatrix} = \begin{bmatrix} a_{21} - \frac{a_{21}}{a_{11}} a_{11} = 0 \\ a_{22} - \frac{a_{21}}{a_{11}} a_{12} \\ \vdots \\ a_{2,n+1} - \frac{a_{21}}{a_{11}} a_{1,n+1} \end{bmatrix}. \tag{2.89}$$

Premultiply $[A, b]$ by $E_{31}\big(-\frac{a_{31}}{a_{11}}\big)$. We modify the third row as follows:

$$\begin{bmatrix} a_{31}^{(1)} \\ a_{32}^{(1)} \\ \vdots \\ a_{3,n+1}^{(1)} \end{bmatrix} = \begin{bmatrix} a_{31} - \frac{a_{31}}{a_{11}} a_{11} = 0 \\ a_{32} - \frac{a_{31}}{a_{11}} a_{12} \\ \vdots \\ a_{3,n+1} - \frac{a_{31}}{a_{11}} a_{1,n+1} \end{bmatrix}. \tag{2.90}$$

Generally, to zero out the terms a_{i1}, we use the transformation E_{i1} (ai1/a11) , which yields the new terms for the i-th row:

$$\begin{bmatrix} a_{i1}^{(1)} \\ a_{i2}^{(1)} \\ \vdots \\ a_{i,n+1}^{(1)} \end{bmatrix} = \begin{bmatrix} a_{i1} - \frac{a_{i1}}{a_{11}} a_{11} = 0 \\ a_{i2} - \frac{a_{i1}}{a_{11}} a_{12} \\ \vdots \\ a_{i,n+1} - \frac{a_{i1}}{a_{11}} a_{1,n+1} \end{bmatrix}. \tag{2.91}$$

Thus, the first step is expressed in general form as:

$$a_{ij}^{(1)} = a_{ij} - \frac{a_{i1}}{a_{11}} a_{1j} \quad \begin{cases} i = 2, \ldots, n \\ j = 2, \ldots, n+1 \end{cases} \tag{2.92}$$

After the first step, the system $[A, b]^{(1)}$ becomes:

$$\begin{bmatrix} a_{11} & a_{12} & \cdots & a_{1n} \\ 0 & a_{22}^{(1)} & \cdots & a_{2n}^{(1)} \\ \vdots & \vdots & \ddots & \vdots \\ 0 & a_{n2}^{(1)} & \cdots & a_{nn}^{(1)} \end{bmatrix} \begin{bmatrix} x_1 \\ x_2 \\ \vdots \\ x_n \end{bmatrix} = \begin{bmatrix} a_{1,n+1}^{(1)} \\ a_{2,n+1}^{(1)} \\ \vdots \\ a_{n,n+1}^{(1)} \end{bmatrix}. \tag{2.93}$$

second step

During this phase, we must eliminate the sub-diagonal terms of the second column:

$$a_{32}^{(2)} = a_{42}^{(2)} = \cdots = a_{n2}^{(2)} = 0. \tag{2.94}$$

Premultiply $[A,b]^{(1)}$ by $E_{i2}\big(-\frac{a_{i2}^{(1)}}{a_{22}^{(1)}}\big)$. This modifies the i-th row as follows:

$$\begin{bmatrix} a_{i2}^{(2)} \\ a_{i3}^{(2)} \\ \vdots \\ a_{i,n+1}^{(2)} \end{bmatrix} = \begin{bmatrix} a_{i2}^{(1)} - \frac{a_{i2}^{(1)}}{a_{22}^{(1)}} a_{22}^{(1)} = 0 \\ a_{i3}^{(1)} - \frac{a_{i2}^{(1)}}{a_{22}^{(1)}} a_{23}^{(1)} \\ \vdots \\ a_{i,n+1}^{(1)} - \frac{a_{i2}^{(1)}}{a_{22}^{(1)}} a_{2,n+1}^{(1)} \end{bmatrix}. \tag{2.95}$$

The second step is therefore written:

$$a_{ij}^{(2)} = a_{ij}^{(1)} - \frac{a_{i2}^{(1)}}{a_{22}^{(1)}} a_{2j}^{(1)} \quad \begin{cases} i = 3, \ldots, n \\ \\ j = 3, \ldots, n+1. \end{cases} \tag{2.96}$$

At the end of this step, the system $[A,b]^{(2)}$ is written as:

$$\begin{bmatrix} a_{11} & a_{12} & a_{13} & \cdots & a_{1n} \\ 0 & a_{22}^{(1)} & a_{23}^{(1)} & \cdots & a_{2n}^{(1)} \\ 0 & 0 & a_{33}^{(2)} & \cdots & a_{3n}^{(2)} \\ \vdots & \vdots & \vdots & \ddots & \vdots \\ 0 & 0 & a_{n3}^{(2)} & \cdots & a_{nn}^{(2)} \end{bmatrix} \begin{bmatrix} x_1 \\ x_2 \\ x_3 \\ \vdots \\ x_n \end{bmatrix} = \begin{bmatrix} a_{1,n+1}^{(1)} \\ a_{2,n+1}^{(1)} \\ a_{3,n+1}^{(2)} \\ \vdots \\ a_{n,n+1}^{(2)} \end{bmatrix}. \tag{2.97}$$

K-th step

We can thus summarize the transformations at the kk-th step as:

$$a_{ij}^{(k)} = a_{ij}^{(k-1)} - \frac{a_{ik}^{(k-1)}}{a_{kk}^{(k-1)}} a_{kj}^{(k-1)} \quad \begin{cases} i = k+1, \ldots, n \\ \\ j = k+1, \ldots, n+1. \end{cases} \tag{2.98}$$

Note that all these transformations assume the pivot terms a_k are non-zero. Therefore, a phase must be added to verify pivot non-nullity. In practice, to minimize rounding errors, division by small pivots is avoided as much as possible.

2.8 General algorithm

2.8.1 First phase

Partial Pivot Method

We choose as the pivot the element $a_{rk}^{(k-1)}$ such that:

$$a_{rk}^{(k-1)} = \max \left| a_{ik}^{(k-1)} \right| \quad \text{with} \quad i = k, \ldots, n. \tag{2.99}$$

And we swap rows K and r.

2.8.2 Second step

The matrix $[A, b]^{(k-1)}$, potentially modified by the first phase, requires computation of its non-zero elements corresponding to:

$$a_{ij}^{(k)} = a_{ij}^{(k-1)} - \frac{a_{ik}^{(k-1)}}{a_{kk}^{(k-1)}} a_{kj}^{(k-1)} \quad \begin{cases} k = 1, \ldots, n-1 \\ i = k+1, \ldots, n \\ j = k+1, \ldots, n+1. \end{cases} \tag{2.100}$$

2.8.3 Third Phase

After obtaining the triangular system $A^{(n-1)}x = b^{(n-1)}$, we solve it using the following formula:

$$x_i = \frac{1}{a_{ii}} \left[b_i - \sum_{j=i+1}^{n} a_{ij}^{(n-1)} x_j \right] \quad \text{for} \quad i = n, n-1, \ldots, 1. \tag{2.101}$$

NOTE:

In our case, we must solve a system of nonlinear equations (12 equations), and the resulting Jacobian is:

$$\begin{bmatrix} \frac{\partial f_1}{\partial x_1} & \frac{\partial f_1}{\partial x_2} & \cdots & \frac{\partial f_1}{\partial x_n} \\ \vdots & \vdots & \ddots & \vdots \\ \frac{\partial f_n}{\partial x_1} & \frac{\partial f_n}{\partial x_2} & \cdots & \frac{\partial f_n}{\partial x_n} \end{bmatrix}$$

2.9 Conclusion

This chapter has rigorously examined the fundamental principles and practical methodologies necessary for accurate combustion analysis. Essential parameters such as mass and mole fractions, mixture equivalence ratio, stoichiometry, and dissociation effects were defined to build a robust foundation for understanding reactive flows and combustion behavior. Advanced numerical techniques, including the Newton-Raphson and Gaussian elimination methods, were applied with the aid of Futron to solve the complex systems governing combustion reactions and to precisely calculate the adiabatic flame temperature using the bisection method.

The systematic approach demonstrated here ensures reliable determination of reactant and product enthalpies, providing clear insight into optimizing combustion efficiency while minimizing pollutant formation. Overall, the theoretical and computational framework developed in this chapter is directly applicable to the design of cleaner and more energy-efficient combustion systems, highlighting the crucial role of detailed combustion analysis in addressing modern environmental and technological challenges.

Chapter 3

Experimental Study

3.1 Introduction

Active experimental research on the performance of diesel and gasoline internal combustion engines, conducted entirely by our team. We carried out these studies at the University of M'Hamed Bouguerra Boumerdès (Department of Mechanics) using the TD200 test bench for the single-cylinder gasoline engine, and at the University Saad Dahleb of Blida 1 using the TD43 universal test bench for the variable This chapter presents our compression ratio diesel engine (FARRYMAN A30). Our approach included designing protocols, executing tests, and analyzing data, ensuring rigorous methodological consistency across both experimental platforms.

Our methodology centered on the systematic variation of rotational speeds (1500–4000 rpm for gasoline; 1000–2500 rpm for diesel) and precise control of operating parameters (compression ratio, load, ignition timing). We measured real-time primary data (torque, fuel consumption, airflow rate, exhaust gas temperatures) using calibrated instruments, then calculated key performance indicators: effective power, specific consumption, thermal efficiency, and volumetric efficiency. This protocol standardization enables a direct comparison of combustion mechanisms (spark ignition vs. compression ignition) and their energy implications.

The fundamental objective of this dual study is to establish a unified analytical framework highlighting the inherent trade-offs between both technologies. Through systematic

comparison of results, we identify optimal operating ranges, quantify energy losses (friction, unburned fuel), and evaluate the impact of structural differences (compression ratios, injection systems). This original contribution provides robust empirical foundations for optimizing existing engines and reducing their environmental footprint, while serving as an academic benchmark for thermal engineering research.

3.2 Diesel Internal Combustion Engine

3.2.1 Operating Principle

Four-Stroke Cycle

The base engine selected for the TD43 operates on a four-stroke cycle, which can be represented by a pressure-volume diagram similar to the one shown in the figure below:

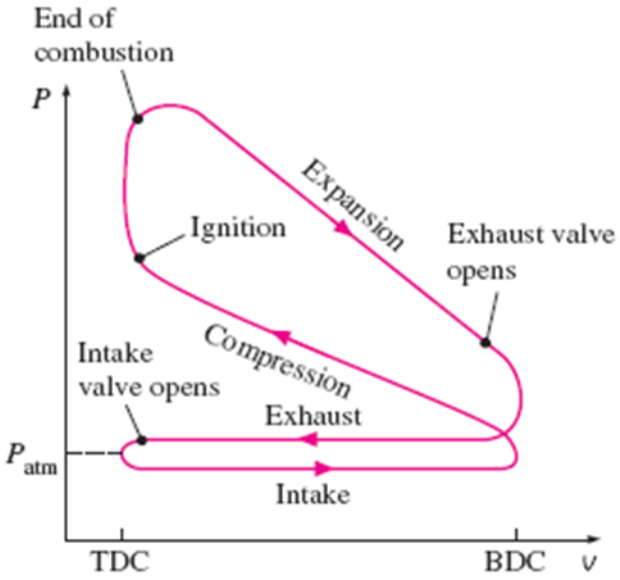

Figure 3.1: Operating Cycle of an Internal Combustion Engine. [13]

The pressure-volume loop can be determined experimentally using a pressure indicator (piezoelectric sensor) and a volume angle indicator.

The piston being at TDC and beginning to descend, air (for diesel engines) or air-fuel mixture (for gasoline engines) is drawn in through the intake valve - this is the first stroke of the cycle, or intake stroke. The intake occurs at a pressure slightly below atmospheric

pressure. After passing BDC, the piston rises and compresses the admitted charge in the cylinder. Combustion is initiated just before the piston reaches TDC again. In gasoline or gas engines, ignition is caused by a spark. In diesel engines, however, fuel is injected at this moment and spontaneously ignites upon contact, causing a significant increase in pressure and temperature.

The flywheel's inertia carries the piston beyond TDC, and as the gases expand, they push the piston downward. The exhaust valve opens slightly before the end of the stroke, so that some gases are expelled from the cylinder by the pressure difference. The power stroke or expansion stroke is represented in the previous figures. The piston then begins to rise again, expelling most of the exhaust gases. This final phase of the cycle is called the exhaust stroke.

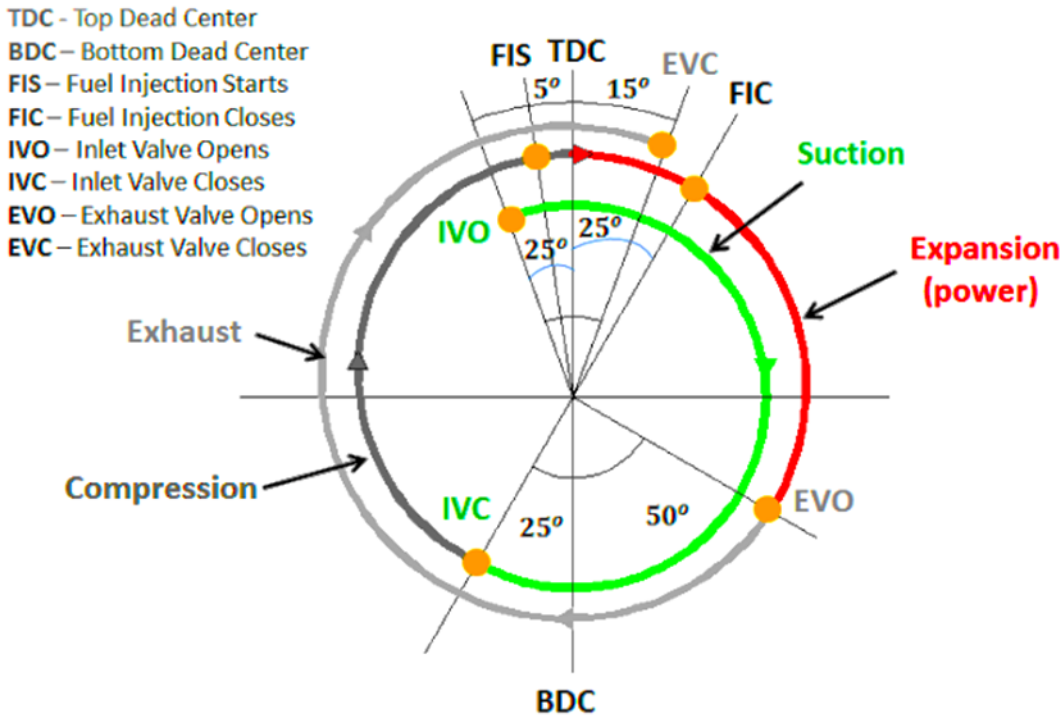

Figure 3.2: Valve Timing and Ignition Timing Diagram. [14]

The valve timing diagram in the following figure illustrates the actual opening and closing of the valves. Ideally, the valve timing for gasoline engines differs from that of diesel engines. However, for practical purposes, the valve timing of the TD43 engine represents a compromise between the optimal solutions for gasoline, diesel, and gas engines.

3.2.2 Performance Criteria

Indicated Power

The work delivered by the engine is represented by the area of the loop. The corresponding power is called indicated power; the loops are obtained using an indicator.

The indicated power is greater than the power available at the engine's crankshaft, as it does not account for mechanical losses. The area enclosed by the loop can be divided by the displacement volume (Vc) to obtain the indicated mean effective pressure (IMEP).

$$\text{Network delivered per cycle} = (\text{Area of the HP loop}) - (\text{Area of the LP loop}) = Vc \times \text{IMEP} \tag{3.1}$$

With:

- HP loop = High Pressure loop.
- LP loop = Low Pressure loop.
- Vc = Displacement volume.
- PMI $\rightarrow$ IMEP (Indicated Mean Effective Pressure).

Indicated power depends on the frequency of power strokes in a four-stroke engine. The cycle is completed in two full revolutions. Hence, if N is the engine speed in revolutions per minute (rpm), then:

$$\text{Indicated power } (Pi) = \text{IMEP} \times Vc \times N_0 \text{ (watts)} \tag{3.2}$$

With:

- Pi = Indicated power.
- IMEP = (Indicated Mean Effective Pressure).
- Vc = Displacement volume.
- N_0 = Number of working cycles per second.

Effective Power

Brake Power (Effective Power) refers to the power available at the engine crankshaft. It is typically measured by determining the engine torque while the motor operates against a braking device. This brake can consist of:

- A friction band acting on the flywheel,
- A hydraulic brake,
- An electric brake that dissipates energy through a resistor network.

The engine torque (C) is read from an electric indicator (or linear potentiometer) that measures the displacement of a spring. This spring absorbs the reaction force exerted by the dynamometer housing, which tends to rotate with the engine.

$$P_e(\text{effective power}) = C \cdot \omega = C_m \cdot 2 \cdot \pi \cdot \frac{N}{60} \text{ (Watt)} \tag{3.3}$$

Mechanical Losses and Mechanical Efficiency

The energy lost to mechanical friction is equal to the difference between indicated power and brake power.

$$\text{Friction mechanical losses} = \text{Indicated power} - \text{Brake power} \tag{3.4}$$

Mechanical friction losses are measured directly by recording the torque required to rotate the engine using a dynamometer configured as an electric motor.

$$\text{friction losses} = 2 \cdot \pi \cdot \frac{N}{60} \cdot C_f \tag{3.5}$$

With:

- C_f: the friction torque indicated by the measuring instrument.

Mechanical efficiency is defined by:

$$\eta_m = \frac{\text{effective power}}{\text{indicated power}} \tag{3.6}$$

Specific Consumption

Fuel Specific Consumption (FSC) serves as a key metric for evaluating the economic efficiency of delivered energy. It is defined as follows:

$$S_c = \frac{\text{Hourly fuel consumption}}{\text{effective power}} = \frac{m_c}{P_e} \left(\frac{\text{Kg}}{\text{KW.h}} \right) \tag{3.7}$$

Specific consumption is a performance parameter of engines. On the one hand, it allows controlling the engine's consumption level for a certain effective delivery power, and on the other hand, it enables comparing the consumption of engines of different sizes. An engine is economical if its specific consumption is low for a given effective power.

The fuel consumption (mc) is determined by measuring the time (t) required for the engine to consume a given volume of fuel (8,16, or 32 ml).

$$m_c = \frac{\rho_c \cdot (8, 16 \text{ or } 32) \cdot 10^{-3}}{t} \left(\frac{\text{kg}}{\text{s}} \right) \tag{3.8}$$

With:

- ρ_c: Fuel density in kg/L (0.84 for diesel).

A similar method is used to determine gas consumption, except a domestic gas meter is employed instead of a pipette. The measurement involves timing the consumption of 10 liters (0.01 m^3) of gas. The density of propane is approximately 1.92 kg/m^3 at 15°C and 1013 mbar, such that:

$$m_{\text{gas}} = \frac{0.0192}{t} \left(\frac{\text{Kg}}{\text{second}} \right) \tag{3.9}$$

A correction must be applied to this value when the temperature and pressure of the fuel gas differ from standard conditions.

$$m_{\text{gas}} = \frac{0.0192}{t} \cdot \frac{P_{\text{réel}}}{1013} \cdot \frac{(273 + 15)}{T_{\text{réel}}} \tag{3.10}$$

Overall Efficiency

Overall efficiency provides an assessment of the engine's total efficiency and is defined as follows:

$$\eta_g = \frac{\text{effective power}}{\text{supplied power}} \tag{3.11}$$

When accounting for the power supplied during combustion, the overall efficiency becomes:

$$\eta_g = \frac{P_e}{m_c \cdot \text{PCI}} = \frac{1}{S_c \cdot \text{PCI}} \tag{3.12}$$

Consequently, the overall efficiency is inversely proportional to the specific fuel consumption. To use this, a consistent set of units must be employed. In practice, specific fuel consumption is measured in grams/kWh and the lower heating value in kJ/kg. To obtain the correct value of η_g using these units, equation (3.12) must be multiplied by $3,6 \cdot 10^6$.

Volumetric Efficiency

The power delivered by an engine depends on the load, specifically the amount of charge that can be introduced into the cylinder. In practice, the engine does not intake a full cylinder volume of air during each intake stroke. Therefore, the volumetric efficiency is defined as follows:

$$\eta_v = \frac{\text{Air flow rate}}{\text{mass of air occupying the cylinder volume at atmospheric conditions}} \tag{3.13}$$

The displacement of the TD43 engine is 582 cm^3, and the mass of air required to fill this volume per unit time is given by:

$$\rho_a \cdot 582 \cdot 10^{-6} \cdot n_0 \tag{3.14}$$

$$\rho_a = \frac{P_a}{r \cdot T_a} \text{ (ambient air density)}$$

$$n_0 = \frac{N}{120} \text{ (number of cycles per second for a 4-stroke engine)}$$

Thus, the volumetric efficiency is expressed as:

$$\eta_v = \frac{\text{Air flow rate}}{\rho_a \cdot 582 \cdot 10^{-6} \cdot n_0} \tag{3.15}$$

Air/Fuel Ratio

The air/fuel ratio (AFR) is the quotient of the mass flow rate of air to the mass flow rate of fuel. The mass flow rate of air is determined by the calibration curve of the viscous flow meter, while the mass flow rate of fuel is provided by Equation (3.6).

Under ideal conditions, the AFR should be around **15:1** for complete combustion. In practice:

- Maximum overall efficiency is achieved with a relatively **lean mixture (17:1)**.
- Maximum power is obtained with a **richer mixture (12:1)**.

3.2.3 Test Bench Description

TD 43 Test Bench

This test bench features a modified four-stroke marine engine (FARRYMAN A30), a power plant designed for high flexibility in fuel compatibility and performance testing with water cooling. It has an adjustable compression ratio from 5:1 (for low-pressure applications such as natural gas) to 18:1, optimized for high-efficiency diesel combustion, providing a great platform for research and development. It can operate on gasoline fuels (petrol), diesel, propane (LPG), and compressed Ral gas (CNG). This makes it very suitable for testing alternative fuel efficiency, emissions, and engine behavior under different combustion conditions. It also comes with a turbocharger, which improves adaptability since it can provide forced induction both in diesel and direct fuel-injected gasoline configurations. This is important for downsized turbocharged engines.

The engine is mounted linked to a high-precision electric dynamometer that serves both measurement of the torque/power output with ±0.5% calibration and as a motoring sys-

tem to start the engine or simulate the effect of inertia during friction tests. These measurements are vital for mechanical losses in bearings, piston rings, and valve trains; losses are crucial for optimizing engine efficiency. The engine and dynamometer are both mounted on a heavy-duty steel base with four anti-vibration feet of the very best quality to eliminate outside interference and promote consistent, reproducible measurements even at high RPM.

Two ergonomic control panels are placed behind the setup. The left panel incorporates a centralized electrical control system having programmable logic controls (PLCs) for automated test sequences, emergency stop functions, and real-time data logging. The right panel is dedicated to engine performance analysis; it includes digital gauges, a TD 43 engine analyzer with a touchscreen interface, plus external data acquisition system connectivity (e.g., CAN bus or LabVIEW integration). Fuel storage complies with ISO 22734; color-coded tanks: gasoline—red, diesel—brown, plus other safety features (pressure relief valves, grounding straps to static ignition risks).

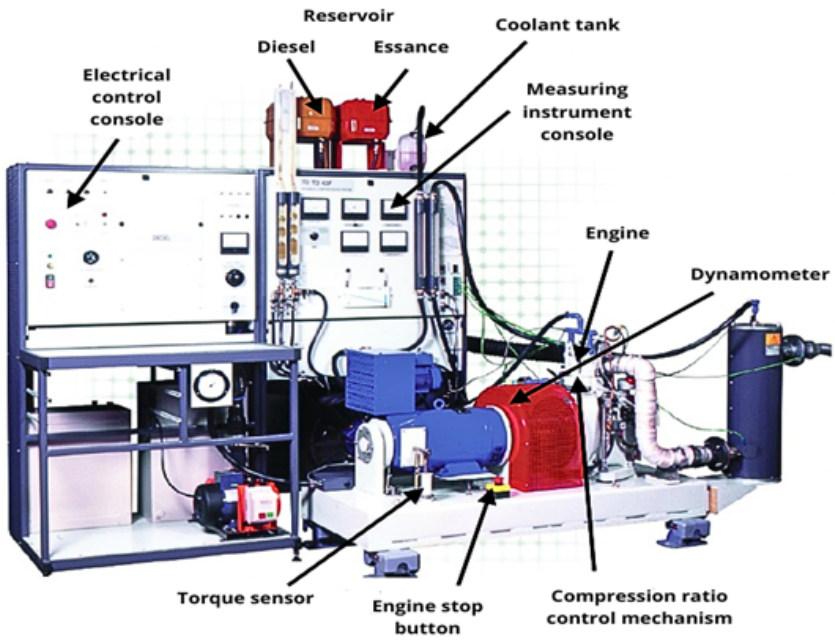

Figure 3.3: TD 43 Benchmark Overview. [15]

The test bench's back panels incorporate modern technical devices for thorough instrumentation diagnostics. As an example, a Meriam LFE series accurately "viscously" measures the air flow (real time) needed for the air consumption meter, which is vital for the

air-fuel ratio and volumetric efficiency calculations. The cooling system is designed to control the temperature with a high degree of accuracy and contains a thermostatically controlled high aluminum radiator, a step electric fan for adjustable airflow, and a centrifugal water pump with flow rate metering. This permits uninterrupted temperature control during endurance testing or high-load simulation. Additional subsystems may include knock sensors, exhaust gas analyzers (measuring NOx, CO, and HC), and pressure transducers for the combustion process analysis aimed at making this bench powerful enough for marine, automotive, and energy industries' engine development, calibration, and compliance tests.

Instrumentation

The engine performance measurement instruments are mounted on the right-hand console. On this console, the following parameters can be read:

Table 3.1: Measured Parameters and Instrumentation.

Parameters	**Measuring Instrument**
Engine speed (tours/minute)	Tachometer (contact or non-contact optical sensor)
Torque (N.m)	Dynamometer (eddy-current or hydraulic type)
Effective power (kW)	Dynamometer + Power Meter
Coolant temperature at engine inlet and outlet (in °C)	RTD (PT100) or K-Type Thermocouples
Exhaust gas temperature (in °C)	K-Type or N-Type Thermocouple (high-temperature probe)
Coolant flow rate (cm H2O)	Differential Pressure Transducer
Air consumption (mm H2O)	Pitot Tube or Orifice Plate + Pressure Transducer
Fuel consumption (ml/s)	Graduated Burette + Flow Sensor (Coriolis or ultrasonic)

Engine Specifications

Four-stroke, multi-fuel, variable compression ratio engine – FARRYMAN A30, water-cooled. Its technical specifications are provided in the following table:

Table 3.2: Technical Specifications.

Parameter	**Value**
compression ratio	12/1 to 18/1
Bore	95 mm
Stroke	82 mm
Displacement	582 cm^3
Speed	1000 to 2500 tr/mn
Maximum power	7 kW
Maximum torque	50 N.m
Ignition timing	30° before to 10° after TDC
Venturi carburetor	19; 21; 23; and 25 mm

Purpose of the Tests

A universal test bench like the TD43 can provide diverse and extensive data. The essential parameters measured on this test bench over a speed range varying from 1000 to 2500 rpm are as follows:

- Torque.
- Friction loss.
- Air/fuel ratio.
- Engine effective power.
- Specific fuel consumption.
- Exhaust gas temperature.
- Heat absorbed by the cooling water.
- Heat carried away by the exhaust gases.

These parameters allow us to construct the performance curves of the tested engine at different operating speeds. The tests can be performed at partial load or full load by varying the rotational speed within the range indicated above using the dynamometer.

3.2.4 Experience steps

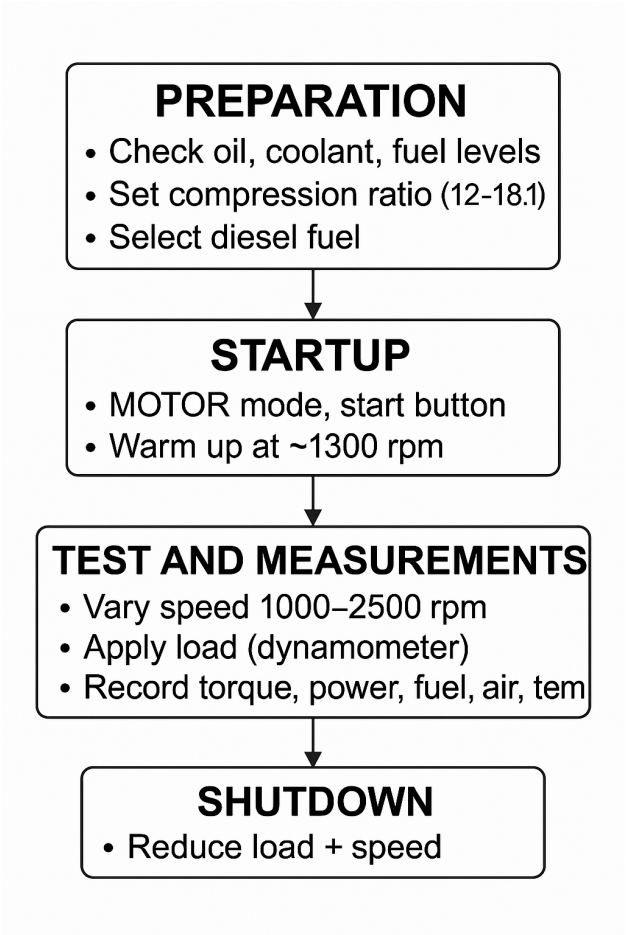

Figure 3.4: Diesel Engine Experimental Procedure (TD43).

3.2.5 Calculation

Effective Power

$$P_e = \mathbf{C_m} \cdot \frac{2 \cdot \pi \cdot \mathbf{N}}{60}$$

- First case:

$$P_e = \mathbf{19} \cdot \frac{2 \cdot \pi \cdot \mathbf{1000}}{60} = \mathbf{1989,68}\ \text{W} = \mathbf{1,990}\ \text{KW}$$

Hourly Consumption

$$m_c = \frac{\rho_c \cdot 8 \cdot 10^{-3}}{\mathbf{t}} \text{ With } \rho_c = 0,84 \text{ (for Diesel)}$$

- First case:

$$m_c = \frac{0,84 \cdot 8 \cdot 10^{-3}}{\mathbf{9,5 \cdot 10^{-3}}} = \mathbf{0,707} \text{ kg/h}$$

Specific Consumption

$$FSC = \frac{\text{Hourly fuel consumption}}{\text{effective power}} = \frac{\mathbf{m_c}}{\mathbf{P_e}}$$

- First case:

$$S_c = \frac{\mathbf{0,707}}{\mathbf{1,990}} = \mathbf{0,355} \frac{\text{Kg}}{\text{KW.h}}$$

Air Flow Rate

$$\text{Air Flow Rate} = AFR = \text{Manometer Reading} \times K$$

With:

$$K = 0,2048 \text{ kg/h per mm } H^2O \text{ (derived empirically)}$$

$$= \text{Conversion factor (calibrated for the test bench).}$$

- First case:

$$AFR = \mathbf{25} \times 0,2048 = \mathbf{5,120} \text{ kg/h}$$

Air/Fuel Ratio

$$A/F = \frac{\text{AFR}}{\mathbf{m_c}}$$

- First case:

$$A/F = \frac{\mathbf{5,120}}{\mathbf{0,707}} = \mathbf{7,241}$$

Water Flow Rate

$$\text{Water Flow Rate} = WFR = \text{Rotameter Reading} \times \text{Calibration Factor}$$

With: calibration factor = 6 L/h per cm (Rotameters for engine testing often use **5–10 L/h per cm**).

- First case:

$$WFR = \mathbf{17,5} \times 6 = \mathbf{105} \text{ L/h}$$

Overall Efficiency

$$\eta_g = \frac{\text{effective power}}{\text{supplied power}} = \frac{\mathbf{P_e}}{\mathbf{m_c} \cdot \text{PCI}} = \frac{1}{\mathbf{S_c} \cdot \text{PCI}}$$

With: PCI (Lower Heating Value) = 42,5 MJ/kg (for diesel, as per ISO standards)

$$\text{PCI} = 42,5 \frac{\text{MJ}}{\text{kg}} \times \frac{1\text{kWh}}{3,6\text{MJ}} = \mathbf{11,81} \text{ kWh/kg}$$

- First case:

$$\eta_g = \frac{1}{\mathbf{0,355} \cdot 11,81} = \mathbf{0,2528} = \mathbf{23,85}\%$$

Volumetric Efficiency

$$\eta_v = \frac{\text{Air flow rate}}{\text{mass of air occupying the cylinder volume at atmospheric conditions}} = \frac{\text{Air flow rate}}{\rho_a \cdot 582 \cdot 10^{-6} \cdot n_0}$$

With:

$$\rho_a = \frac{P_a}{r \cdot T_a} = \frac{101,3}{0,287 \cdot 298} = 1,184 \text{ kg/m}^3 \text{ (ambient air density)}$$

$$(P_a = 1,013 \text{ bar} = 101,3 \text{ KPa and } T_a = 25°\text{C} = 273 + 25 = 298 \text{ K})$$

And:

$$n_0 = \frac{N}{120} \text{ (number of cycles per second for a 4-stroke engine)}$$

- First case:

$$\eta_v = \frac{\mathbf{5,120}}{1,184 \cdot 582 \cdot 10^{-6} \cdot \frac{\mathbf{1000}}{120} \cdot 3600} = \mathbf{0,2477} = \mathbf{24,77}\%$$

Table 3.3: Result of the Diesel Experience.

Rotation speed	1000	1250	1500	1750	2000	2250
Torque (N.M)	19	20	20	19	16	8
Effective power (kw)	**1,990**	**2,617**	**3,141**	**3,481**	**3,351**	**1,884**
Time (s) (8 ml)	34,2	29,5	27,2	23	25,9	33,6
Time$\times 10^{-3}$ (h) (8 ml)	**9,50**	**8,19**	**7,56**	**6,39**	**7,19**	**9,33**
Hourly consumption Kg/h	**0,707**	**0,821**	**0,889**	**1,052**	**0,935**	**0,720**
Specific consumption Kg/(kWh)	**0,355**	**0,314**	**0,283**	**0,302**	**0,279**	**0,382**
Manometer on mm H2O	25	25	29,5	37	47,5	48
Air flow rate (kg/h)	**5,120**	**5,120**	**6,042**	**7,578**	**9,728**	**9,830**
Air-fuel ratio	**7,241**	**6,236**	**6,796**	**7,203**	**10,404**	**13,653**
Inlet temperature (c°)	30	25	20	40	35	45
Outlet temperature (c°)	65	50	70	71	65	75
Rotameter (cm)	17,5	18	17,8	17,5	17,5	17,5
Water flow rate	**105**	**108**	**106,8**	**105**	**105**	**105**
Exhaust gas temperature	350	300	350	380	340	290
Overall efficiency (%)	**23,58**	**26,97**	**29,92**	**28,04**	**30,35**	**22,17**
Volumetric efficiency (%)	**24,77**	**19,81**	**19,48**	**20,95**	**23,53**	**21,13**

3.3 Gasoline Internal Combustion Engine

3.3.1 Operating Principle

Four-Stroke Cycle

The TD200 test bench utilizes a gasoline engine of four-stroke cycle, illustrated below through a pressure-volume (PV) diagram. There are four stages in the cycle:

- **Intake Stroke:**
  - Piston moves from Top Dead Center (TDC) to Bottom Dead Center (BDC).
  - Intake valve is opened; air-fuel mixture comes in at almost below atmospheric pressure.

- **Compression Stroke:**
  - Piston moves from BDC to TDC.
  - Both valves closed; air-fuel mixture compressed.
  - Spark plug ignites the mixture near TDC.
- **Power/Expansion Stroke:**
  - High-pressure gases drive the piston from TDC to BDC.
  - Valves are closed; mechanical work is being performed.
- **Exhaust Stroke:**
  - Piston is traveling from BDC to TDC.
  - Exhaust valve opens; burned gases are expelled.

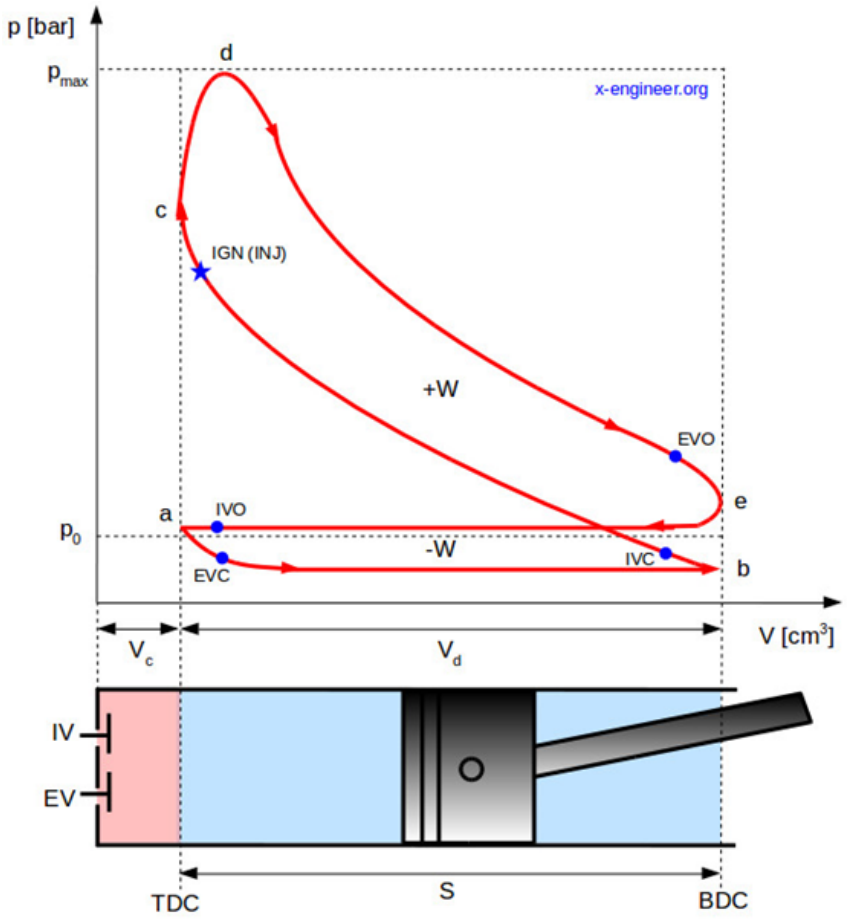

Figure 3.5: PV Diagram of a Gasoline Engine (Four-Stroke Cycle). [13]

Distribution Diagram

Valve timing optimizes engine efficiency by the precise opening/closing of valves relative to piston position. For the TD200-based gasoline engine:

- **Intake Valve:** Opens before TDC (early intake) and closes after BDC (delayed closing).
- **Exhaust Valve:** Opens before BDC (early exhaust) and closes after TDC (delayed closing).
- **Ignition Timing:** Spark is generated a little before TDC on the compression.

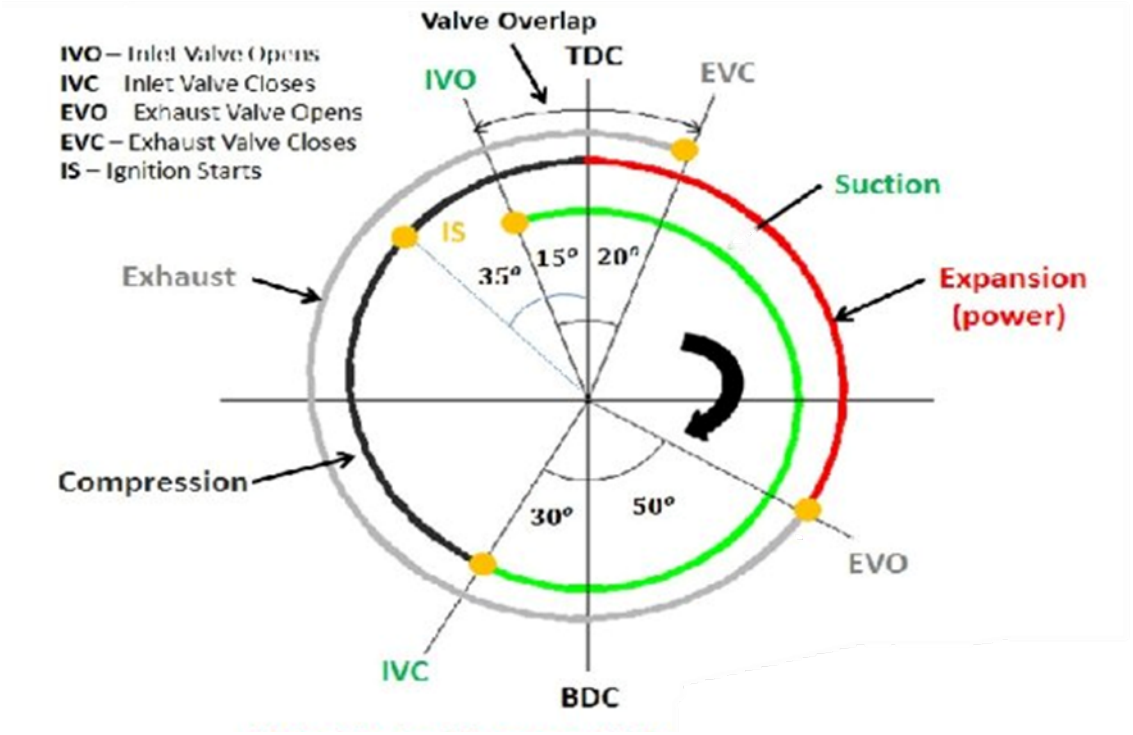

Figure 3.6: Valve timing diagram for gasoline engine. [14]

3.3.2 Performance Criteria

Effective Power

The effective power is the actual power transmitted from the engine to the crankshaft, to do mechanical work. It is calculated after subtracting all the losses inside the engine (pumping, heat, friction). Given by:

$$P_e = \omega_c \cdot \frac{N}{60000 \cdot x} = 4 \cdot \pi \cdot C \cdot \frac{N}{60000 \cdot x} \tag{3.16}$$

With:

- $x = 2$ (4-stroke engine).
- P_e: Effective power (KW).
- C: Torque (N.m).
- N: Rotation speed (tr/min).

Air Consumption

Air consumption is the mass or volumetric flow rate of air taken into an internal combustion engine during running. Given by:

$$\dot{m}_a = C_d \cdot \frac{\pi d^2}{4} \sqrt{\frac{2 \cdot P_a \cdot \Delta P}{r_{\text{air}} \cdot T_a}} \tag{3.17}$$

With:

- $\dot{m}_a$: Air consumption (kg/s).
- $C_d = 0,6$: de-rating coefficient.
- $d = 18,5 \cdot 10^{-3}$m: orifice diameter.
- P_a: ambient pressure (Pa).
- ΔP: differential pressure (Pa).
- T_a: ambient temperature.
- $r_{\text{air}} = 287 \frac{\text{J}}{\text{kg} \cdot \text{K}}$

Hourly Fuel Consumption

Hourly fuel burn is the weight or quantity of fuel consumed by an engine over one hour's running. Given by:

$$\dot{m}_c = \frac{m_c}{t} = \frac{\rho_c \cdot 8 \cdot 10^{-3}}{t} \tag{3.18}$$

with:

- $\dot{m}_c$: Hourly fuel consumption (g/h).
- m_c: Carburant mass (g).
- t: time for burning 8ml of gasoline (h).
- $\rho_c = 0,73$kg/L: for gasoline.

Specific Fuel Consumption

Specific Fuel Consumption (SFC) is a measure of an engine's fuel efficiency as it is the rate of fuel consumption per unit of power output over a period. Given by:

$$s_{\text{fc}} = \frac{\dot{m}_c}{P_e} \tag{3.19}$$

With:

- s_{fc}: Specific Fuel Consumption (g/kW.h).
- $\dot{m}_c$: Hourly fuel consumption (g/h).
- P_e: Effective power (KW).

Air/ Fuel Ratio (Mass Ratio)

Air-Fuel Ratio (AFR) – Mass Ratio is the mass ratio of air to the fuel mass fed to an internal combustion engine in running conditions. Given by:

$$d = \frac{\dot{m}_a}{\dot{m}_c} \tag{3.20}$$

With:

- d: Air/ Fuel ratio (Mass ratio).
- $\dot{m}_a$: Air consumption (kg/s).
- $\dot{m}_c$: Hourly fuel consumption (g/h).

Filling Coefficient

The fill factor is a parameter used to evaluate the efficiency with which an engine or cylinder fills its volume with an air-fuel mixture during the intake cycle.

$$\tau_r = \frac{m_a}{\rho_a \cdot V_{cc}} = \frac{V_{\text{calcul}}}{V_{\text{mesur}}} = \frac{\left(\frac{V_{cc} \cdot N}{60 \cdot x}\right)}{\left(\frac{m_a \cdot r_{\text{air}} \cdot T_a}{P_e}\right)} \tag{3.21}$$

With:

$$m_a = \frac{\dot{m}_{\text{air}}}{\rho_{\text{cycl}}}$$

$$\rho_{\text{cycl}} = \frac{\frac{N}{2}\text{tr}}{\text{min}} = \frac{N}{2} \cdot \frac{1}{60} = \frac{N}{120}\text{Hz}$$

And:

- τ_r: Fill factor.
- $V_{cc} = 200$ cm^3: The displacement (Hz).
- ρ_{cycl}: Frequency (Hz).

Effective Efficiency

Effective efficiency (also called brake thermal efficiency) is how well an engine turns fuel energy into actual usable mechanical power (like power to move a car or run a generator). Given by:

$$\eta_{\text{eff}} = \frac{3,6 \cdot 10^6}{S_{\text{fc}} \cdot \text{PCI}} \tag{3.22}$$

With:

- η_{eff}: Effective efficiency.
- s_{fc}: Specific Fuel Consumption (g/kW.h).
- PCI $= 43,8 \cdot 10^6$kJ/kg.

Mean Effective Pressure

Mean effective pressure is the hypothetical constant pressure that, if applied during the entire power stroke of an engine, would produce the same network output as one full engine cycle. Given by:

$$P_m = \frac{\omega_c}{V_{cc}} = \frac{4 \cdot \pi \cdot C}{V_{cc}} \tag{3.23}$$

With:

- P_m: Mean effective pressure (Pa).
- $V_{cc} = 200$ cm^3: The displacement (Hz).
- C: Torque (N.m).

3.3.3 Test Bench Description

TD200 Engine Test Bench

The TD200 test stand is a trolley-based, universal facility designed to carry out single-cylinder, four-stroke petrol (gasoline) engine testing. Unlike the TD43 facility, which is utilized for multi-fuel marine engines, the TD200 is specifically designed for research and teaching applications in the study of internal combustion engines with gasoline combustion performance as its primary focus.

Figure 3.7: Real Picture of the TD200 Test Bench.

Key Features

- **Hydraulic Dynamometer:**
  - Capable of absorbing up to 7.5 kW @ 7000 rpm (no significant electrical supply needed).
  - Load controlled via adjustable needle valve (water-based cooling).
  - Strain-gauged load cell for precise torque measurement (±0.5% accuracy).
- **Modular Engine Compatibility:**
  - Specifically engineered for TecQuipment's TD201/TD211 petrol engines (not diesel-compatible without modification).
  - Quick-change mounting system (dowel-and-slot alignment) to enable fast engine swaps (¡5 minutes).
- **Instrumentation and Data Acquisition:**
  - Independent instrumentation frame (vibration-isolated) with digital displays for:
    - Torque (N·m), Speed (rpm), Power (kW).
    - Air fuel usage (volumetric flow rate).
    - Exhaust gas temperature (°C).
  - Optional VDAS® software for real-time data logging and performance curve plotting.
- **Citizen's Safety Compliance:**
  - Self-sealing fuel couplings (color-coded for gasoline).
  - Acoustic silencer for sound dampening.
  - Removable fuel tanks discourage unauthorized use.

Instrumentation and Measured Parameters

The TD200's right-hand instrumentation panel includes:

Table 3.4: Measured Parameters and Instrumentation.

Parameter	**Measuring Instrument**
Engine Speed	Proximity sensor + digital tachometer
Torque (N.m)	Hydraulic dynamometer + load cell
Effective Power	Calculated (Torque × Speed)
Fuel Consumption	Volumetric fuel gauge (AVF1 or DVF1)
Air Consumption	Air-box + orifice plate + pressure transducer
Exhaust Temperature	K-type thermocouple
Ambient Air Temperature	Thermocouple + digital display

Advanced Add-Ons (Optional)

- ECA100 Engine Cycle Analyzer: For p-V diagrams and combustion analysis.
- Exhaust Gas Calorimeter (TDX00a): Measures heat loss in exhaust gases.

Engine Specifications

Four-Stroke Petrol Engine, single-cylinder, air-cooled, spark-ignition gasoline engine. Its technical specifications are provided in the following table:

Table 3.5: Technical Specifications.

Parameter	**Value**
Displacement	150–250 cc
Compression Ratio	8:1 to 10:1 (fixed, optimized for petrol)
Max Power	3–4 kW @ 3000 rpm
Max Torque	12–15 N·m
Speed Range	1000–7000 rpm
Fuel System	Carbureted (no direct injection/turbocharging)

3.3.4 Purpose of the Tests

- Verify ignition system performance (spark quality, timing, voltage stability).
- Diagnose faults in distributors, coils, spark plugs, and ignition modules.
- Validate timing advance curves under simulated engine loads.

3.3.5 Operating Procedure

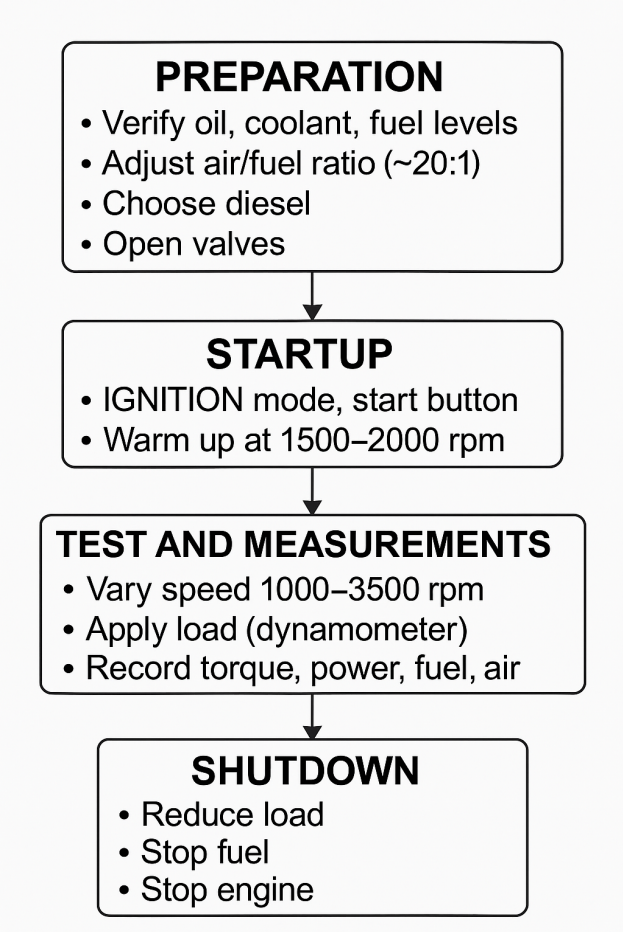

Figure 3.8: Gasoline Engine Experimental Procedure (TD20).

3.3.6 Calculation

Effective Power

$$P_e = \omega_c \cdot \frac{N}{60000 \cdot x} = 4 \cdot \pi \cdot \mathbf{C} \cdot \frac{\mathbf{N}}{60000 \cdot x}$$

- First case:

$$P_e = 4 \cdot \pi \cdot \mathbf{11,1} \cdot \frac{\mathbf{1410}}{60000 \cdot 2} = \mathbf{1,639} \text{ KW} = \mathbf{1639} \text{ W}$$

Air Consumption

$$\dot{m}_a = C_d \cdot \frac{\pi d^2}{4} \sqrt{\frac{2 \cdot P_a \cdot \Delta P}{r_{\text{air}} \cdot T_a}}$$

- First case:

$$\dot{m}_a = 0,6 \cdot \frac{\pi(18,5 \cdot 10^{-3})^2}{4} \sqrt{\frac{2 \cdot \mathbf{1,017 \cdot 10^5 \cdot 55}}{287 \cdot \mathbf{296,1}}} = \mathbf{1,850 \cdot 10^{-3}} \text{ kg/s} = \mathbf{6,660} \text{ kg/h}$$

Hourly Fuel Consumption

$$\dot{m}_c = \frac{m_c}{t} = \frac{\rho_c \cdot 8 \cdot 10^{-3}}{t} = \frac{0,73 \cdot 8 \cdot 10^{-3}}{t} = \frac{5,84 \cdot 10^{-3}}{\mathbf{t}}$$

- First case:

$$\dot{m}_c = \frac{5,84 \cdot 10^{-3}}{\mathbf{11,21 \cdot 10^{-3}}} = \mathbf{0,521} \text{ kg/h}$$

Specific Fuel Consumption

$$s_{\text{fc}} = \frac{\dot{m}_c}{P_e}$$

- First case:

$$s_{\text{fc}} = \frac{\mathbf{0,521}}{\mathbf{1,639}} = \mathbf{0,318} \text{ kg/kW.h}$$

Air/ Fuel Ratio (Mass Ratio)

$$d = \frac{\dot{m}_a}{\dot{m}_c}$$

- First case:

$$d = \frac{\mathbf{6,66}}{\mathbf{0,521}} = \mathbf{12,783}$$

Filling Coefficient

$$\tau_r = \frac{m_a}{\rho_a \cdot V_{cc}} = \frac{V_{\text{calcul}}}{V_{\text{mesur}}} = \frac{\left(\frac{V_{cc} \cdot N}{60 \cdot x}\right)}{\left(\frac{m_a \cdot r_{\text{air}} \cdot T_a}{P_e}\right)}$$

$$\tau_r = \frac{\left(\frac{0,0002 \cdot \mathbf{N}}{60 \cdot 2}\right)}{\left(\frac{\mathbf{m_a} \cdot 287 \cdot \mathbf{T_a}}{\mathbf{P_e}}\right)}$$

With:

$$m_a = \frac{\dot{m}_{\text{air}}}{\rho_{\text{cycl}}}$$

$$\rho_{\text{cycl}} = \frac{\frac{N}{2}\text{tr}}{\text{min}} = \frac{N}{2} \cdot \frac{1}{60} = \frac{N}{120}$$

So:

$$\tau_r = \frac{\left(\frac{0{,}0002 \cdot \mathbf{N}}{60 \cdot 2}\right)}{\left(\frac{120 \cdot \frac{\dot{\mathbf{m}}_{\mathbf{air}}}{\mathbf{N}} \cdot 287 \cdot \mathbf{T_a}}{\mathbf{P_e}}\right)}$$

- First case:

$$\tau_r = \frac{\left(\frac{0{,}0002 \cdot \mathbf{1410}}{60 \cdot 2}\right)}{\left(\frac{120 \cdot \frac{\mathbf{1{,}85 \cdot 10^{-3}}}{\mathbf{1410}} \cdot 287 \cdot \mathbf{21{,}1}}{\mathbf{1639}}\right)} = \mathbf{4{,}040}$$

Effective Efficiency

$$\eta_{\text{eff}} = \frac{3{,}6 \cdot 10^6}{\mathbf{S_{fc}} \cdot 43{,}8 \cdot 10^6}$$

- First case:

$$\eta_{\text{eff}} = \frac{3{,}6 \cdot 10^6}{\mathbf{0{,}318} \cdot 43{,}8 \cdot 10^6} = \mathbf{0{,}2585} = \mathbf{25{,}85}\%$$

Mean Effective Pressure

$$P_m = \frac{\omega_c}{V_{cc}} = \frac{4 \cdot \pi \cdot C}{V_{cc}} = \frac{4 \cdot \pi \cdot \mathbf{C}}{0{,}0002}$$

- First case:

$$P_m = \frac{4 \cdot \pi \cdot \mathbf{11{,}1}}{0{,}0002} = \mathbf{697433{,}57}\ \text{Pa} = \mathbf{6{,}97}\ \text{bar}$$

Table 3.6: Result of the Gasoline Experience.

Rotation speed (tr/min)	**1410**	**1710**	**2014**	**2310**	**2610**	**3036**	**3599**
Torque (N.M)	11,1	12,2	12,9	13,4	13,4	13,5	10,9
Effective power (Kw)	**1,639**	**2,185**	**2,721**	**3,241**	**3,662**	**4,292**	**4,108**
Effective power (w)	**1639**	**2185**	**2721**	**3241**	**3662**	**4292**	**4108**
Ambient pressure$\times 10^5$(Pa)	1,017	1,017	1,017	1,017	1,018	1,018	1,018
Ambient temp(°C)	21,1	20,8	20,9	20,8	20,9	21,9	23,2
Ambient temp (K)	**296,1**	**295,8**	**295,9**	**295,8**	**295,9**	**296,9**	**298,2**
Differential pressureΔP(Pa)	55	86	97	146	187	259	302
Air-cons$\times 10^{-3}$ (kg/s)	**1,850**	**2,315**	**2,458**	**3,016**	**3,413**	**4,010**	**4,321**
Air-cons (kg/h)	**6,660**	**8,334**	**8,849**	**10,858**	**12,287**	**14,436**	**15,556**
Time (s) (8 ml)	40,34	30,38	33,57	24,87	23,88	19,20	17,20
Time$\times 10^{-3}$ (h) (8 ml)	**11,21**	**8,44**	**9,33**	**6,91**	**6,63**	**5,33**	**4,78**
Hourly-cons Kg/h	**0,521**	**0,692**	**0,626**	**0,845**	**0,881**	**1,096**	**1,222**
Speci-cons Kg/(KW.h)	**0,318**	**0,317**	**0,230**	**0,261**	**0,241**	**0,255**	**0,297**
Air/Fuel ratio	**12,783**	**12,043**	**14,136**	**12,850**	**13,947**	**13,172**	**12,730**
Filling coefficient	**4,040**	**6,342**	**10,397**	**13,341**	**16,924**	**21,800**	**25,649**
Effective efficiency (%)	**25,85**	**25,93**	**35,74**	**31,49**	**34,10**	**32,23**	**27,67**
M E P (Pa)	**6,97**	**7,67**	**8,11**	**8,42**	**8,42**	**8,48**	**6,85**
Exhaust gas temp °C	469	526	542	600	615	668	725

3.4 Conclusion

This chapter presented a detailed experimental study comparing the performance of diesel and gasoline internal combustion engines. The experiments were conducted using specialized test benches (TD43 for diesel and TD200 for gasoline) under controlled conditions, with systematic variations in rotational speeds and precise measurements of key parameters such as torque, fuel consumption, airflow rate, and exhaust temperatures. The data collected enabled the calculation of critical performance indicators, including effective power, specific fuel consumption, thermal efficiency, and volumetric efficiency. The results from both engines were analyzed separately, providing insights into their respec-

tive operational characteristics and efficiencies. The diesel engine demonstrated notable performance in terms of torque and specific fuel consumption at lower speeds, while the gasoline engine exhibited higher power output and efficiency at elevated speeds. These findings highlight the inherent trade-offs between the two technologies, influenced by factors such as combustion mechanisms, compression ratios, and fuel properties. In Chapter 5 (Results and Discussion), the results of these experiments will be compared in depth. Graphical representations of the data will be used to illustrate the differences and similarities between the diesel and gasoline engines, focusing on their performance metrics across varying operational conditions. This comparative analysis will provide a clearer understanding of the strengths and limitations of each engine type, contributing to the broader goal of optimizing engine performance and reducing environmental impact.

Chapter 4

Computational Modeling (ANSYS)

4.1 Introduction

This chapter presents the computational modeling approach for simulating methane-air combustion in an internal combustion engine using ANSYS. The study focuses on establishing the fundamental framework for combustion analysis, including the mathematical formulation of governing equations (continuity, momentum, and energy), turbulence modeling (k-ε standard and RNG approaches), and combustion modeling techniques. The first phase of the simulation work covers the essential preprocessing steps, including the creation of the combustion chamber geometry and the generation of a high-quality computational mesh. These preparatory steps lay the foundation for subsequent numerical analysis of the combustion process under varying operating conditions. The chapter details the methodology employed in setting up the simulation environment and the considerations taken into account to ensure accurate representation of the physical system.

4.2 Mathematical Modeling

4.2.1 Fundamental Equations of Fluid Dynamics

These equations represent the mathematical formulation of three fundamental physical principles that form the foundation of fluid dynamics [17]:

- Conservation of mass.

- Conservation of momentum.
- Conservation of energy.

The Continuity Equation (Mass Conservation Equation)

The continuity equation, formulated in the 19th century by the French mathematician and physicist Augustin-Louis Cauchy, is a cornerstone of fluid dynamics. It mathematically expresses the principle of mass conservation within a fluid flow. This principle asserts that the rate of mass entering or leaving a control volume must be equal to the rate of change of mass within that volume. The non-conservative form of the continuity equation is given by [17]:

$$\frac{\partial \rho}{\partial t} + \frac{\partial \left(\rho u_i\right)}{\partial x_i} = 0 \tag{4.1}$$

This equation ensures that mass is neither created nor destroyed in the system.

When considering the conservation of mass for a chemical species (partial mass balance), the continuity equation is expressed as [17]:

$$\nabla \cdot (\rho D_k \nabla Y_k) = \dot{W}_k \tag{4.2}$$

where:

- Y_k: is the mass fraction of species k.
- D_k: is the diffusion coefficient (or diffusion velocity) of species k.
- $\dot{W}_k$: is the mass production rate per unit volume of species k due to chemical reactions.

Alternatively, the equation can be written in the following general form [17]:

$$\frac{\partial \rho Y_k}{\partial t} + \frac{\partial}{\partial x_i}(\rho u_i Y_k + J_{i,k}) = \dot{W}_k \quad \text{for } k = 1, \ldots, N \tag{4.3}$$

where:

- $J_{i,k}$: is the **i-th component of the diffusion flux** of species k.

- $\dot{W}_k$: is the reaction rate of species k.

By definition, the total mass diffusion and the total reaction rate across all species satisfy the following conditions [17]:

$$\sum_{k=1}^{N} J_{i,k} = 0 \quad \text{and} \quad \sum_{k=1}^{N} \dot{W}_k = 0 \tag{4.4}$$

These constraints ensure overall mass conservation in multicomponent reacting flows.

Momentum Equation: The Navier-Stokes Equations

The Navier-Stokes equations represent the momentum conservation law in fluid dynamics. They are typically written in differential form and describe how the velocity of fluid particles evolves under the influence of various forces. These include:

- Pressure gradients,
- Viscous forces, and
- External body forces (e.g., gravity).

The general form of the momentum equation is [17]:

$$\rho \left(\frac{\partial u_i}{\partial t} + u_j \frac{\partial u_i}{\partial x_j} \right) = -\frac{\partial p}{\partial x_i} + \frac{\partial \tau_{ij}}{\partial x_j}$$

Where:

- ρ: mass density (kg/m^3).
- u_i: velocity component in the i-direction.
- p: pressure.
- τ_{ij}: viscous stress tensor.

Energy Equation

The energy equation expresses the conservation of energy within a fluid system and is based on the first law of thermodynamics $\Delta U = Q - W$.[17]

It accounts for the changes in internal, kinetic, and potential energy of the fluid. The general differential form of the energy conservation equation can be written as [17]:

$$\frac{\partial}{\partial t}(\rho e + \frac{1}{2}\rho u_i u_i) + \frac{\partial}{\partial x_j}\left[\rho u_j(h + \frac{1}{2}u_i u_i)\right] = \frac{\partial q_j}{\partial x_j} - \frac{\partial}{\partial x_j}(u_i \tau_{ij}) \tag{4.6}$$

Where:

- e: is the **specific internal energy**.
- h: is the **specific enthalpy**.

$$h = e + \frac{p}{\rho} \tag{4.7}$$

- q_j: is the **heat flux vector**, defined by **Fourier's law** as:

$$q_j = -\lambda \frac{\partial T}{\partial x_j} \tag{4.8}$$

With:

- λ: being the thermal conductivity.
- T: the temperature.

The viscous dissipation term in the energy equation uses the velocity gradient tensor and is given by [17]:

$$\tau_{ij} = 2\mu S_{ij} + \lambda \delta_{ij} \frac{\partial u_k}{\partial x_k} \tag{4.9}$$

Where:

- S_{ij}: is the symmetric part of the velocity gradient tensor,
- μ: is the dynamic viscosity,
- δ_{ij}: is the Kronecker delta.

The Transportation Equation of Chemical Species

$$\frac{\partial \rho y}{\partial t} + \sum_{a=1}^{3} \frac{\partial (\rho v y)}{\partial x} = \sum_{a=1}^{3} \frac{\partial \left(-j_{i,a}\right)}{\partial x} + \rho w \tag{4.10}$$

$$\frac{\partial \rho u}{\partial t} + \sum_{a=1}^{3} \frac{\partial (\rho v y)}{\partial x} = \sum_{a=1}^{3} \frac{\partial \left(-j_{q,a} - \sum_{i=1}^{3} j_{i,a} + \sum_{=1}^{3} v\tau\right)}{\partial x} + \sum_{=1}^{3} vF \tag{4.11}$$

The molecular diffusion flux equation $j_{i,a}$, the diffusion of mass $j_{q,a}$, the quantity of movement τ, must be expressed with their aforementioned expressions the energy equation can also be written by showing the reaction rate to process the reactive flow. [17]

$$h = \overline{c}T + \sum_{i=1}^{n} y h_{i,0} \tag{4.12}$$

$$u = \overline{c_v}T + \sum_{i=1}^{n} y h_{i,0} \tag{4.13}$$

4.2.2 Turbulence

Turbulent flows are characterized by fluctuating velocity fields. In addition to causing the transported amounts to fluctuate, these fluctuations also mix transported quantities including momentum, energy, and species concentration. These fluctuations are too computationally expensive to directly mimic in real-world engineering computations since they can occur at small scales and high frequencies. Alternatively, the small scales can be eliminated from the instantaneous governing equations by temporal averaging, ensemble averaging, or other manipulations that provide a modified set of equations that require less computing power to solve. [17]

Characteristics of Turbulent Flows

The major characteristics of a turbulent flow regime are [17]:

- Diffusivity
- Irregularity
- Large Reynolds number

- 3D vorticity fluctuations
- Dissipation
- Continuum

The instantaneous value ϕ, of any flow property (velocity, temperature, pressure, etc.) can be expressed as the sum of a mean component and a fluctuating component. Hence any flow variable is given as the expression [17] :

$$\phi = \overline{\phi} + \phi' \tag{4.14}$$

4.2.3 Effect of Turbulence on Time-Averaged Navier-Stokes Equations

Turbulent flows depict eddying motions over a wide variety of length scales, constituting a key contrast from laminar flow visualizations. Turbulent flows with a high Reynolds number and a 0.1 by 0.1 m flow domain have eddies as small as 10 to 100 μm. In order to characterize processes at all length scales, this calls for computational meshes of 10^9 to 10^{12} points.

Significant advances in computer hardware are needed to solve the time-dependent Navier-Stokes equations of completely turbulent flows at high Reynolds numbers, which is an amazing computing challenge. [17]

Reynolds Equations

The mean Φ of a flow property ϕ is given by the relation [17]:

$$\Phi = \frac{1}{\Delta t}\int_0^{\Delta t} \phi(t)dt \tag{4.15}$$

Theoretically, Δt should approach infinity; nonetheless, Δt is sufficiently long if it is greater than the time scales of the property ϕ's slowest changes (caused by the biggest eddies). For stable mean flows, this definition of a flow property's mean is sufficient. In time-dependent flows, the so-called ensemble average the mean of a property at time t

is determined by averaging the instantaneous values of the property over a significant number of repeated experiments.

The flow property ϕ is time dependent and can be thought of as a sum of a steady mean component Φ and a time-varying fluctuating component ϕ' with zero mean value; hence [17]:

$$\phi(t) = \Phi + \phi'(t) \tag{4.16}$$

Or writing in an implicit manner [17]:

$$\phi = \Phi + \phi' \tag{4.17}$$

The time average of the fluctuations ϕ' is, by definition, zero [17]:

$$\phi' = \frac{1}{\Delta t}\int_0^{\Delta t} \phi'(t)dt \equiv 0 \tag{4.18}$$

The kinetic energy k (per unit mass) associated with turbulence is defined as [17]:

$$k = \frac{1}{2}(\overline{u'^2} + \overline{v'^2} + \overline{w'^2}) \tag{4.19}$$

The turbulence intensity Ti is linked to kinetic energy and a reference means flow velocity as follows [17]:

$$Ti = \frac{\left(\frac{2}{3}k\right)^{1/2}}{U_{ref}} \tag{4.20}$$

To investigate the effects of fluctuations, the flow variables $\overrightarrow{u}$, p, ρ, h, and e are replaced by the sum of a mean and a fluctuating component. Thus [17]:

$$\rho = \overline{\rho} + \rho', \quad u_i = \overline{u_i} + u_i', \quad p = P + p', \quad h = \overline{h} + h', \quad e = \overline{e} + e'$$

The above equations indicate the new terms that were added as a result of time averaging. Because of the velocity variations, these terms involve products of variable velocities and

represent convective momentum transfer. These terms are typically positioned on the right side of the aforementioned equations to represent their function as extra turbulent stresses on the U, V, and W mean velocity components.

Hence, the equations (4.1), (4.5), (4.6), and (1.5) get modified to [17]:

$$\frac{\partial \overline{\rho}}{\partial t} + \frac{\partial(\overline{\rho u}_j)}{\partial x_i} = 0 \tag{4.21}$$

$$\frac{\partial(\rho \overline{u}_j)}{\partial t} + \frac{\partial(\overline{\rho u}_i \overline{u}_j)}{\partial x_j} = \frac{\partial \overline{\rho}}{\partial x_i} + \frac{\partial(\overline{\tau}_{ij})}{\partial x_i} - \frac{\partial(\overline{\rho u''_i u''_j})}{\partial x_i} \tag{4.22}$$

$$\begin{aligned} &\frac{\partial}{\partial t}\left[\rho\left(\overline{e} + \frac{\overline{u}_i \overline{u}_i}{2}\right) + \frac{\overline{\rho u''_i u''_i}}{2}\right] + \frac{\partial}{\partial x_j}\left[\rho \overline{u}_j\left(\overline{h} + \frac{\overline{u}_i \overline{u}_i}{2}\right) + \frac{\overline{\rho u''_i u''_i}}{2}\right] \\ &= \frac{\partial}{\partial x_j}\left[-\overline{q}_j - \overline{\rho u''_j h''} + \overline{u''_i \tau_{ij}} - \frac{\overline{\rho u''_j u''_i u''_i}}{2}\right] + \frac{\partial}{\partial t}\left[\overline{u}_i\left(\overline{\tau}_{ij} - \rho u''_i u''_j\right)\right] \end{aligned} \tag{4.23}$$

$$\overline{P} = \overline{pr}^{\frac{\gamma}{\gamma-1}} \tag{4.24}$$

The extra terms:

- $\overline{\rho u'_i u'_j}$: Reynolds stress tensor.
- $\overline{\frac{\rho u''_i u''_i}{2}}$: turbulent kinetic energy.
- $\overline{\rho u''_j h''}$: turbulent heat flux.
- $\overline{u''_i \tau_{ij}}$: molecular diffusion.
- $\overline{\frac{\rho u''_j u''_i u''_i}{2}}$: turbulent energy transport.

4.2.4 Turbulence Models

A computer process to conclude the system of mean flow equations and solve a relatively large range of flow issues is known as a turbulence model. Generally, in engineering, one just looks for turbulence's impacts on the mean flow. In a general-purpose CFD code, a turbulence model needs to be accurate, easy to use, low computational cost, and have a broad range of applications. Below is a classification of the several turbulence models used in CFD [17]:

- **BASED ON RANS (CLASSICAL MODELS) - REYNOLDS AVERAGE NAVIER-STOKES**
  - Zero equation-Mixing length model.
  - One equation Spalart-Allmaras model.
  - Two equation – The k-ε and k-ω models.
  - Seven equation – Reynolds stress model.

The k-ε Standard Model

This model emphasizes the mechanisms affecting turbulent kinetic energy based on the modeling of two transport equations. The first is that of the turbulent kinetic energy (κ), and the second is its viscous dissipation rate (ε). [17]

$$\frac{\partial\left(\bar{\rho}k\right)}{\partial t}+\frac{\partial\left(\overline{\rho u}_{j}k\right)}{\partial x_{j}}=2\tau_{RIJ}\frac{\partial\widetilde{U}_{l}}{\partial x_{j}}-\rho\bar{\varepsilon}+\left(\frac{\mu_{t}}{\sigma_{k}}+\mu\right)\left(\frac{\partial k}{\partial x_{j}}\right)+P_{b} \tag{4.25}$$

$$\frac{\partial\left(\bar{\rho}\varepsilon\right)}{\partial t}+\frac{\partial\left(\bar{\rho}u_{j}\varepsilon\right)}{\partial x_{j}}=C_{\varepsilon1}\frac{\bar{\rho}\varepsilon}{k}\tau_{RIJ}\frac{\partial\widetilde{U}_{i}}{\partial x_{j}}-C_{\varepsilon2}\frac{\bar{\rho}\varepsilon^{2}}{k}+\left(\frac{\mu_{t}}{\sigma_{\varepsilon}}+\mu\right)\frac{\partial k}{\partial x_{j}}+C_{\varepsilon1}C_{\varepsilon3}\frac{\varepsilon\overline{\rho}}{k}\frac{\varepsilon}{k}P_{b} \tag{4.26}$$

Thus, the turbulent dynamic viscosity μ_t is calculated by [17]:

$$\mu_{t}=\rho C_{\mu}\frac{k^{2}}{\varepsilon} \tag{4.27}$$

$$C_{\mu}=0.09$$

P_b, the production of turbulent kinetic energy due to volume forces.

$$P_{b}=\beta^{''}g_{i}\frac{\mu_{t}}{Pr_{t}}\frac{\partial T}{\partial x_{i}} \tag{4.28}$$

Where:

g_i is the component of the vector gravity in direction i.

$Pr_t = 0.85$ or the model k-ε standard and realizable.

$C_{\varepsilon 1}\frac{\bar{\rho}\varepsilon}{k}\tau_{RIJ}\frac{\partial \widetilde{U}_i}{\partial x_j}$ dissipation production deadline.

$2\tau_{RIJ}\frac{\partial \widetilde{U}_i}{\partial x_j}$ term of production of turbulent kinetic energy.

$C_{\varepsilon 1}\frac{\bar{\rho}\varepsilon}{k}$ dissipation term.

$\bar{\rho}\varepsilon$ Dissipation term turbulent kinetic energy.

$\left(\frac{\mu_t}{\sigma_\varepsilon}+\mu\right)\frac{\partial k}{\partial x_j}$ Term of the sum of turbulent kinetic energy diffusion and transport.

4.2.5 Combustion Modeling

Flames are dynamic phenomena that involve the transport of gases through convection and diffusion. Gases escape at a specific speed due to reservoir pressure, creating a reaction zone in the mixture. This zone is formed when gases and air mix continuously. As gases escape, heat is released, and the gas escape and heat released also mix. This process is explained by thermodynamics laws, mathematical models, and the impact of turbulence on combustion and the impact of burning on turbulentness. [17]

4.2.6 Species Transport (Models of Combustion)

ANSYS FLUENT predicts the local mass fraction of each chemical species, Y_i by solving a convection-diffusion equation specific to the i-th species. This equation represents the conservation of mass and has a general form [17]:

$$\frac{\partial}{\partial t}\left(\rho Y_i\right)+\nabla\cdot\left(\rho\overrightarrow{v}Y_{iv}\right)=-\nabla.\overrightarrow{J}_i+R_i+S_i \tag{4.29}$$

Where:

Y is the rate of creation by addition from the scattered phase plus any user-defined sources, and N is the net rate of formation of species Y through chemical reaction.

For $N-1$ species, an equation of this type will be solved, where N is the total number of fluid phase chemical species in the system.

The i-th mass fraction is calculated as one minus the sum of the $N-1$ solved mass fractions since the mass fraction of the species must add up to unity. To reduce numerical

inaccuracy, the species with the biggest mass fraction overall, such as $N-2$ in the case of air as the oxidant, should be chosen as the i-th species.

Eddy Dissipation Model

This work deals with the problem of non-premixed turbulent flames (diffusion). This model was therefore used for the modeling of reaction rates. The eddy dissipation model is based on the work of Magnussen and Hjertager, in which chemistry is considered very fast relative to turbulence. In this case, combustion, which is controlled only by turbulence, transports the mixture of fresh gases and hot products into the reaction zone where chemical kinetics is rapidly carried out. The latter can therefore be neglected. [17]

$$\begin{aligned} R_{i,r} &= v_{i,r}^{'} M_{w,i} A \rho \left(\frac{\varepsilon}{k}\right) \min\left(\frac{Y_R}{v_R^{'} M_{w,R}}\right) \\ R_{i,r} &= v_{i,r}^{'} M_{w,i} A B \rho \frac{\varepsilon}{k} \left(\frac{\sum pY_p}{\sum_J^N v_{j,r}^{''} M_{w,j}}\right) \end{aligned} \tag{4.30}$$

Where:

- Y_R: is the mass fraction of a species p in the products; Yr: is the mass fraction of a species r in the reagents.
- A and B: are empirical constants with values 4 and 5 respectively.
- $M_{w,i}$: is the molar mass of the species i.

4.3 Numerical Resolution

4.3.1 Pressure-Based Solver

Density remains constant and independent of pressure in the case of an incompressible flow. In this scenario, the coupling of pressure and velocity affects the solution of the flow field, and the resulting velocity field satisfies the continuity equation when the appropriate pressure field is substituted into the conservation equations for momentum.

The pressure-based solver allows you to solve your flow problem separately or in a coupled manner. Different algorithms are used depending on the case. These five pressure-velocity coupling algorithms are: SIMPLE, SIMPLER, SINGLE, PISO, and Coupled.

The pressure-based solver is chosen for its ability to handle combustion and compressible flow simulations. It utilizes the projection method to ensure mass conservation in the velocity field by solving a pressure equation derived from the continuity and momentum equations. [17]

4.3.2 Meshing

A mesh is created by dividing a physical domain into smaller, typically convex subdomains. An EDP is resolved by it. There are two main categories of numerical simulation codes in fluid mechanics. The two classes, structure mesh and non-structure mesh, are equivalent to the types of mesh utilized in simulations. Each of these two mesh types has benefits and drawbacks. [17]

Structured Mesh

A structured mesh is a line of mesh or a mesh by space direction such that, in dimensions 2 and 3, each node of the mesh can be uniquely identified by a double (x, y) or a triple (x, y, z). The table below enumerates this mesh's benefits and drawbacks. [17]

Table 4.1: Advantages and Disadvantages of Structured Mesh. [17]

Advantages	**Disadvantages**
- Their description is light, and with a small number of parameters, it is possible to define a whole mesh.	- Human expertise is necessary. A structured mesh must meet a specific specification for the charges.
- Their modification is very easy, on the one hand because of the few parameters to modify and, on the other hand, because of the possibility of using projection algorithms.	- They do not allow complex geometries to be woven into a single block. For example, it is impossible to mesh a disk through a single-block structure mesh.
- Calculations are generally faster in a structured mesh than in an unstructured mesh.	- Its implementation is difficult.

Non-Structured Mesh

An unstructured mesh is constructed with at least the following elements [17]:

- The number of nodes in the grid, and each node being identified by the coordinates (X_i, Y_i, Z_i).
- The number of volumes in the mesh, with each volume being defined by the N tops of the cell, and this is the connectivity table of the elements of the mesh.

The advantages and disadvantages of this mesh are listed in the table below [17]:

Table 4.2: Advantages and Disadvantages of Non-Structured Mesh. [17]

Advantages	**Disadvantages**
- Their generation is more automatic.	- Their generation requires more computational resources.
- They are adapted to complex shapes without the operator having to interfere too much.	- They may require more memory and processing power compared to structured meshes.
- They require fewer points compared to structured mesh for the same geometry.	- Solution accuracy may be slightly lower for some applications.

4.3.3 Computational Fluid Dynamics

Through computer-based simulation, systems including fluid flow, heat transport, and related phenomena like chemical reactions are analyzed in computational fluid dynamics, or CFD. The method has a broad variety of industrial and non-industrial application sectors and is highly powerful.

The primary cause of CFD's lag is the underlying behavior's extreme complexity, which makes it impossible to describe fluid flows in a way that is both sufficiently complete and inexpensive.

Fluent is a CFD software capable of modeling fluid flows involving complex physical phenomena such as turbulence, thermal transfer, chemical reactions, and multiphase flows

in complex geometry areas. It is widely used in the aerospace industry. It offers a simple interface, allowing the user access to the functions required for the calculation of the solution and the display of the results.

The numerical techniques that can solve fluid flow issues are the foundation of CFD codes. All commercial CFD packages feature sophisticated user interfaces for entering problem parameters and examining outcomes, making their solution capabilities easily accessible.

Thus, there are three primary components to all codes [17]:

- Preprocessor.
- Solver.
- Post-processor.

4.4 Combustor Modeling and FLUENT Setup

4.4.1 Combustion Chamber Geometry

This Figure shows a combustion chamber model for an internal combustion engine (ICE) piston, created in Ansys. It has a wider top section and a narrower cylindrical section below.

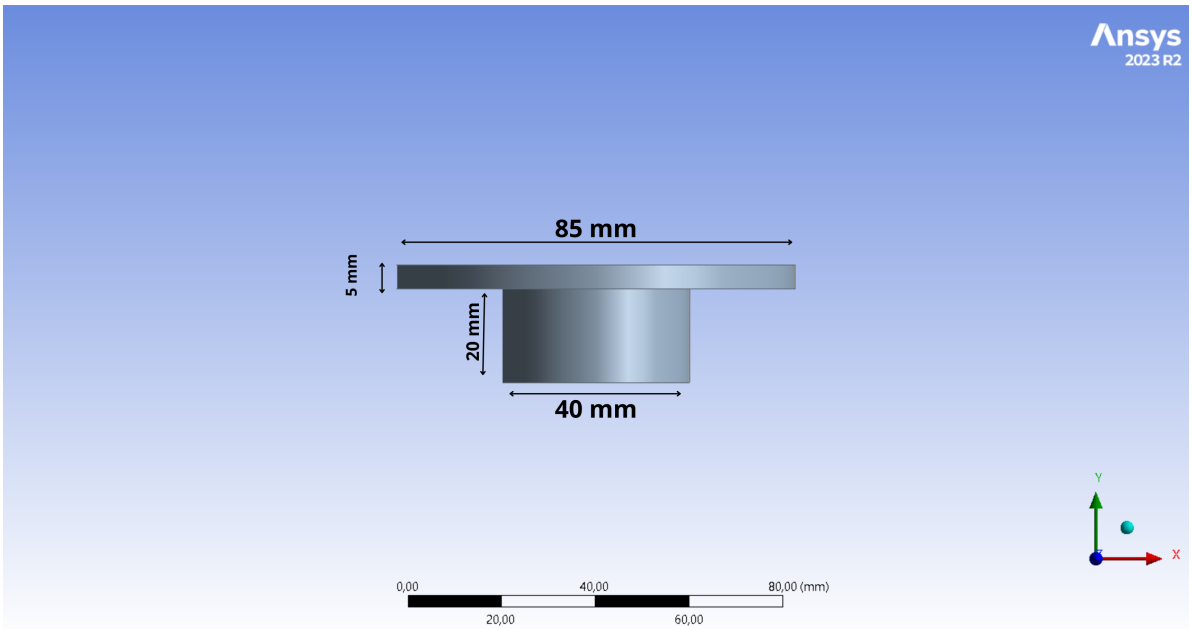

Figure 4.1: IC Engine Combustion Chamber Geometry and Dimensions.[16]

4.4.2 Combustion Chamber Mesh

This image shows the meshed model of the internal combustion engine piston chamber in Ansys. The mesh is composed of many small elements covering the entire geometry, including the wider top section and the narrower cylindrical section below.

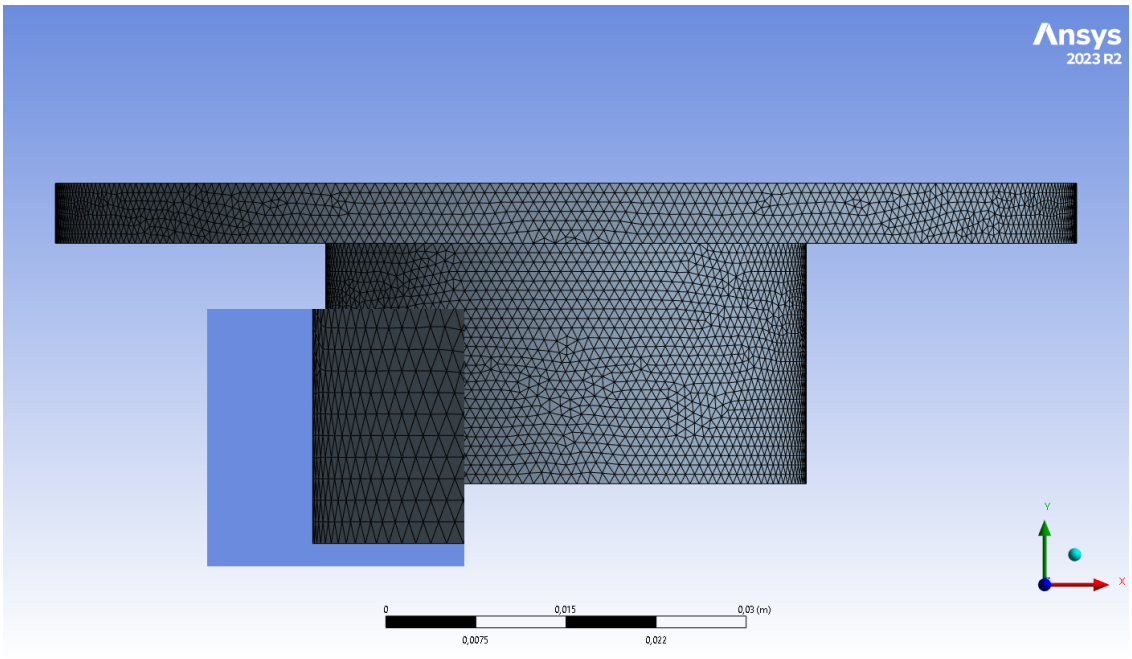

Figure 4.2: Combustion chamber mesh.

Orthogonal Quality

We use the orthogonality quality metric to assess whether our mesh is well-structured. This metric has an established standard, as shown in Figure 4.3. By comparing our interval from Figure 4.4 with this standard, we observe that the orthogonality values of our mesh fall between 0.2 and 1. This indicates that our meshing is of good quality and within the acceptable range.

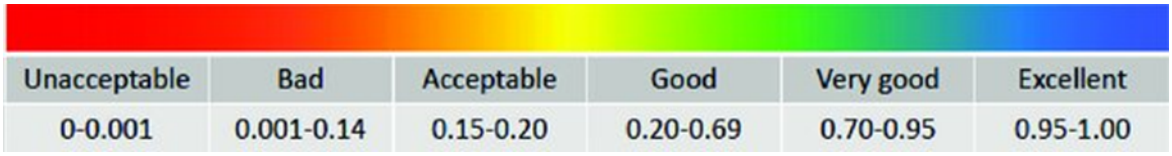

Figure 4.3: orthogonal quality mesh spectrum. [17]

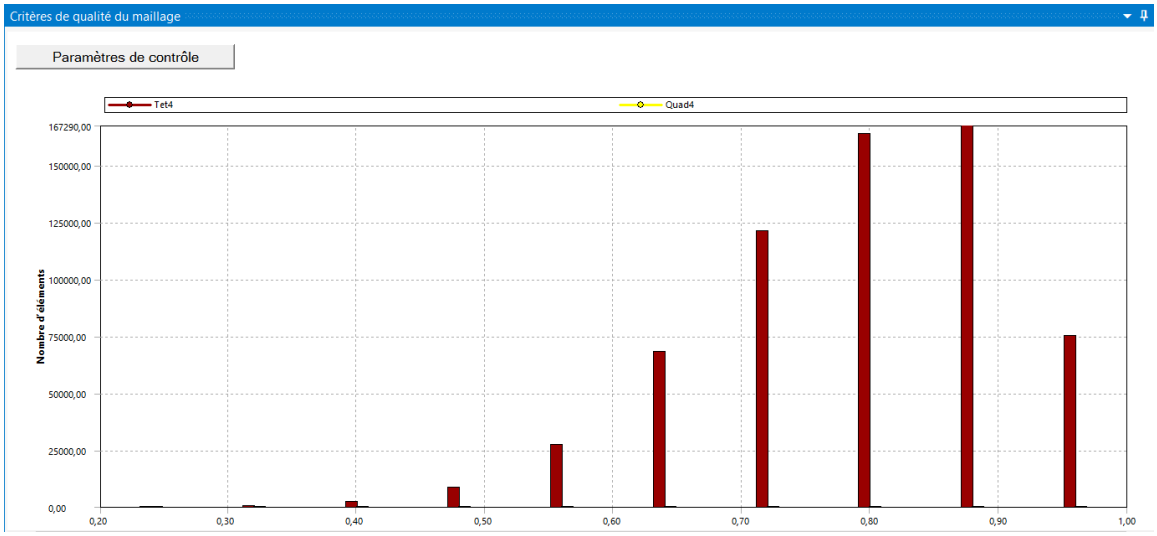

Figure 4.4: Orthogonal quality of IC engine combustion chamber.

As we can see in Figure 4.5, which represents the number of elements and nodes, our mesh includes both 633177 elements and 116104 nodes.

Statistiques	
Nœuds	116104
Eléments	633177

Figure 4.5: Statistic of mesh.

4.4.3 Boundary Conditions

Naming Section

We name all boundary wall:

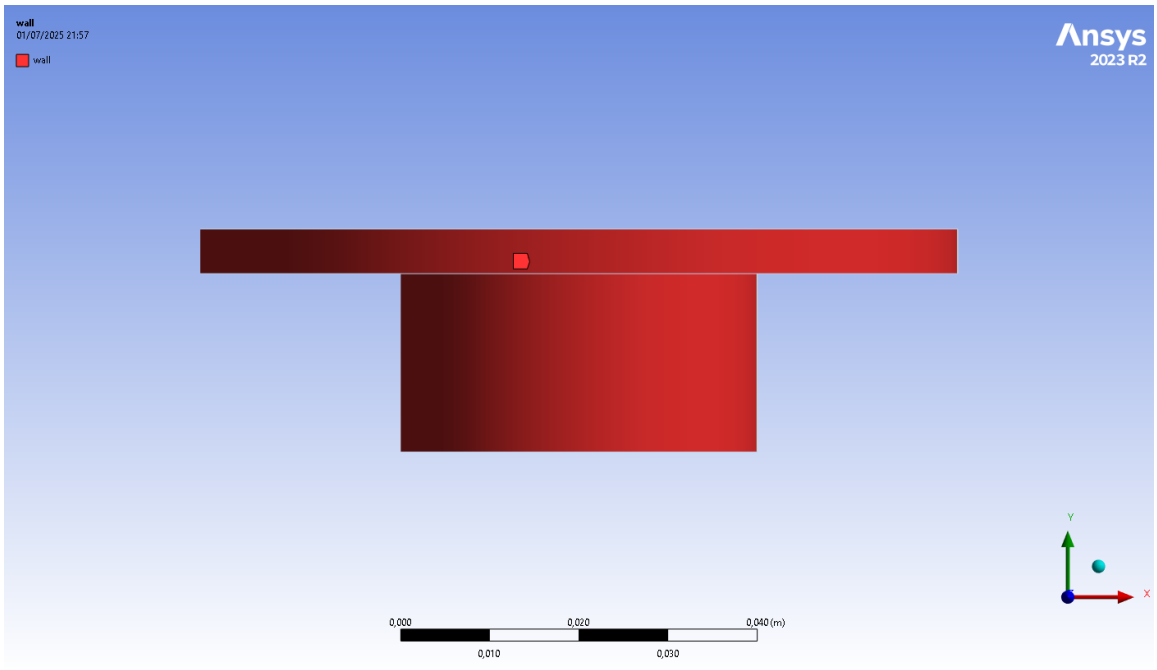

Figure 4.6: Wall section of IC engine combustion chamber.

Boundary Conditions Identification

Since all boundaries are walls in this closed system:

Table 4.3: Wall Boundary Condition

Parameter	**Setting**	**Rationale**
Thermal Condition	Adiabatic	Matches theoretical adiabatic assumption.
Species Flux	Zero diffusive flux	Closed system (no mass transfer).
Velocity	No-slip ($u = v = w = 0$)	Static mesh, no piston motion.

Table 4.4: Thermodynamic Conditions.

Parameter	**Value**	**Justification**
Pressure	20 bar	Typical peak compression pressure in CI engines.
Temperature	900 K	Based on adiabatic compression of methane-air mixture.
Turbulence	5% intensity	Represents residual swirl from intake stroke.

Initial Conditions

We calculate the mass fraction of each species to include it in our simulation, in order to determine the resulting combustion temperature under different conditions.

Table 4.5: Mass Fraction Composition (Methane-Air).

Species	$\phi = 0.8$ **(lean)**	$\phi = 1$ **(stoichiometric)**	$\phi = 1.2$ **(rich)**
CH_4	0.0445	0.0551	0.0655
O_2	0.2227	0.2203	0.2176
N_2	0.7320	0.7246	0.7169

4.4.4 Simulation Result

This figures (4.7, 4.8 and 4.9) shows the temperature contour of the combustion chamber simulated in Ansys at an equivalence ratio $\Phi = 0.8$ Φ =1.2 and Φ =1. High temperatures appear in the central zone, while lower temperatures are distributed toward the outer regions.

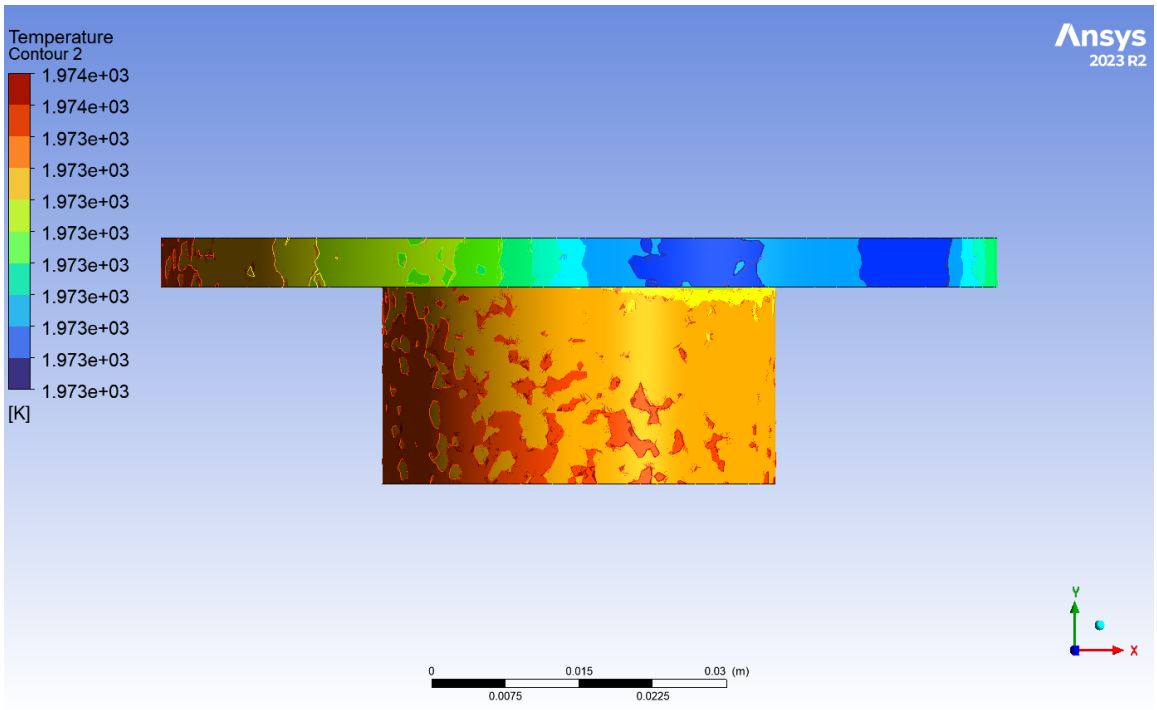

Figure 4.7: Contour of combustion temperature Φ=0.8.

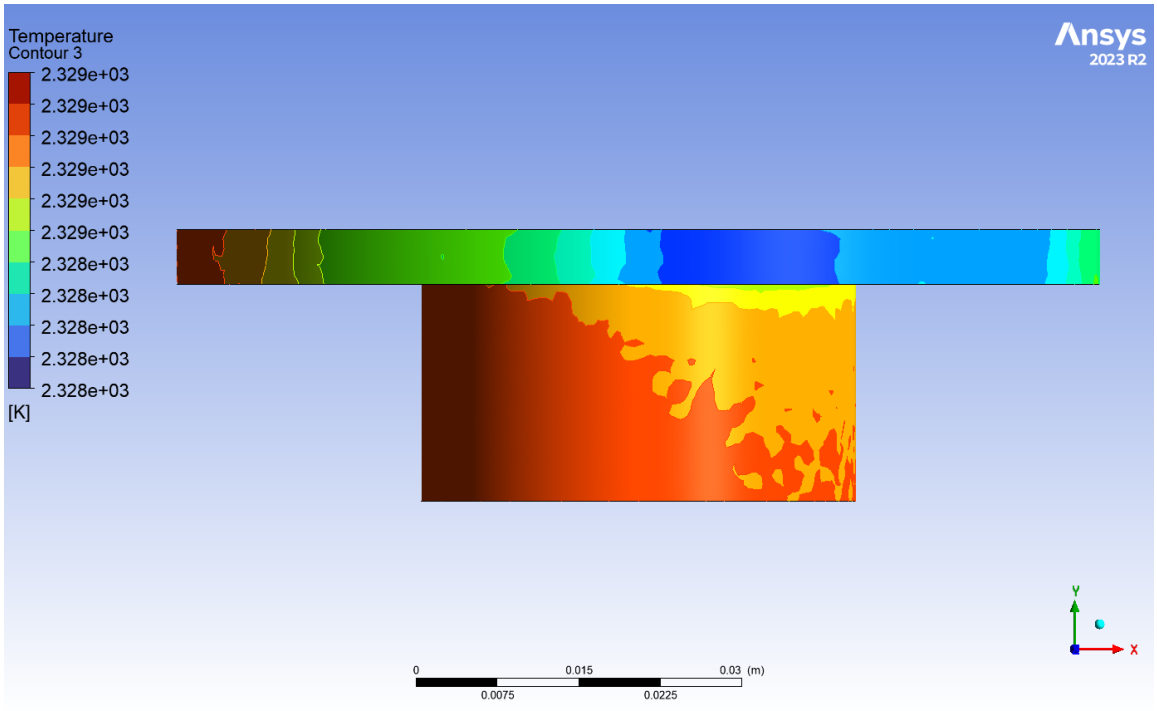

Figure 4.8: Contour of combustion temperature Φ=1.

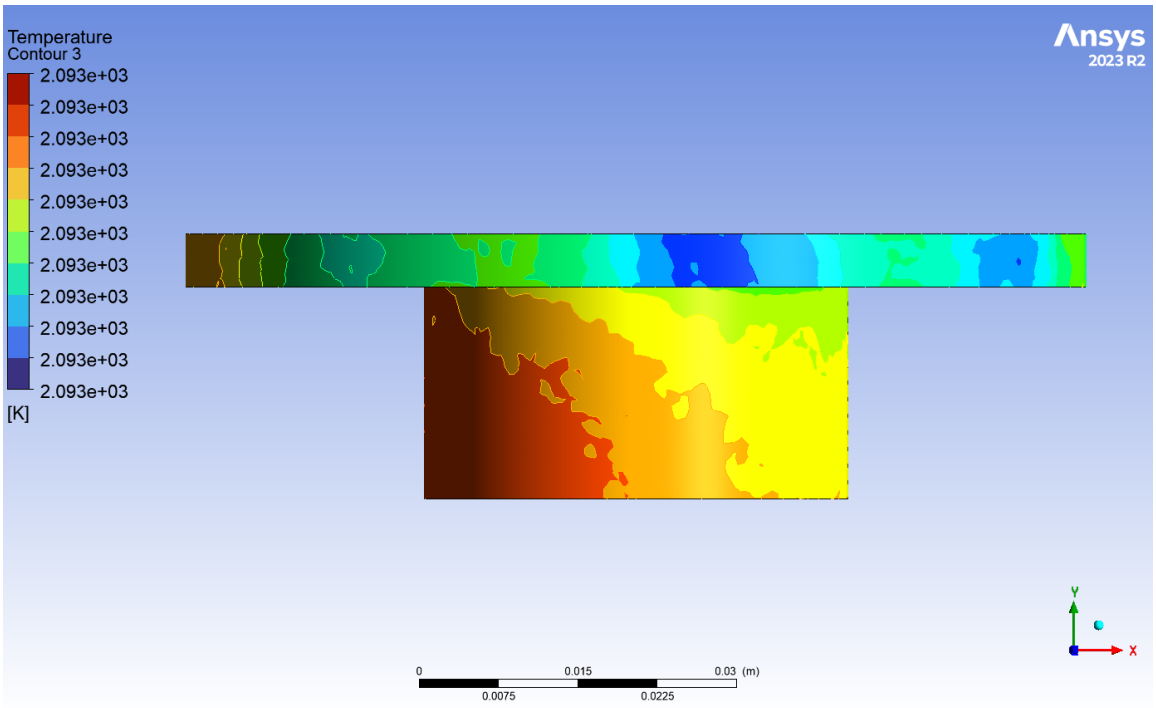

Figure 4.9: Contour of Combustion Temperature Φ=1.2.

As we can see in the following table, the simulation results show that the combustion temperature changes as the equivalence ratio varies.

Table 4.6: Combustion Temperature for Different Equivalence Ratios.

Equivalence Ratio ϕ	**Combustion Temperature (K)**
0.8	1974
1.0	2329
1.2	2093

This figure 4.10 illustrates how the combustion temperature varies with the equivalence ratio. The temperature increases up to $\Phi = 1.0$, reaching a peak, and then decreases as the equivalence ratio increases further.

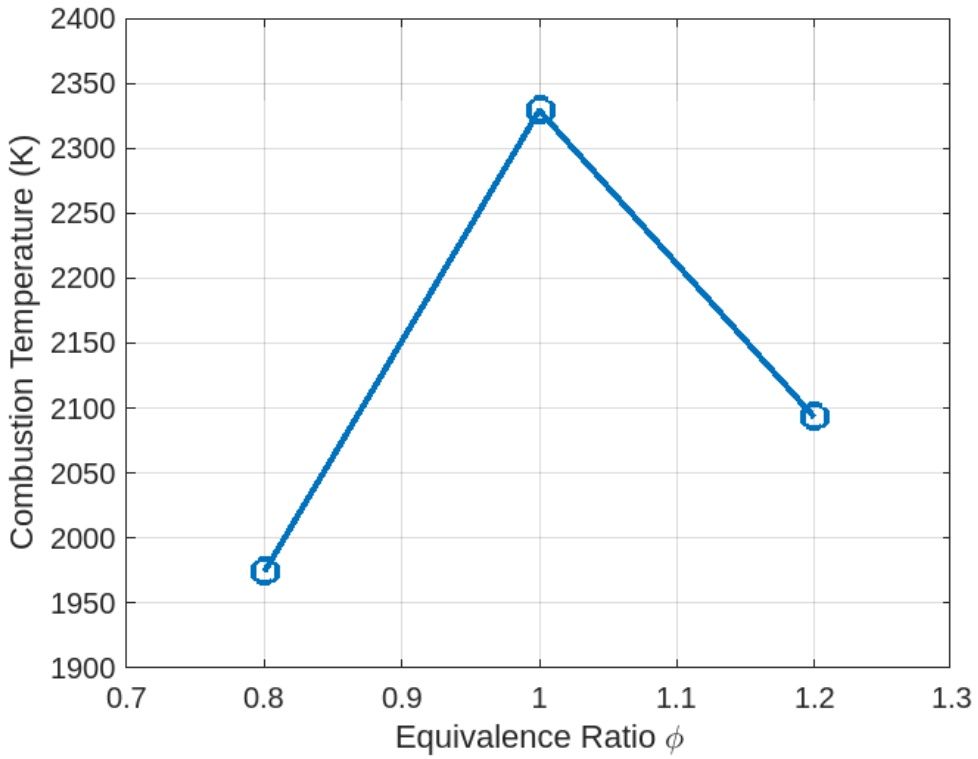

Figure 4.10: Effect of Equivalence Ratio on Combustion Temperature.

Comment

The analysis reveals that the combustion temperature peaks at an equivalence ratio (Φ) of 1, which corresponds to the stoichiometric condition—the ideal balance of fuel and air for complete combustion. At this point, the chemical reaction is most efficient, resulting in the maximum release of heat and the highest flame temperature (2329 K).

When the equivalence ratio is reduced to 0.8, the mixture becomes lean, meaning it contains excess air relative to fuel. This surplus air absorbs part of the generated heat, leading to a lower combustion temperature (1974 K). The reduced thermal energy per unit mass of the mixture diminishes the flame temperature due to energy dilution and reduced thermal efficiency.

On the other hand, increasing the equivalence ratio to 1.2 creates a rich mixture, with more fuel than needed for complete combustion. While additional fuel is available, the limited oxygen inhibits full combustion, resulting in incomplete oxidation and less heat released per unit of fuel. Consequently, the combustion temperature decreases to 2093 K, falling below the peak observed at the stoichiometric point.

In summary, maximum combustion temperature occurs at $\Phi = 1$, while both lean ($\Phi = 0.8$) and rich ($\Phi = 1.2$) mixtures result in lower flame temperatures due to inefficiencies introduced by non-ideal fuel–air proportions.

4.5 Conclusion

This chapter described the initial setup for simulating methane-air combustion in an internal combustion engine using ANSYS Fluent. The geometry, mesh quality, boundary conditions, and solver parameters were all carefully defined. Although the simulation encountered convergence difficulties, it produced preliminary results that, while not fully accurate, offer a meaningful starting point for further development.

The results obtained do not yet reflect a complete or fully validated combustion model. However, they represent an important initial phase in the simulation process, providing insights that can guide future refinements. Continued work will focus on improving numerical stability, adjusting model parameters, and enhancing solution accuracy. These early outcomes serve as a foundation upon which more advanced and reliable simulations can be built in the next stages of the study.

Chapter 5

Result and Discussion

5.1 Introduction

This project focuses on analyzing the effect of inlet air temperature and fuel-air equivalence ratio on the adiabatic flame temperature and combustion characteristics of various fuels, including diesel, kerosene, and methane. Through a series of numerical studies, the influence of preheating and fuel equivalence ratio on flame temperature and the formation of combustion products such as CO, CO, H, NO, and others is evaluated. Particular attention is given to understanding how these variables affect combustion efficiency and pollutant emissions. The second part of the study presents experimental data comparing the performance of diesel and gasoline engines, including torque, effective power, fuel consumption, exhaust temperature, and efficiency across different engine speeds. Together, these analyses aim to highlight the thermal and environmental benefits of optimized combustion conditions and engine design.

5.2 Part 01: Numerical results

The effect of the inlet air temperature on the adiabatic flame temperature for the combustion of diesel and kerosene at different equivalence ratios

Figures (5.1) and (5.2) demonstrate that substantial fuel savings can be achieved by using heat recuperator to recycle part of the thermal energy. This function is implemented by closed-loop digital regulators in modern thermal systems, automotive engines, and aircraft

engines, since the maximum temperature increases due to air preheating.

For example, with an inlet air temperature of 600 K, the adiabatic flame temperature rises by 250 K compared to the 300 K air baseline. In other words, preheating air from 300 K at an equivalence ratio ϕ of 0.7 yields a combustion temperature gain of $\approx 250K|equivalenttothetemperatureachievedat\phi \approx 0.9$ without preheating. This avoids the energy waste associated with operating at higher fuel-rich conditions.

The Results

Thus, as key results: Air preheating is essential to minimize fuel consumption and enhance combustion performance

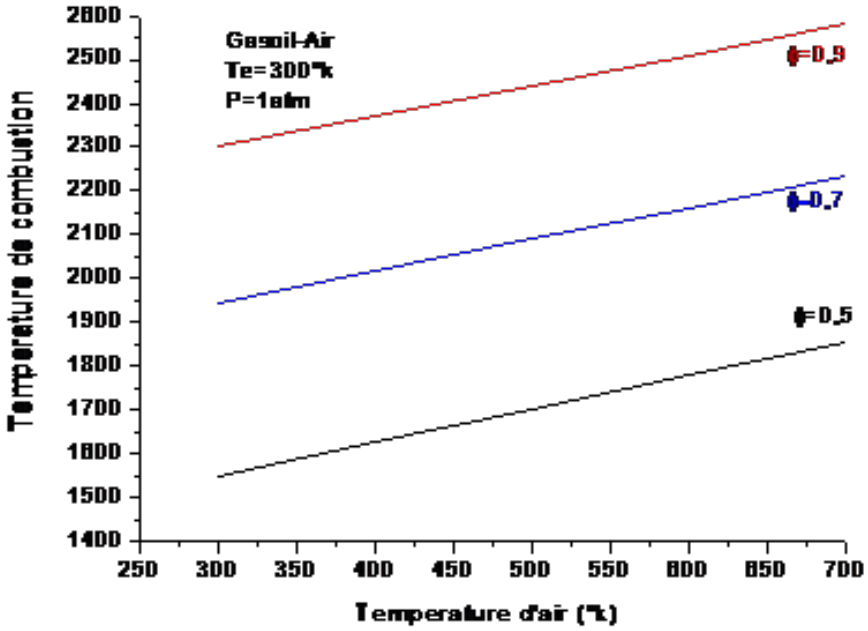

Figure 5.1: Evolution of the combustion temperature of the gas oil with air as a function of the preheating temperature for different equivalence ratio.

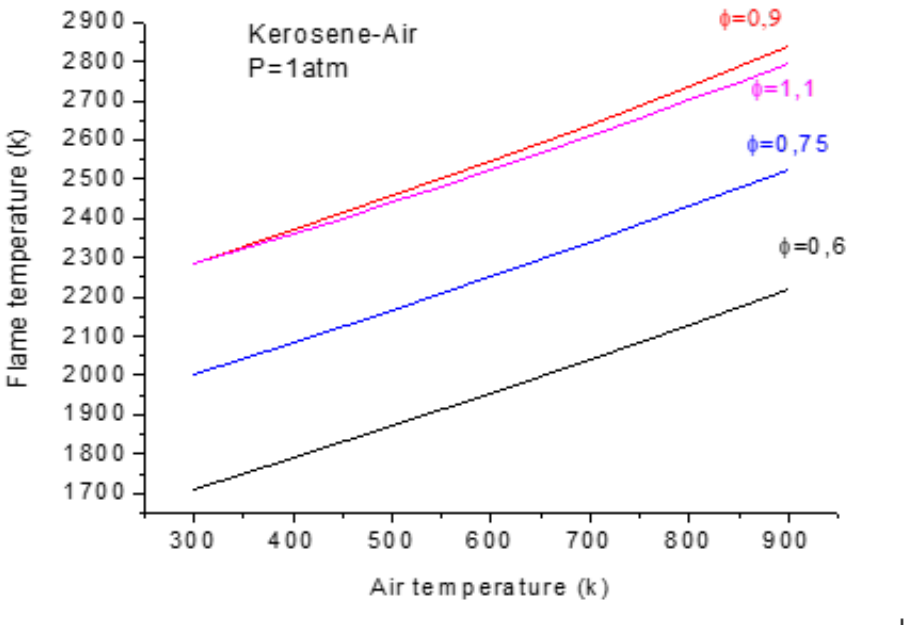

Figure 5.2: Evolution of the Kerosene combustion temperature with air as a function of the preheating temperature for different equivalence ratio.

Effect of the Equivalence Ratio ϕ on the adiabatic flame temperature for methane combustion

Figures (5.3) and (5.4) presents the evolution of the adiabatic flame temperature as a function of the equivalence ratio for different preheating temperatures. It is interesting to note that the maximum temperature is around 2420 K of the flame occurs at stoichiometry (equivalence ratio...F=1). Also, the flame temperature decreases when f exceeds unity; the decrease in flame temperature is dominated by the increase in the number of moles of the products formed per mole of fuel burned. Moreover, the decrease in combustion temperature is caused by the phenomenon of molecular dissociation and chemical species caused by high temperatures. This phenomenon is created by elementary reactions whose endothermic nature causes the decrease in combustion temperature.

The Result

From the two previous figures, it is observed that there are two combustion zones: a lean zone with an equivalence ratio less than unity and a rich zone where the equivalence ratio is greater than unity. To minimize fuel consumption, equivalence ratios less than unity can be found that provide the same temperatures as equivalence ratios greater than unity.

It is also noted that the trends in both figures are nearly identical compared to reference. It should be noted that Figures (5.3) and (5.4) were obtained using the (Gordon-McBride) polynomials published by NASA in 2004 for the first and in 1996 for the second.

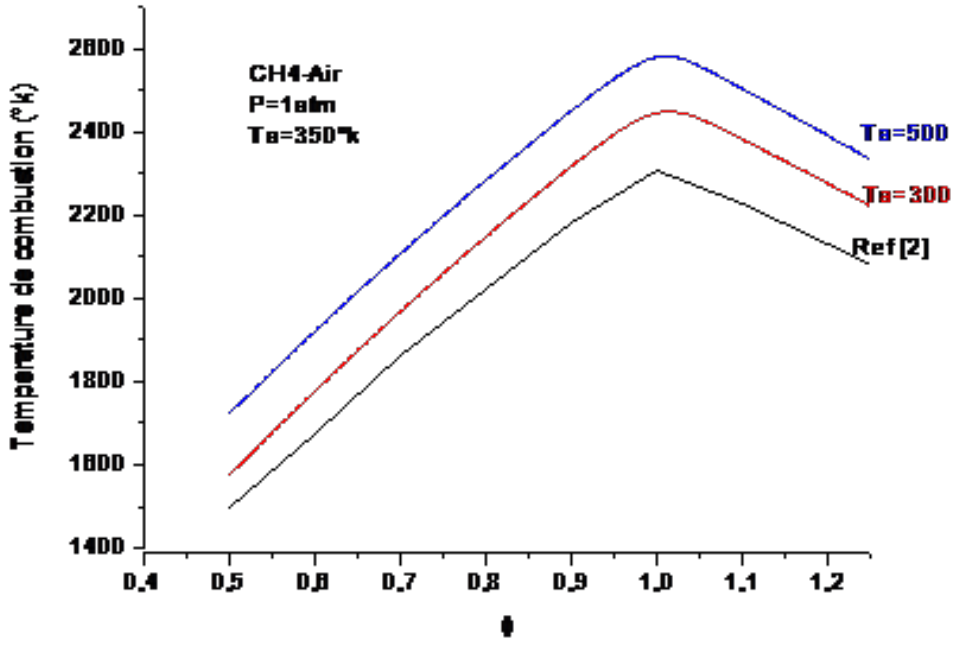

Figure 5.3: Evolution of the combustion temperature as a function of equivalence ratio.

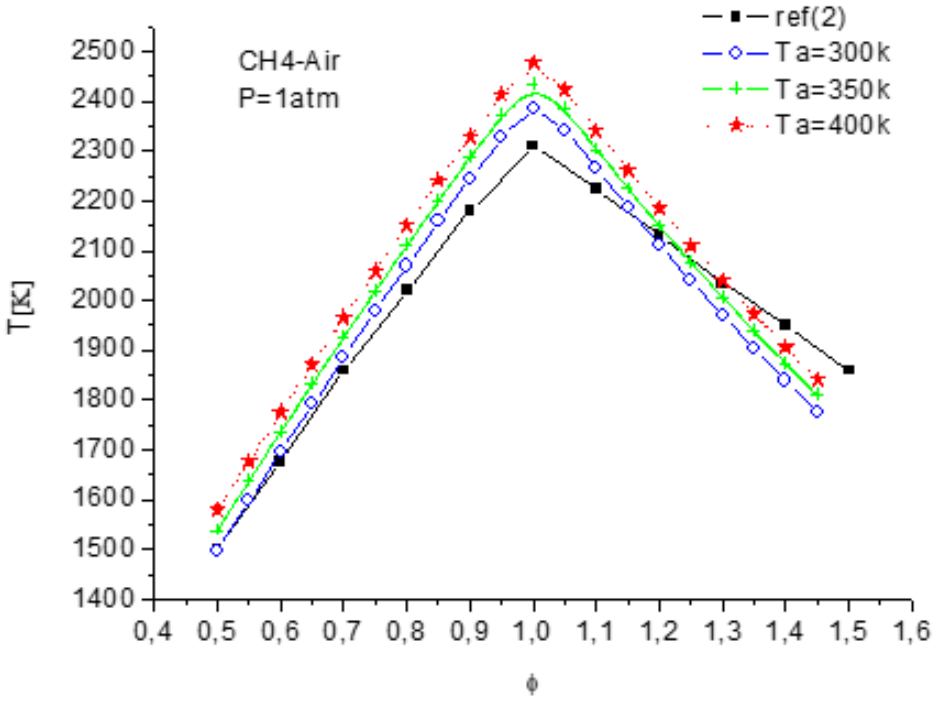

Figure 5.4: Evolution of the combustion temperature as a function of equivalence ratio.

Effect of the Equivalence Ratio ϕ on the evolution of the molar composition of the kerosene-air combustion products

Figure (5.5) illustrate the evolution of combustion products (CO_2, CO, H_O, H_2, H, OH, O_2, O, NO, N_2, and N) as a function of equivalence ratio (ϕ). The primary products in lean combustion are H_O, CO_2 , O_2, and N_2, whereas rich combustion yields additional species such as CO, H_2, and residual N_2. Furthermore, due to dissociation effects, even stoichiometric conditions (ϕ= 1) exhibit simultaneous presence of O_2, CO, and H_2. This demonstrates the approximate nature of the "complete combustion" assumption. Minor species in equilibrium combustion of kerosene-air mixtures are shown in Figure (2.6), while Figure (2.7) presents analogous results for diesel-air combustion.

Key observations from the figures include:

1. Mild reduction of N_2 concentration with trace yields of NO and N.
2. Monotonic increase of CO_2 and H_2O (dominant products of combustion) with ϕ, along with O_2 consumption (oxidizer depletion):
    - For lean zones ($\phi < 1$), O_2 consumption is slow due to the absence of fuel to

burn off available oxygen.

- For rich zones ($\phi > 1$), O_2 is depleted faster due to excess fuel.

3. Emergence of pollutants such as carbon monoxide (CO) and nitric oxide (NO):
   - CO formation is extremely tiny in lean combustion but rises significantly in rich burning.

The Result

To minimize pollutant emissions (notably CO and NO), lean combustion is preferable.

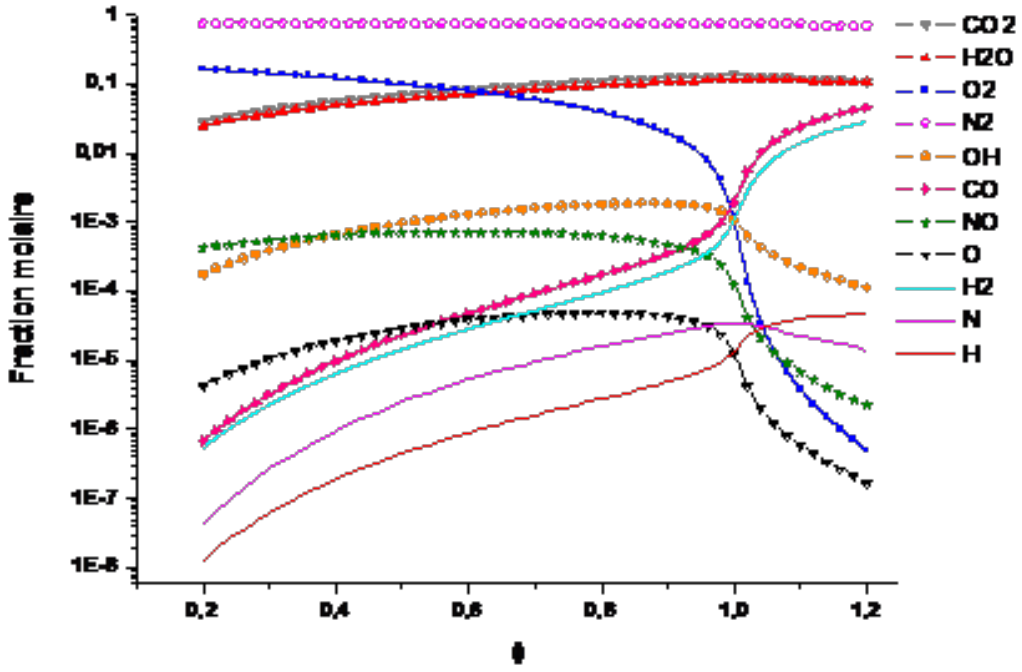

Figure 5.5: Variation of the different species according to the equivalence ratio for combustion (Kerosene-Air).

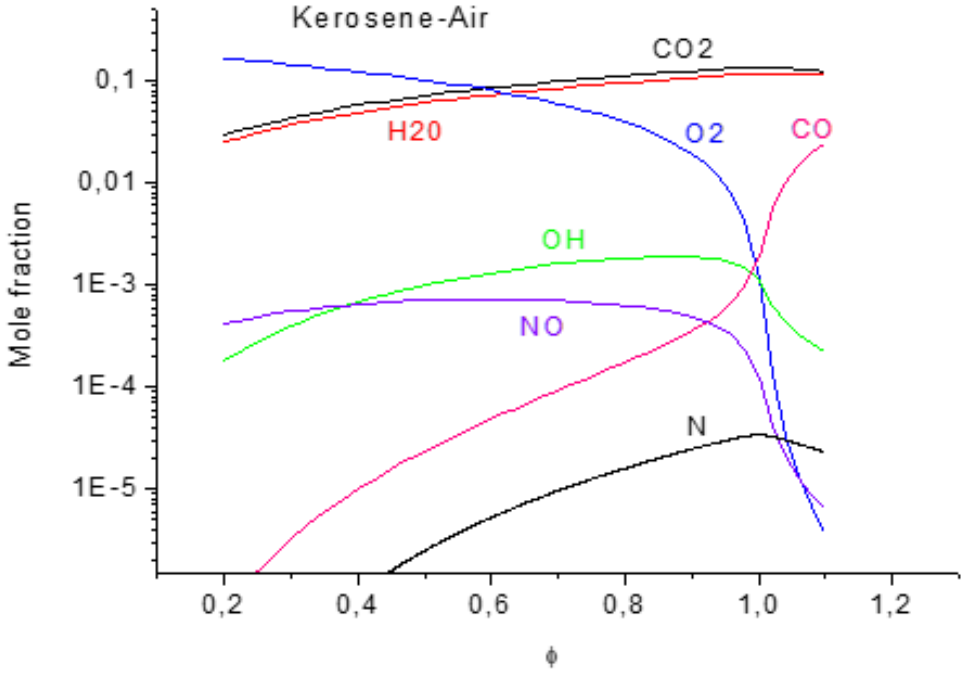

Figure 5.6: Variation of the main species according to equivalence ratio for combustion (Kerosene-Air).

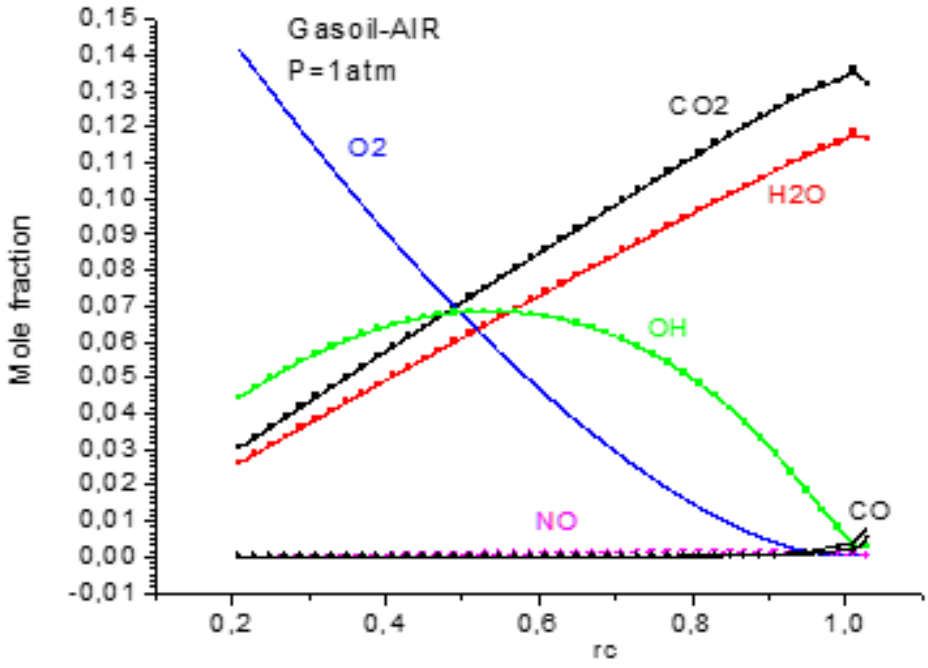

Figure 5.7: Variation of main species according to equivalence ratio for combustion (diesel-air).

Effect of Preheat Temperature on Pollutant Formation Across Equivalence Ratios

figure (5.8) show that the preheat temperature (T_p) is instrumental in pollutant emissions (CO, NO, CO_2) and combustion efficiency. This technique is most commonly used in the design of gas turbine and industrial thermal systems to achieve:

1. **Pollutant Reduction:**
    - CO: Decreased at high T_p in lean burning (enhanced oxidation kinetics).
    - NO: Decreased under fuel-rich conditions ($\phi > 1.2$) but maximizes near stoichiometry ($\phi \approx 1$) due to thermal-NO dominance at higher T_p.
    - CO_2: Reduced indirectly by improved combustion efficiency (less fuel consumed to produce the same output).
2. **Performance Benefits:**
    - Higher Thermal Efficiency: Preheating reactants reduces energy losses and stabilizes flame propagation.
    - Fuel Economy: Complete combustion at optimized T_p minimizes specific fuel consumption (SFC).
3. **Engineering Implications:**
    - Lean-Premixed Combustion (gas turbines): High T_p with $\phi < 1$ suppresses CO/CO_2 and lowers NO via rapid quenching.
    - Industrial Burners: Rich-lean staging is used to control preheating, minimizing NO (by reburning) and unburned hydrocarbons.

Conclusion: Optimizing the preheat temperature is imperative to ensure emission compliance and operational efficiency, in line with contemporary clean-combustion approaches.

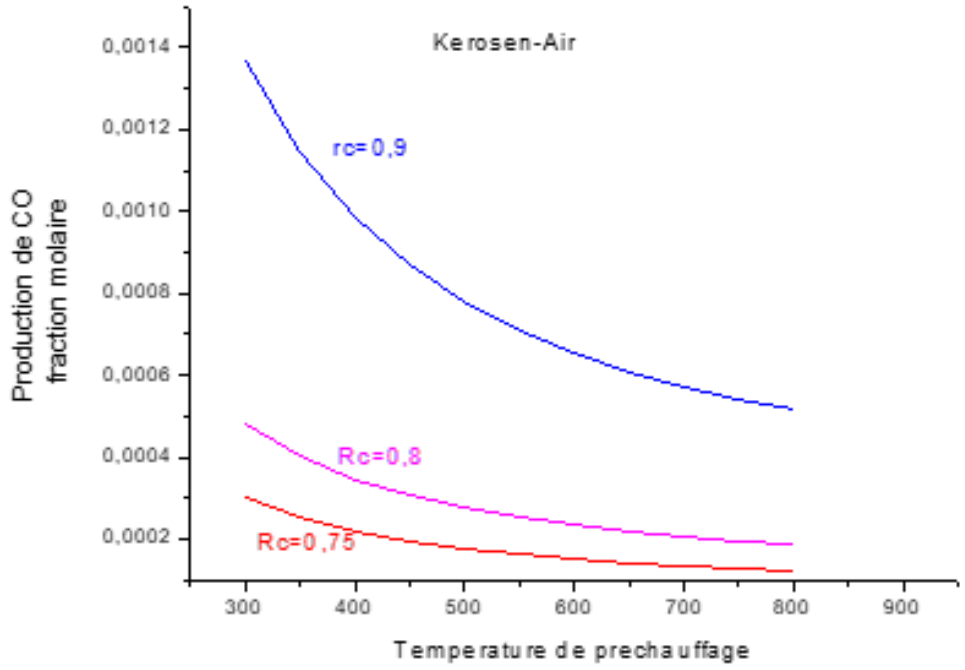

Figure 5.8: Evolution of carbon monoxide (CO) as a function of the preheating temperature for different equivalence ratio.

5.3 Part 02: Engine Performance Characteristics results (experimental)

5.3.1 Torque

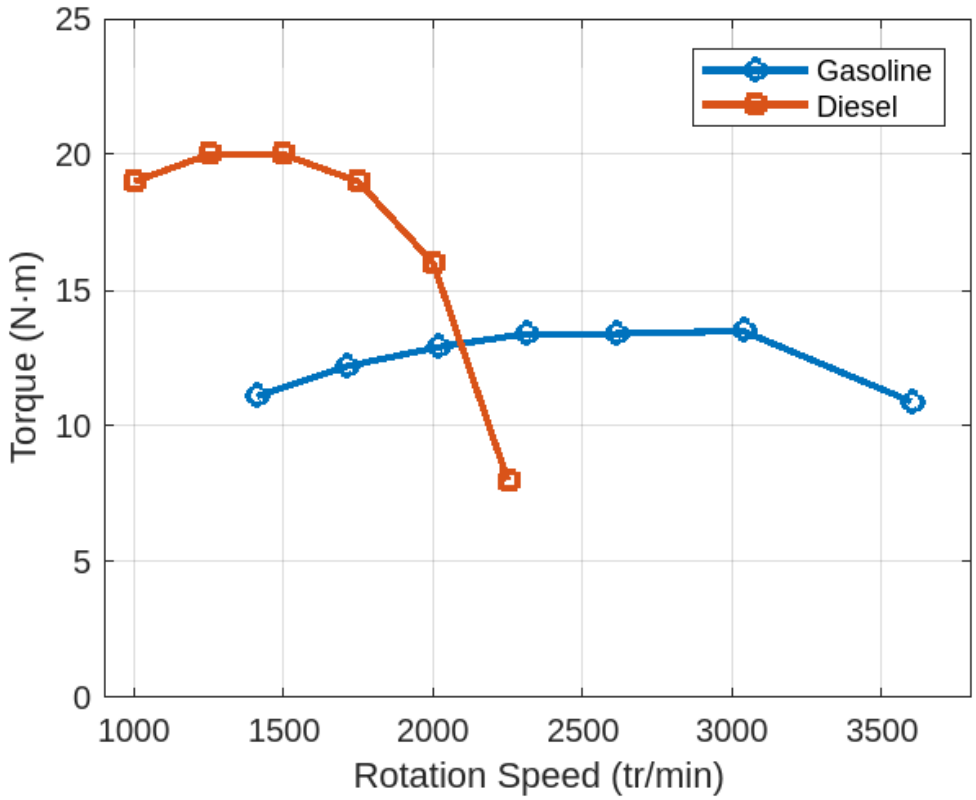

Figure 5.9: Comparative Analysis of Torque Characteristics: Gasoline vs. Diesel Engines Across Engine Speeds.

Comment

Diesel engines have higher torque (20–25 N·m) and strong low-RPM performance due to higher compression ratios and flat torque curves. Gasoline engines produce lower torque (10–15 N·m), with a bell-shaped curve peaking mid-range and declining at high RPMs. As a result, diesel suits heavy loads, while gasoline fits passenger cars and high-RPM needs.

analysis

- The Diesel engine produces higher torque than the Gasoline engine up to around 2000 tr/min, peaking at about 20 N·m before declining sharply.
- Beyond 2000 tr/min, Diesel torque drops quickly to below 10 N·m, indicating reduced efficiency at higher speeds.
- In contrast, the Gasoline engine shows a steadier torque curve, maintaining about 13–14 N·m across a wide speed range.
- This suggests Diesel is better for low-speed, high-torque applications, while Gasoline offers more consistent performance over higher speeds.
- Overall, engine selection depends on whether peak low-end torque or stable higher-speed operation is prioritized.

5.3.2 Air fuel ratio

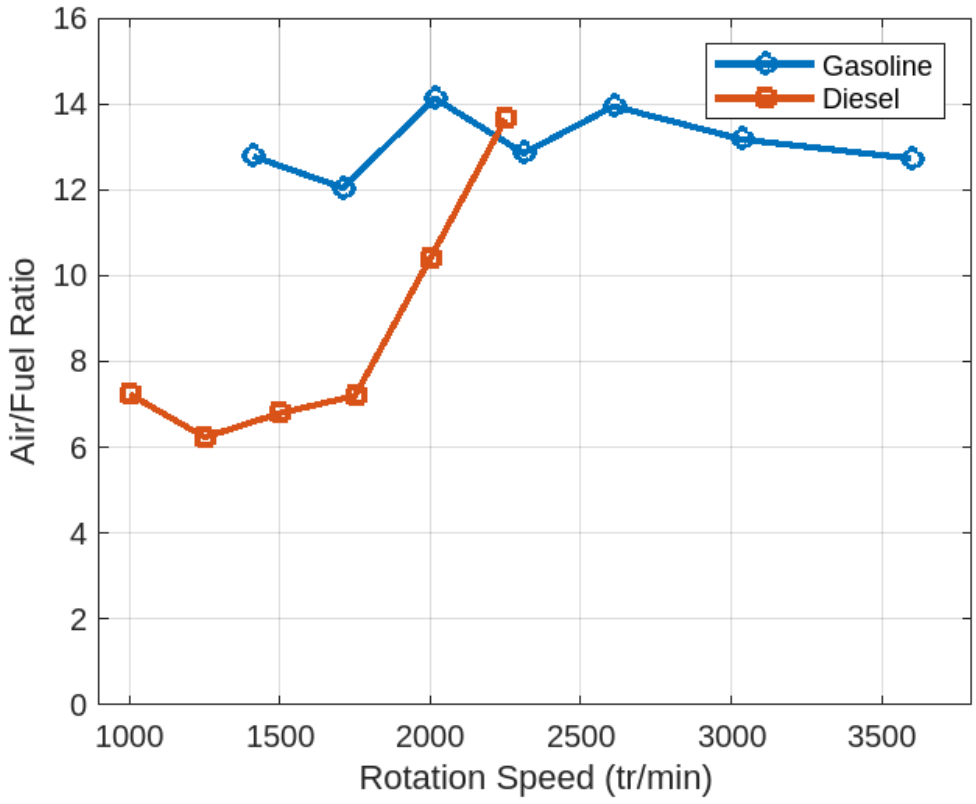

Figure 5.10: Comparative Analysis of air/fuel ratio Characteristics: Gasoline vs. Diesel Engines Across Engine Speeds.

Comment

Diesel engines operate with leaner air-fuel ratios (AFR), ranging from about 8–16, while gasoline engines use a narrower range around 8–14 and require near-stoichiometric mixtures (14.7) for combustion. Diesel maintains efficiency by adjusting AFR more flexibly, enabling lean combustion and a wider operating window, especially at low and mid RPMs. In contrast, gasoline engines enrich mixtures under load for power but are limited by spark ignition requirements.

analysis

- The Diesel engine starts with a lower Air/Fuel ratio (around 7) and gradually increases to about 14 as rotation speed rises.
- The Gasoline engine maintains a consistently higher Air/Fuel ratio between 12 and 14 over the entire speed range.
- At low speeds, Diesel operates richer (more fuel), enhancing torque but reducing efficiency.
- At higher speeds, Diesel's Air/Fuel ratio approaches that of Gasoline, improving combustion and emissions.
- Overall, Gasoline shows stable mixture control, while Diesel transitions from rich to lean mixtures as speed increases.

5.3.3 Effective Power

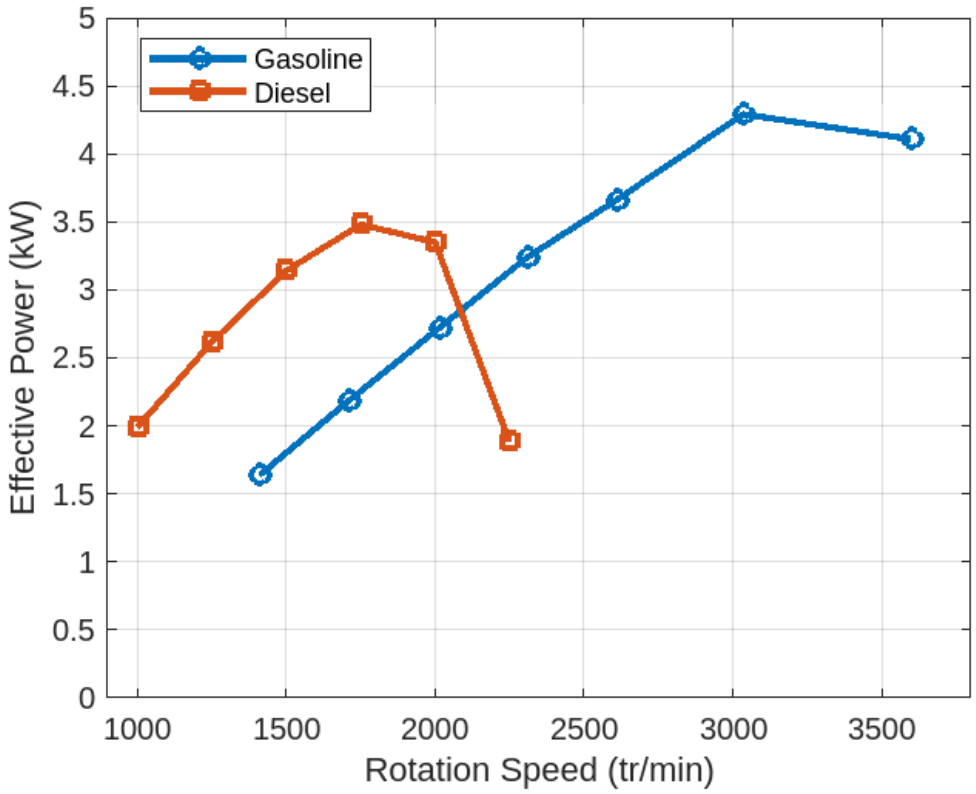

Figure 5.11: Comparative Analysis of effective power Characteristics: Gasoline vs. Diesel Engines Across Engine Speeds.

Comment

Diesel engines produce more effective power across most RPM ranges, being up to 67% stronger at low speeds thanks to higher torque and better combustion. This advantage remains through mid-range RPMs, where diesel maintains a sustained torque curve and delivers more power. At higher RPMs (3000–3500), the power difference narrows as gasoline engines perform better at high speeds.

analysis

- The Diesel engine shows higher effective power up to around 2000 tr/min, peaking near 3.5 kW before declining.
- In contrast, the Gasoline engine's power increases steadily with rotation speed, reaching about 4.3 kW at 3000 tr/min.

- Beyond 2000 tr/min, Gasoline clearly surpasses Diesel in power output.
- This indicates Diesel is optimal for lower-speed applications requiring strong initial power.
- Gasoline is better suited for high-speed operation with continuously increasing power.

5.3.4 Exhaust Temperature

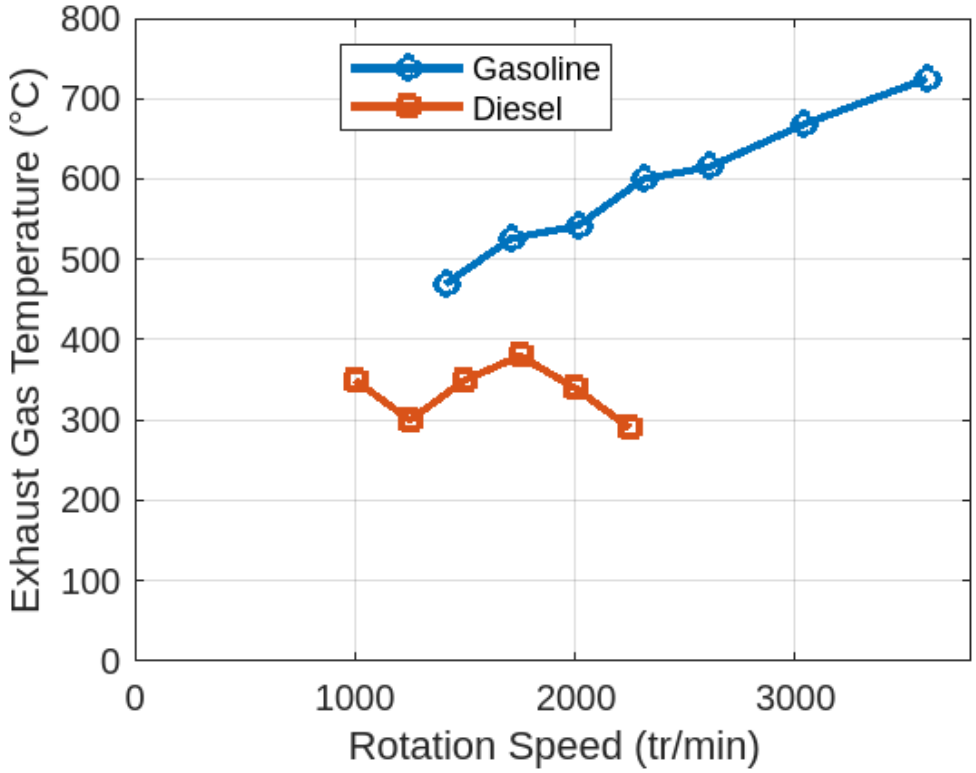

Figure 5.12: Comparative Analysis of Exhaust gaz temperature Characteristics: Gasoline vs. Diesel Engines Across Engine Speeds.

Comment

Gasoline engines have significantly higher exhaust temperatures, ranging from 400–800°C, while diesel exhaust stays cooler between 200–500°C. The difference increases with RPM, reaching up to +300°C at high speeds. This is because diesel's lean combustion and expansion cooling lower temperatures, whereas gasoline's stoichiometric combustion generates more heat.

analysis

- The Gasoline engine shows a continuous rise in exhaust temperature, reaching about 720 °C at high speeds.
- The Diesel engine maintains significantly lower exhaust temperatures, mostly between 300–390 °C.
- This indicates higher combustion temperatures in Gasoline engines due to faster burn rates.
- Diesel engines operate cooler, contributing to better thermal efficiency and less heat stress.
- Overall, Gasoline engines produce hotter exhaust gases, especially at higher rotation speeds.

5.3.5 Hourly consumption

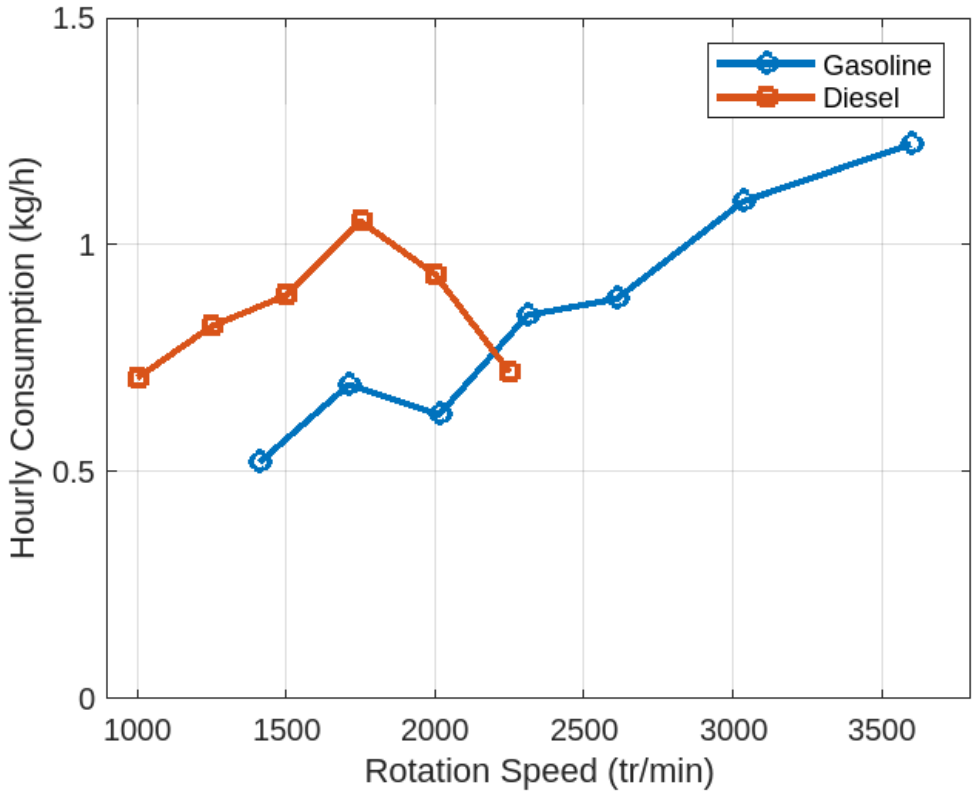

Figure 5.13: Comparative Analysis of Hourly consumption Characteristics: Gasoline vs. Diesel Engines Across Engine Speeds.

Comment

Diesel engines consume less fuel per hour across all RPM ranges, using about 20–40% less than gasoline engines. This efficiency comes from lean burn combustion, higher energy density, and better thermal performance. While the gap narrows at high loads, diesel remains consistently more economical in fuel consumption.

analysis

- The Diesel engine shows higher consumption at lower speeds, peaking near 1.1 kg/h around 1750 tr/min.
- Gasoline consumption starts lower and increases steadily with rotation speed, surpassing Diesel after 2250 tr/min.
- At high speeds, Gasoline reaches about 1.3 kg/h, indicating higher fuel demand.
- Diesel consumption decreases beyond mid-range speeds, reflecting better efficiency under certain conditions.
- Overall, Diesel is more economical at higher speeds, while Gasoline requires more fuel as speed rises.

5.3.6 Specific consumption

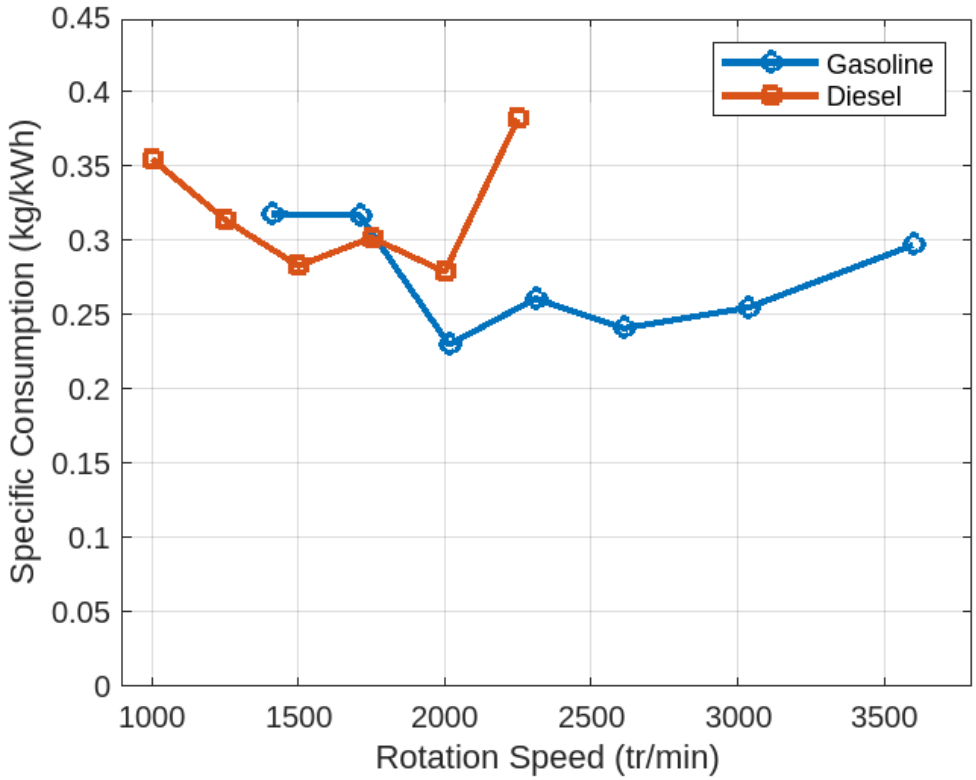

Figure 5.14: Comparative Analysis of specific consumption Characteristics: Gasoline vs. Diesel Engines Across Engine Speeds.

Comment

Diesel engines show lower specific consumption by about 15–25% compared to gasoline engines across all RPM ranges. This advantage comes from lean combustion, better thermal efficiency, and slower efficiency decline at higher loads. Diesel maintains a consistent fuel economy edge, especially at low and mid RPMs.

analysis

- The Diesel engine starts with higher specific consumption (around 0.35 kg/kWh) at low speeds, then decreases towards mid-range.
- Around 2000 tr/min, Diesel shows its lowest specific consumption, indicating better fuel efficiency.
- At higher speeds, Diesel consumption rises sharply, exceeding 0.38 kg/kWh.

- The Gasoline engine maintains more stable specific consumption between 0.23 and 0.32 kg/kWh across speeds.
- Overall, Gasoline demonstrates more consistent efficiency, while Diesel efficiency varies more with speed.

5.3.7 Time (s)

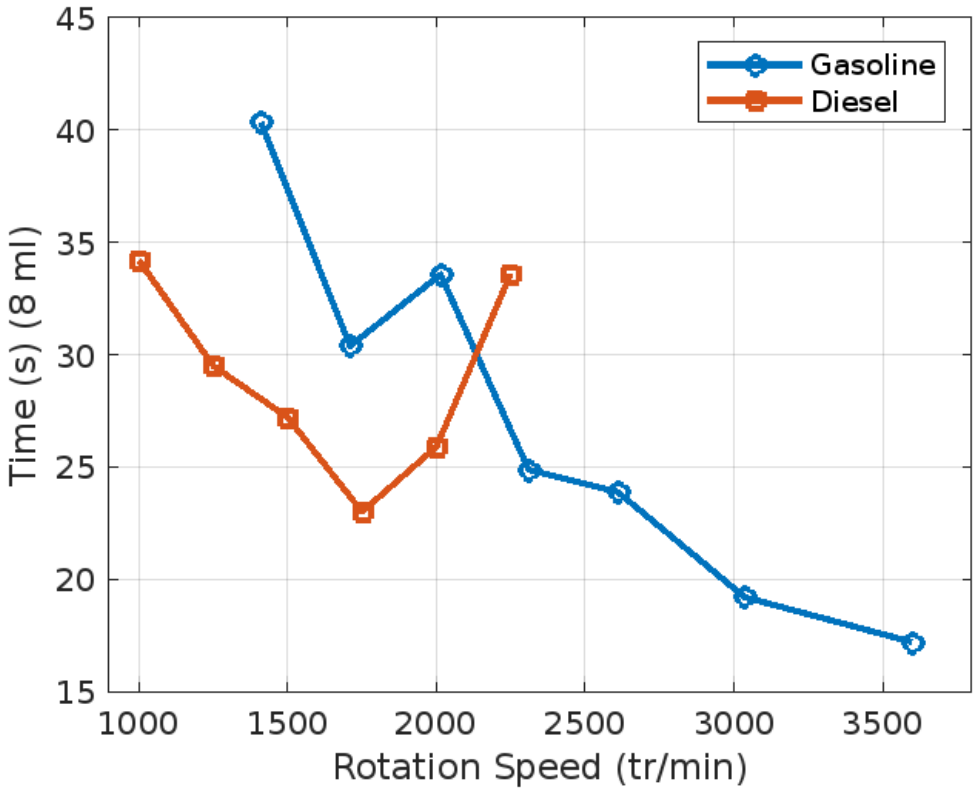

Figure 5.15: Comparative Analysis of time Characteristics: Gasoline vs. Diesel Engines Across Engine Speeds.

Comment

The chart shows that diesel engines generally require less time to consume 8 ml of fuel across most rotation speeds, reflecting higher efficiency at low and mid RPMs. Gasoline engines take longer, especially below 2300 tr/min, but become faster as RPM increases beyond 2500. This trend highlights diesel's better fuel economy at lower speeds and gasoline's advantage at higher rotation rates.

analysis

- The Diesel engine shows shorter times to consume 8 ml fuel at low speeds (around 23 s at 1750 tr/min).
- At higher speeds, Diesel times increase slightly, indicating reduced relative consumption.
- The Gasoline engine has longer times at low speeds (over 40 s), reflecting lower consumption rates.
- As rotation speed increases, Gasoline times decrease significantly, reaching about 17 s at 3500 tr/min.
- Overall, Diesel consumes fuel faster at low speeds, while Gasoline consumption accelerates with speed.

5.3.8 Gasoline Engine Air Consumption Analysis

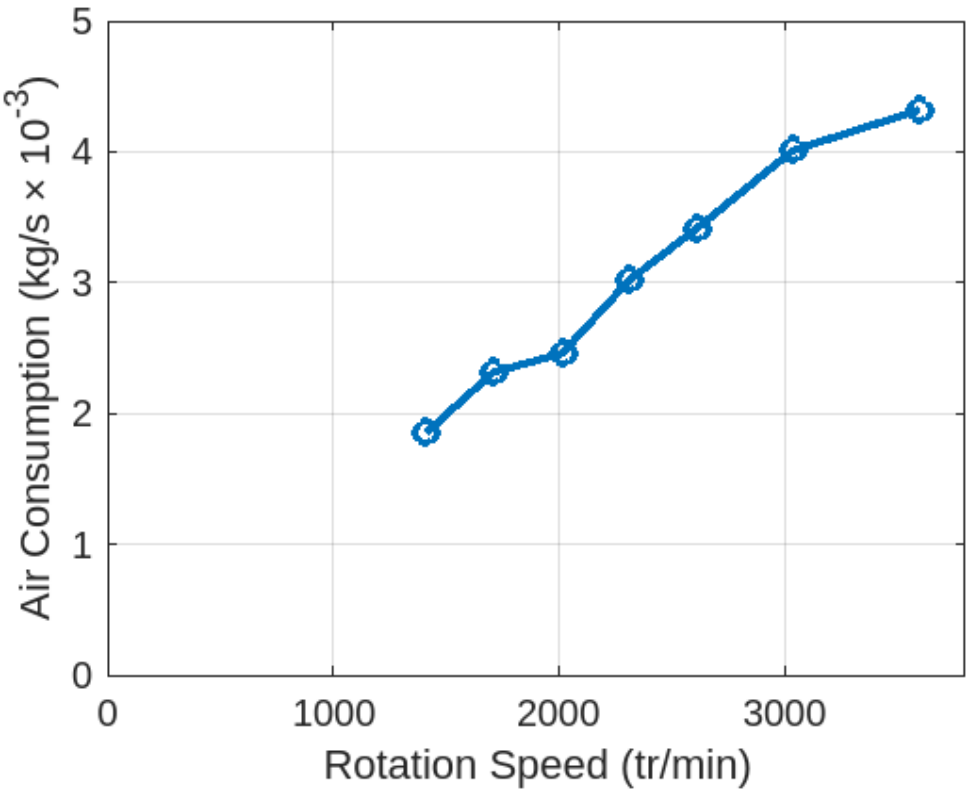

Figure 5.16: Gasoline Engine Air Consumption Analysis.

Comment

Diesel engines consume less fuel per hour across all RPM ranges, using about 20–40 % less than gasoline engines. This efficiency comes from lean burn combustion, higher energy density, and better thermal performance. While the gap narrows at high loads, diesel remains consistently more economical in fuel consumption.

analysis

- Air consumption increases steadily with rotation speed.
- At low speeds (around 1500 tr/min), consumption is about 1.8×10^{-3} kg/s.
- As speed rises to 3500 tr/min, air consumption exceeds 4.2×10^{-3} kg/s.
- This trend indicates higher air intake required to support combustion at higher speeds.
- Overall, air consumption nearly doubles from minimum to maximum rotation speed.

5.3.9 Gasoline Engine Effective Efficiency Analysis

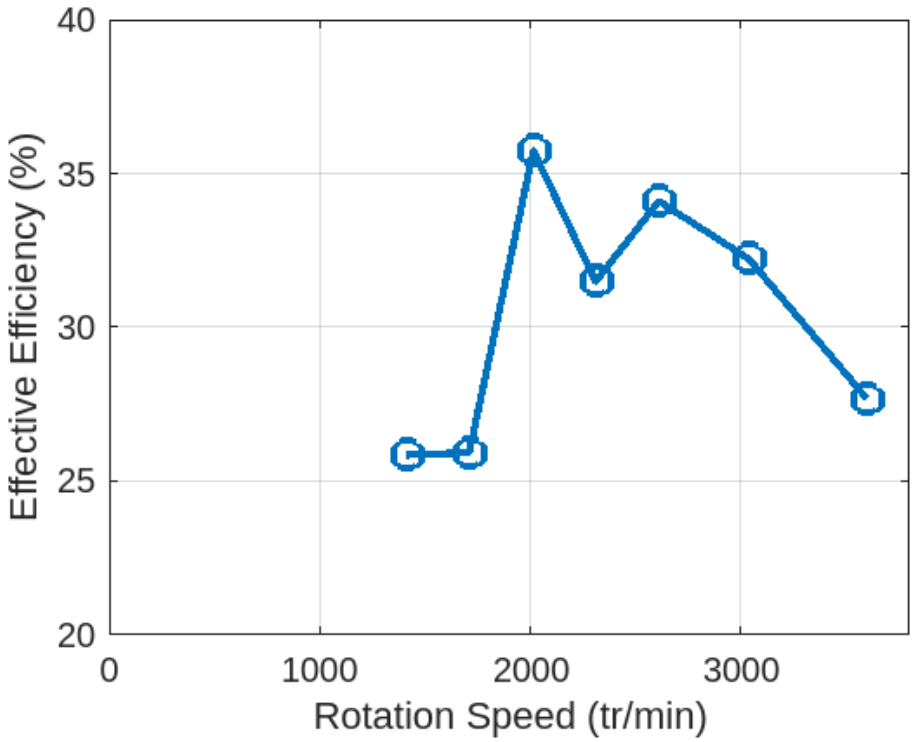

Figure 5.17: Gasoline Engine Effective Efficiency Analysis.

Comment

Engine efficiency improves gradually from 22–26% at low RPMs to an optimal 26–31% around 1500–2000 rpm due to best fuel consumption. Beyond 2000 rpm, efficiency peaks and then declines sharply, dropping to 20% by 3500 rpm. This reduction is caused by increased friction, knock-limited spark timing, and poor volumetric efficiency at high speeds.

analysis

- Efficiency remains around 26% at lower speeds (1500–1750 tr/min).
- A sharp peak occurs at 2000 tr/min, reaching approximately 36% efficiency.
- Beyond this peak, efficiency decreases moderately, stabilizing between 31–34%.
- At the highest speeds, efficiency drops again to about 28%.
- Overall, the engine achieves maximum efficiency near mid-range rotation speeds.

5.3.10 Diesel Engine Volumetric Efficiency Analysis

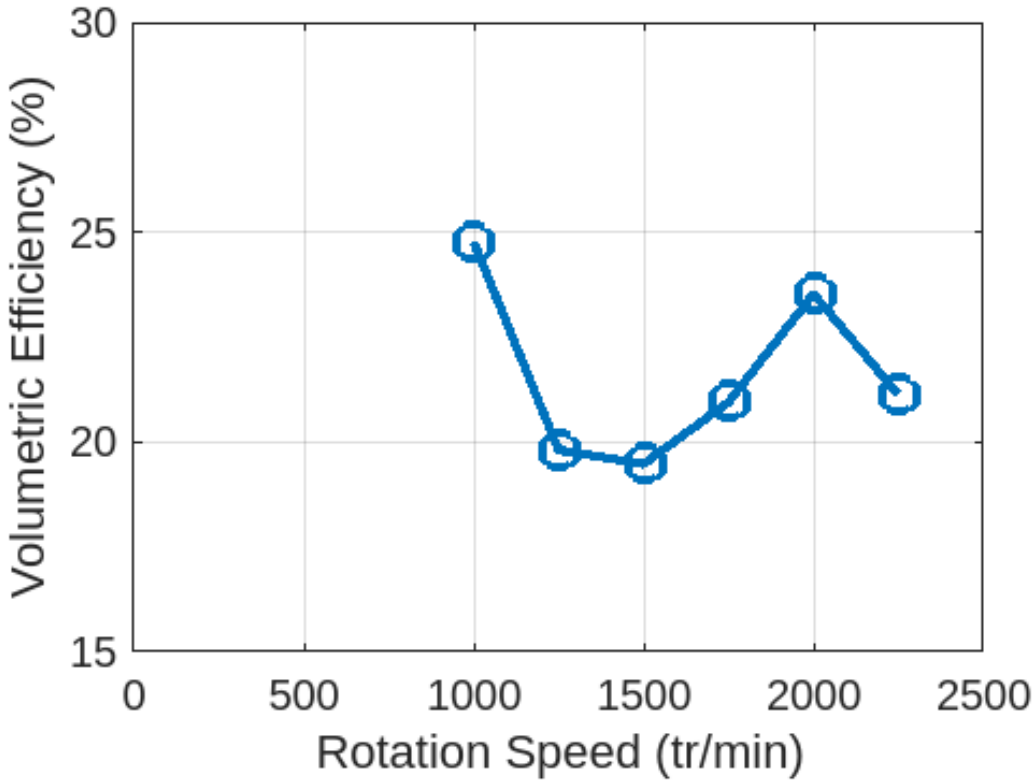

Figure 5.18: Diesel Engine Volumetric Efficiency Analysis.

Comment

Volumetric efficiency increases rapidly from 65–80% at low RPMs thanks to turbo spool-up improving airflow and peaks at 88% between 1500–2000 rpm with optimal boost. As RPM rises beyond 2000, efficiency gradually declines due to pumping losses and turbo speed limits. At the highest RPMs, it drops sharply to around 68% because of valve float restrictions.

analysis

- Volumetric efficiency peaks near 25% at around 1000 tr/min.
- As rotation speed increases to 1400 tr/min, efficiency drops to about 19.5%.
- From mid-range speeds, efficiency gradually recovers, reaching approximately 23% near 2000 tr/min.
- At the highest measured speeds, efficiency decreases again slightly.
- Overall, volumetric efficiency shows a non-linear trend with a maximum at low speeds and moderate recovery at higher speeds.

5.3.11 Diesel Engine Overall Efficiency Analysis

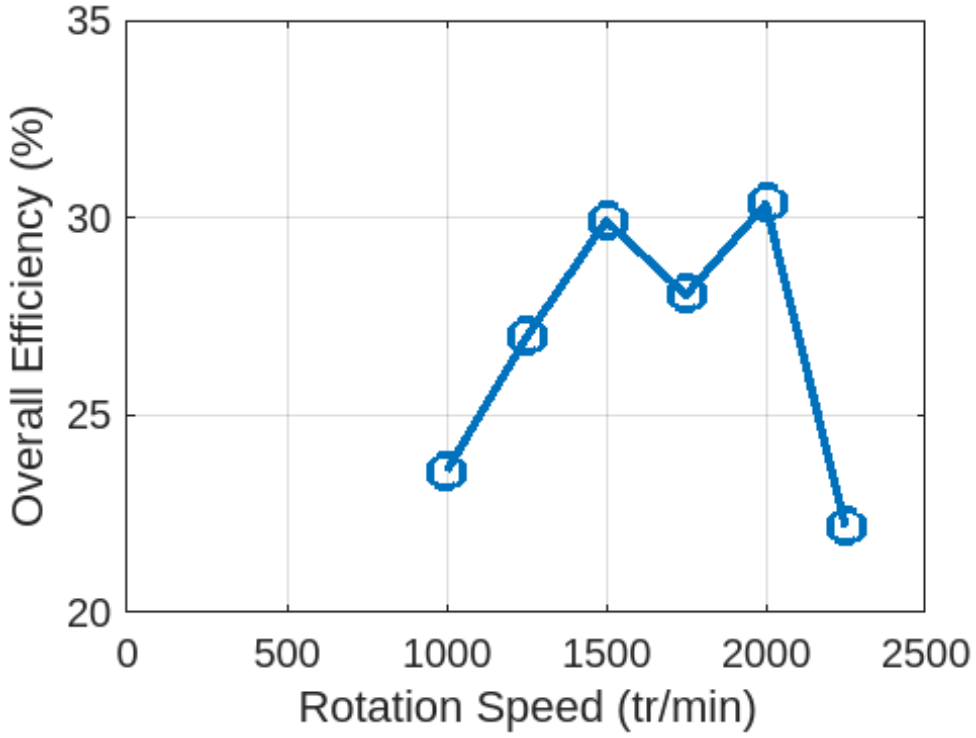

Figure 5.19: Diesel Engine Overall Efficiency Analysis.

Comment

The graph shows that overall efficiency rises from about 23% at low rotation speeds, peaking near 30% around 1500–2000 tr/min. This indicates the engine operates most efficiently in the mid-RPM range. Beyond 2000 tr/min, efficiency declines sharply, highlighting increased losses at higher speeds.

analysis

- Overall efficiency increases from about 23% at 1000 tr/min to a peak near 30% at 1500 tr/min.
- A slight dip follows at 1700 tr/min, where efficiency decreases to roughly 28%.
- Efficiency rises again to about 31% near 2000 tr/min, marking the highest value recorded.
- At higher speeds (2300 tr/min), efficiency drops noticeably to around 22%.

- Overall, the curve shows two efficiency peaks, with performance best in the mid-speed range.

5.4 Sources of Error

Analytical / Numerical Data

- Simplified combustion models (polynomial approximations).
- Approximations in thermochemical data.

Experimental Measurements

- Torque measurement error (±1–2%).
- Fuel consumption measurement error (±0.5–1%).
- Exhaust temperature sensor accuracy (±5–10 °C).
- Variations in ambient conditions (temperature, humidity, pressure).
- Operator variability when adjusting loads or RPM.

5.5 Estimated Experimental Error Margins

Table 5.1: Estimated Experimental Error Margins.

Measurement	**Instrument Accuracy**	**Estimated Error / Dispersion**
Torque	±1–2% full scale	∼ 2–3%
Effective Power	Derived from torque and RPM	∼ 3–4% cumulative error
Fuel Consumption	±0.5–1%	∼ 1–2%
Exhaust Gas Temperature	±5–10 °C	∼ 2–3%
Air/Fuel Ratio	±0.1–0.2 AFR units	∼ 1–2%
Volumetric Efficiency	Calculated via intake airflow	∼ 2–3%

Overall, the measurements are credible within these uncertainty ranges.

5.6 Recap Table: Gasoline vs Diesel Engine Results

Table 5.2: Recap Table: Gasoline vs Diesel Engine Results.

Parameter	**Diesel Engine**	**Gasoline Engine**
Torque	High at low RPM (excellent low-end torque)	Lower at low RPM, better at high RPM
Effective Power	30–70% higher especially at 1000–2000 RPM	Gains power at high RPM; power gap narrows
Hourly Fuel Consumption	20–40% lower across all RPM	Higher, reflecting performance combustion
Specific Consumption	15–25% better efficiency	Less efficient, especially at low RPM
Exhaust Gas Temperature	Lower (max $\sim 500\,^{\circ}\mathrm{C}$)	Higher (max $\sim 800\,^{\circ}\mathrm{C}$)
Air/Fuel Ratio	Leaner (14–16 AFR); wider operating range	Richer (12–14 AFR); more precise control
Volumetric Efficiency	¿80% mid-RPM due to turbocharging	Peaks mid-RPM; declines faster at high RPM
Overall Efficiency	Stable 32–35%, high across RPM range	Peaks mid-RPM, falls at high RPM
Emissions	Lower CO/CO_2 when operating lean	Higher CO/CO_2 and NO, especially at high RPM
Best Use	Heavy-duty, low-mid RPM operation	High-speed performance, lighter-duty

5.7 Key Takeaways

- Preheating and lean combustion strategies significantly improve combustion efficiency and reduce emissions.
- Diesel engines are best suited for applications requiring low RPM torque and fuel economy.

- Gasoline engines excel in high RPM operation but consume more fuel and produce higher exhaust temperatures.
- Measurement precision is good, but results should be interpreted considering the estimated error margins.

5.8 Conclusion

The results clearly show that increasing the inlet air temperature significantly enhances the adiabatic flame temperature, improving thermal efficiency and reducing the need for fuel-rich mixtures. This leads to lower fuel consumption and fewer emissions. Lean mixtures proved to be more effective in minimizing pollutants such as CO and NO, while still maintaining desirable combustion temperatures when preheating is applied. The analysis of combustion product composition also revealed the presence of incomplete combustion species even at stoichiometric conditions, highlighting the role of dissociation at high temperatures. In the experimental section, diesel engines demonstrated superior performance at low engine speeds, delivering higher torque and better fuel economy due to their high compression ratios and lean combustion characteristics. Gasoline engines, on the other hand, performed better at higher RPMs and maintained lower exhaust gas temperatures. Overall, the study emphasizes that careful control of equivalence ratio and preheating, along with a proper choice of engine type, can significantly enhance both energy efficiency and environmental performance.

General Conclusion

In terms of numerical modeling, it is important to emphasize that the Computational Fluid Dynamics (CFD) simulations performed in ANSYS Fluent yielded approximate results that should be interpreted as preliminary estimates rather than fully validated predictions. Although these simulations successfully captured the main combustion dynamics and produced valuable information about flow structures and temperature distributions, they remain limited by simplifications in the turbulence and combustion models employed. Recognizing these limitations, future efforts will be directed toward developing and refining these numerical models to improve their reliability and accuracy. This includes integrating more advanced turbulence–chemistry interaction frameworks capable of representing transient combustion behavior in greater detail and capturing local phenomena such as flame front instabilities and pollutant formation mechanisms. Moreover, extending the simulation framework to evaluate alternative fuels, including bio-fuel blends and synthetic fuels, will enhance the models' relevance for addressing emerging energy challenges.

Experimentally, it would be valuable to investigate a broader range of engine configurations and operating conditions to expand the dataset and further validate numerical predictions. Additional testing campaigns could include variations in injection strategies, intake air management, and combustion chamber geometry to better understand their combined effects on performance and emissions. Integrating real-time emissions analysis and high-resolution in-cylinder pressure measurement will also provide a more comprehensive basis for assessing environmental impacts and refining the thermodynamic and CFD models accordingly.

Finally, from a technological standpoint, the combined experimental–numerical approach developed in this project has demonstrated significant potential for supporting combustion optimization strategies. The validated models—while still subject to further improvement—can serve as a foundation for exploring techniques such as optimizing injection timing, adopting advanced ignition systems, and adjusting air–fuel mixture preparation to enhance efficiency and reduce pollutant emissions. These contributions will help accelerate the development of cleaner, more energy-efficient internal combustion engine technologies that align with increasingly stringent environmental regulations and growing demands for sustainable mobility.

Bibliography

[1] Brahim Mahfoud and Allalou Azzedine. Numerical simulation of combustion in an internal combustion engine. Technical report, University of Bouira, Bouira, Algeria, July 2021.

[2] Willard W. Pulkrabek. *Fundamentals of Internal Combustion Engines*. Personal copy, PDF version. Accessed from local storage on 27 June 2025.

[3] V. Ganesan. *IC Engine*. Department of Mechanical Engineering, Indian Institute of Technology Madras, Chennai, India, 4th edition, 2012. Professor Emeritus.

[4] How a Car Works. How a two-stroke engine works, n.d. Accessed: 2025-06-27.

[5] DriveSpark. Four-stroke engines: A simple guide to the basics, n.d. Accessed: 2025-06-26.

[6] 4BT Engines. Indirect injection vs direct injection engines, n.d. Accessed: 2025-06-27.

[7] TopOne Power. What are diesel engines and how do they work?, n.d. Accessed: 2025-06-27.

[8] Thermal Engineering. Qu'est-ce qu'un cycle diesel réel et idéal ? - définition, n.d. Accessed: 2025-06-27.

[9] Encyclopædia Britannica. Gasoline engine, n.d. Accessed: 2025-06-27.

[10] Learning in the Leaves. The fire triangle, n.d. Accessed: 2025-06-27.

[11] Chimie du Feu. Chapitre 4: Les flammes. PDF, 2014. Accessed: 2025-06-27.

[12] B. Ashoka, A. Naresh Kumar, Ashwin Jacob, and R. Vignesh. Emission formation in ic engines. In *Chapter 01, Department of Mechanical Engineering, Lakireddy Bali Reddy College of Engineering*. Mylavaram, Andhra Pradesh, India, November 2021.

[13] X-Engineer.org. Pressure-volume (pv) diagram. `https://x-engineer.org/pressure-volume-pv-diagram/`. Accessed: 2024-07-04.

[14] Kanchan Ganvir and N. D. Pachkawade. Synthesis and performance analysis of acetylene for dual fuel mode using s.i engine, September 2019.

[15] TecSolutions. Small engine test set, tecquipment products. `https://tecsolutions.us/tecquipment/product/small-engine-test-set`. Accessed: 2024-07-04.

[16] Abdul Shaik and Mohammed Rafi. A review on c.i engine combustion chamber geometry and optimization. *International Journal of Core Engineering & Management (IJCEM)*, 3(5):1–7, August 2016.

[17] Hamama Remmal. Numerical simulation of turbulent methane combustion process in can-type combustors. Master's thesis, University of Blida, Blida, Algeria, 2024.

[18] BYJU'S. Difference between diesel and petrol engines, n.d. Accessed: 2025-06-27.

[19] SPAREX. Standard piston 68258 – technical specifications, n.d. Accessed: 2025-06-27.

[20] Alexander Schekochihin. Handout 1: Thermodynamics and statistical mechanics. `https://www-thphys.physics.ox.ac.uk/people/AlexanderSchekochihin/A1/2011/handout1.pdf`, 2011. University of Oxford.

[21] ScienceDirect. Closed system. `https://www.sciencedirect.com/topics/mathematics/closed-system`. Accessed: 2025-07-01.

[22] ScienceDirect. Thermodynamic equilibrium. `https://www.sciencedirect.com/topics/engineering/thermodynamic-equilibrium`. Accessed: 2025-07-01.

[23] OpenStax. 12.3 second law of thermodynamics: Entropy, 2021. Accessed: 2025-06-26.

[24] Wikipedia contributors. Enthalpy, 2025. Accessed: 2025-06-10.

[25] J. B. Heywood. *Internal Combustion Engine Fundamentals*. McGraw-Hill, New York, 1988.

[26] Rudolf Diesel. *Theorie und Konstruktion eines rationellen Wärmemotors*. Springer, Berlin, 1913.

[27] Klaus Mollenhauer and Helmut Tschöke. *Handbook of Diesel Engines*. Springer, Berlin, Heidelberg, 2010.

[28] Richard Stone. *Introduction to Internal Combustion Engines*. Palgrave Macmillan, London, 4th edition, 2012.

[29] Testbook. Ic engine - full form, diagram and classification, n.d. Accessed: 2025-06-27.

[30] Inspenet. Diesel engines: Operation and applications, n.d. Accessed: 2025-06-27.

[31] Rato Generator. Working principle of gasoline engine, n.d. Accessed: 2025-06-27.

[32] Aouda Bouzidi and Zahra Daoudi. Study of the hydrodynamic instability of a flat flame. Master's thesis, University Saad Dahleb Blida 1, Blida, Algeria, 2007. Thesis.

[33] Emergent Tech. Fire triangle explained, n.d. Accessed: 2025-06-27.

[34] Quora. What is the meaning of a flame?, n.d. Accessed: 2025-06-27.

[35] A. Evlampiev. *Numerical Combustion Modeling for Complex Reaction Systems*. Phd thesis, Technic University Eindhoven, 2007.

[36] Brahim Mahfoud and Allalou Azzedine. Numerical simulation of combustion in an internal combustion engine. Academic report, July 2021. Final year engineering project.

[37] T. Yusaf, I. Hamawand, P. Baker, and G. Najafi. Experimental study on emissions and performance of an internal combustion engine fueled with gasoline and gasoline/n-butanol blends. *Renewable Energy*, 68:222–229, 2014.

[38] B.-F. Lin, J.-H. Huang, and D.-Y. Huang. Experimental studies on the combustion characteristics and performance of a direct injection engine fueled with biodiesel/diesel blends. *Fuel*, 89(8):2217–2226, 2010.

[39] Abdelkrim Bouamoul. Modélisation mathématique d'une flamme de diffusion méthane-air avec viciation et en configuration contre courant. Master's thesis, Univer-

sité du Québec à Chicoutimi, 1999. Available at: Université du Québec à Chicoutimi Institutional Repository.

[40] R. Stephen Turns. *An Introduction to Combustion: Concepts and Applications*. McGraw-Hill, New York, 3rd edition, 2012. Propulsion Engineering Research Center and Department of Mechanical Engineering, The Pennsylvania State University.

[41] Save My Exams. First law of thermodynamics, 2025. DP IB Physics: HL Revision Notes, Accessed: 2025-06-26.

[42] NASA Glenn Research Center. What is thermodynamics?, 2025. Accessed: 2025-06-26.

[43] Parts of a Car Engine. Car engine parts and their functions, n.d. Accessed: 2025-06-26.

[44] William H. Crouse and Donald L. Anglin. *Automotive Mechanics*. McGraw-Hill Education, New York, 10th edition, 2010.

[45] IndiaMart. Cummins engine block – indiamart product listing, n.d. Accessed: 2025-06-27.

[46] M. J. Nunney. *Light and Heavy Vehicle Technology*. Routledge, London, 4th edition, 2012.

[47] Ronyu Auto Parts. Engine block structure and manufacturing process, 2025. Accessed: 2025-06-27.

[48] Sandvik Coromant. Automotive engine components: Cylinder block machining solutions, 2025. Accessed: 2025-06-27.

[49] F. Payri and J. M. Desantes. *Internal Combustion Engines*. Editorial de la UPV, Valencia, Spain, 2011.

[50] Counterman. Here's what you need to know about replacing a head gasket in your car, 2025. Accessed: 2025-06-27.

[51] J. B. Heywood. *Internal Combustion Engine Fundamentals*. McGraw-Hill Education, New York, 2nd edition, 2018.

[52] SPAREX. Standard piston 68258 – technical specifications, 2025. Accessed: 2025-06-27.

[53] C. F. Taylor. *The Internal Combustion Engine in Theory and Practice, Vol. 1*. MIT Press, Cambridge, MA, 2nd edition, 1985.

[54] Perkins Engines. Crankshaft – major overhaul components, 2025. Accessed: 2025-06-27.

[55] Willard W. Pulkrabek. *Engineering Fundamentals of the Internal Combustion Engine*. Pearson Prentice Hall, Upper Saddle River, NJ, 2nd edition, 2004.

[56] Cylinder Head Manufacturing. Camshaft technical specifications, 2025. Accessed: 2025-06-27.

[57] Heinz Heisler. *Vehicle and Engine Technology*. Butterworth-Heinemann, 2nd edition, 2002.

[58] The Rod Shop. Performance flywheels - technical specifications, 2025. Accessed: 2025-06-27.

[59] M. J. Nunney. *Light and Heavy Vehicle Technology*. Butterworth-Heinemann, 4th edition, 2007.

[60] Ornikar. Vehicle mechanics course: Engine valves, 2025. Accessed: 2025-06-27.

[61] Suraj Kumar. Design and simulation of connecting rod using finite element analysis, July 2021. Unpublished work.

[62] Robert Bosch. *Diesel Engine Management*. Wiley, 5th edition, 2014.

[63] Delphi Technologies. Diesel fuel injection – car and light commercial vehicle, 2025. Accessed: 2025-06-26.

[64] Deanna Sclar. *How to Assess Trouble by Checking Your Spark Plugs*. Wiley, December 2021. Accessed from printed source.

[65] J. B. Heywood. *Internal Combustion Engine Fundamentals*. McGraw-Hill Education, 2018.

[66] H. Zhao. *Advanced Direct Injection Combustion Engine Technologies and Development*. Woodhead Publishing, 2020.

[67] R. D. Reitz and G. Duraisamy. Review of high-efficiency and clean reactivity controlled compression ignition (rcci) combustion in internal combustion engines. *Progress in Energy and Combustion Science*, 46:12–47, 2020.

[68] S. C. Kong, R. D. Reitz, and W. Zeng. Recent advances in modeling turbulent combustion in engines. *Combustion Theory and Modelling*, 26(1):67–92, 2022.